

PUBLISHER :



Address of Publisher & Editor's Office :

GDAŃSK UNIVERSITY
OF TECHNOLOGY
Faculty

of Ocean Engineering
& Ship Technology

ul. Narutowicza 11/12
80-952 Gdańsk, POLAND
tel.: +48 58 347 13 66
fax : +48 58 341 13 66
e-mail : office.pmr@pg.gda.pl

Account number :
BANK ZACHODNI WBK S.A.
I Oddział w Gdańsku
41 1090 1098 0000 0000 0901 5569

Editorial Staff :

Tadeusz Borzęcki Editor in Chief
e-mail : tadbtor@pg.gda.pl

Przemysław Wierzchowski Scientific Editor
e-mail : e.wierzchowski@chello.pl

Jan Michalski Editor for review matters
e-mail : janmi@pg.gda.pl

Aleksander Kniat Editor for international relations
e-mail : olek@pg.gda.pl

Kazimierz Kempa Technical Editor
e-mail : kkempa@pg.gda.pl

Piotr Bzura Managing Editor
e-mail : pbzura@pg.gda.pl

Cezary Spigarski Computer Design
e-mail : biuro@oficynamorska.pl

Domestic price :
single issue : 20 zł

Prices for abroad :
single issue :
- in Europe EURO 15
- overseas US\$ 20

ISSN 1233-2585



POLISH MARITIME RESEARCH

in internet

www.bg.pg.gda.pl/pmr/pmr.php



POLISH MARITIME RESEARCH

No 4(62) 2009 Vol 16

CONTENTS

- 3** **TADEUSZ SZELANGIEWICZ, TOMASZ ABRAMOWSKI**
Numerical analysis of influence of ship hull form modification on ship resistance and propulsion characteristics (Part I)
- 9** **JANUSZ KOZAK**
Selected problems on application of steel sandwich panels to marine structures
- 16** **ZYGMUNT PASZOTA**
The operating field of a hydrostatic drive system parameters of the energy efficiency investigations of pumps and hydraulic motors
- 22** **RYSZARD JASIŃSKI**
Problems of the starting and operating of hydraulic components and systems in low ambient temperature (Part III)
- 31** **ALEKSANDER KNIAT**
Optimization of transformation of measurements of ship hull blocks
- 37** **KRZYSZTOF DUDZIK, MIROSLAW CZECHOWSKI**
Analysis of possible shipbuilding application of friction stir welding (FSW) method to joining elements made of AlZn5Mg1 alloy
- 41** **WOJCIECH LITWIN**
Water-lubricated bearings of ship propeller shafts - problems, experimental tests and theoretical investigations
- 50** **CZESŁAW DYMARSKI, JACEK NAKIELSKI**
Calculation of motion trajectory and geometric parameters of the trawl during pelagic fishing
- 56** **MAREK DZIEWICKI, CEZARY SPECHT**
Position accuracy evaluation of the modernized Polish DGPS
- 61** **ANDRZEJ PIĘTAK, MACIEJ MIKULSKI**
On the adaptation of CAN BUS network for use in the ship electronic systems

Editorial

POLISH MARITIME RESEARCH is a scientific journal of worldwide circulation. The journal appears as a quarterly four times a year. The first issue of it was published in September 1994. Its main aim is to present original, innovative scientific ideas and Research & Development achievements in the field of :

Engineering, Computing & Technology, Mechanical Engineering,

which could find applications in the broad domain of maritime economy. Hence there are published papers which concern methods of the designing, manufacturing and operating processes of such technical objects and devices as : ships, port equipment, ocean engineering units, underwater vehicles and equipment as well as harbour facilities, with accounting for marine environment protection.

The Editors of POLISH MARITIME RESEARCH make also efforts to present problems dealing with education of engineers and scientific and teaching personnel. As a rule, the basic papers are supplemented by information on conferences , important scientific events as well as cooperation in carrying out international scientific research projects.

Scientific Board

Chairman : Prof. **JERZY GIRTLEK** - Gdańsk University of Technology, Poland

Vice-chairman : Prof. **ANTONI JANKOWSKI** - Institute of Aeronautics, Poland

Vice-chairman : Prof. **MIROSLAW L. WYSZYŃSKI** - University of Birmingham, United Kingdom

Dr **POUL ANDERSEN**
Technical University
of Denmark
Denmark

Prof. **STANISŁAW GUCMA**
Maritime University of Szczecin
Poland

Dr **YOSHIO SATO**
National Traffic Safety
and Environment Laboratory
Japan

Dr **MEHMET ATLAR**
University of Newcastle
United Kingdom

Prof. **ANTONI ISKRA**
Poznań University
of Technology
Poland

Prof. **KLAUS SCHIER**
University of Applied Sciences
Germany

Prof. **GÖRAN BARK**
Chalmers University
of Technology
Sweden

Prof. **JAN KICIŃSKI**
Institute of Fluid-Flow Machinery
of PASci
Poland

Prof. **FREDERICK STERN**
University of Iowa,
IA, USA

Prof. **SERGEY BARSUKOV**
Army Institute of Odessa
Ukraine

Prof. **ZYGMUNT KITOWSKI**
Naval University
Poland

Prof. **JÓZEF SZALA**
Bydgoszcz University
of Technology and Agriculture
Poland

Prof. **MUSTAFA BAYHAN**
Süleyman Demirel University
Turkey

Prof. **JAN KULCZYK**
Wrocław University of Technology
Poland

Prof. **TADEUSZ SZELANGIEWICZ**
Technical University
of Szczecin
Poland

Prof. **MAREK DZIDA**
Gdańsk University
of Technology
Poland

Prof. **NICOS LADOMMATOS**
University College London
United Kingdom

Prof. **WITALIJ SZCZAGIN**
State Technical University
of Kaliningrad
Russia

Prof. **ODD M. FALTINSEN**
Norwegian University
of Science and Technology
Norway

Prof. **JÓZEF LISOWSKI**
Gdynia Maritime University
Poland

Prof. **BORIS TIKHOMIROV**
State Marine University
of St. Petersburg
Russia

Prof. **PATRICK V. FARRELL**
University of Wisconsin
Madison, WI
USA

Prof. **JERZY MATUSIAK**
Helsinki University
of Technology
Finland

Prof. **DRACOS VASSALOS**
University of Glasgow
and Strathclyde
United Kingdom

Prof. **WOLFGANG FRICKE**
Technical University
Hamburg-Harburg
Germany

Prof. **EUGEN NEGRUS**
University of Bucharest
Romania

Prof. **YASUHIKO OHTA**
Nagoya Institute of Technology
Japan

Numerical analysis of influence of ship hull form modification on ship resistance and propulsion characteristics

Part I

Influence of hull form modification on ship resistance characteristics

Tadeusz Szelangiewicz, Prof.

Tomasz Abramowski, Ph. D.

West Pomeranian University of Technology, Szczecin

ABSTRACT

After signing ship building contract shipyard's design office orders performance of ship resistance and propulsion model tests aimed at, apart from resistance measurements, also determination of ship speed, propeller rotational speed and propulsion engine power for the designed ship, as well as improvement of its hull form, if necessary. Range of ship hull modifications is practically very limited due to cost and time reasons. Hence numerical methods, mainly CFD ones are more and more often used for such tests. In this paper consisted of 3 parts, are presented results of numerical calculations of hull resistance, wake and efficiency of propeller operating in non-homogenous velocity field, performed for research on 18 hull versions of B573 ship designed and built by Szczecin Nowa Shipyard.

Keywords: ship hull geometry; computational fluid dynamics (CFD); resistance; wake; propeller efficiency

INTRODUCTION

The whole ship design process consisted of 6 ÷ 7 stages can be split into two parts: pre-contractual design, i.e. before signing contract, and post-contractual design. In the design process the designer has to find an optimum design of a given ship, which fulfils shipowner's requirements as well as technical conditions resulting from rules of ship classification institutions and/or organizations dealing with safety at sea (e.g. IMO). However crucial decisions are made already during pre-contractual design phase in the situation where very scarce information is known about designed ship. The basic and simultaneously important parameters determined by shipowner, which have decisive impact on future operational profitability of the ship are: ship speed, propeller rotational speed and propulsion engine power at which the ship speed could be maintained. Overall propulsion efficiency which should be obviously as high as possible, is associated with ship speed and propulsion engine power.

The shipowner obviously expects that the designed ship will reach its assumed service speed at the highest value of propulsion efficiency, i.e. at the possible lowest power delivered to propeller, that also leads to the possible lowest hourly or daily fuel consumption.

Already in the preliminary design stage the ship designer, basing on approximate methods, e.g. [4, 5], determines ship resistance, propulsion power, propeller parameters and overall propulsion efficiency.

After signing the contract further improving the design with respect to available speed and propulsion efficiency takes place mainly on the basis of appropriate resistance and propulsion model tests of the ship in question. During model tests in an experimental tank, apart from resistance measurements, nominal wake and propeller design, also propulsion engine power, propeller rotational speed, and necessary modifications of ship hull form, mainly of its stern part, aimed at obtaining the maximum available ship propulsion efficiency, are determined. However number and range of ship hull modifications during model tests is limited because of high cost and time consumption of such tests. Hence it is not certain whether the elaborated ship hull form together with the designed propeller will ensure the lowest propulsion power, simultaneously at the highest propulsion efficiency, for the assumed speed.

Such possibilities are offered by numerical methods especially those of the computational fluid dynamics (CFD) [1, 2, 3, 6, 8, 9]. The methods can be successfully applied just before contract signing that should contribute to improving designed ship's quality as well as to rising competitiveness of a shipyard which applies such methods. This paper presents results of numerical analyses of influence of ship hull form modifications on resistance characteristics, wake and propeller efficiency, performed for a ship designed and built by Szczecin Nowa Shipyard. Hull form of the built ship is assumed initial one for process of its successive modifications, and to verify the numerical calculations available results of basin model tests and sea trials are used.

COMPUTER SYSTEM APPLIED TO NUMERICAL ANALYSES

Research on flow around floating objects as well as modelling process of their form can be performed by means of various computer programs making use of CFD methods. Commercial packages of computational programs such as CFX, Fluent, Commet, V-Shallo, Marine or the programs elaborated and implemented by research centres, such as PANSHIP, BOS, HPSDK, are in wide use. Prior to actual calculations, hull form of an investigated ship is prepared by using e.g. ACAD or MaxSurf software, and next computational grid is prepared by means of such programs as Gridgen, ICEM, or Gambit.

On the basis of analyzed possibilities of available computer programs, FLUENT system was chosen to investigate viscous flow around ship hull, propeller and rudder, and GAMBIT system was applied to build numerical grids. Both the systems (multi-processor licence) in 64-bit version was installed under control of LINUX operational system.

The selection of FLUENT system has been mainly justified by its wide computational capability for complex systems such as ship hull, rotating propeller, blade rudder (possible application of sliding computational grids), as well as by possible performance of simulation calculations for non-stationary states (e.g. a ship moving with non-stationary speed).

Preparatory calculations were performed by using PC computers, and actual numerical calculations by means of NEPTUN computer cluster installed in the Department of

Ocean Engineering and Design of Marine Systems, Faculty of Maritime Technology, West-Pomeranian University of Technology, Szczecin. The NEPTUN cluster is built of Xeon 4-core processors and its capacity is of about 1T floops. Such computer system makes it possible to shorten calculation time and to conduct calculations for modelled ship hull also in natural scale.

In the frame of realization of the research project in question a few tests and experiments were performed in advance to determine most optimum configuration of the cluster with a view of effectiveness of calculations conducted by means of the multi-processor version of FLUENT system.

For the processing of calculation results in graphical form a graphical work station fitted with Xeon 4-core processors, PNY 3500 professional graphical card, as well as Raid disk matrices (archiving the data and calculation results), was used.

NUMERICAL CALCULATIONS OF B 573 SHIP'S HULL MODEL

On the basis of an agreement signed between the head of Ship Design Office of Szczecin Nowa Shipyard and the head of the Department, numerical analyses in question were performed for a B 573 ship (Tab. 1) for which almost full scope of design documentation including results of basin model tests and sea trials of the built ship, was available.

The ship's hull body lines are shown in Fig. 1 – this is the initial hull form taken for further modification of its geometry.

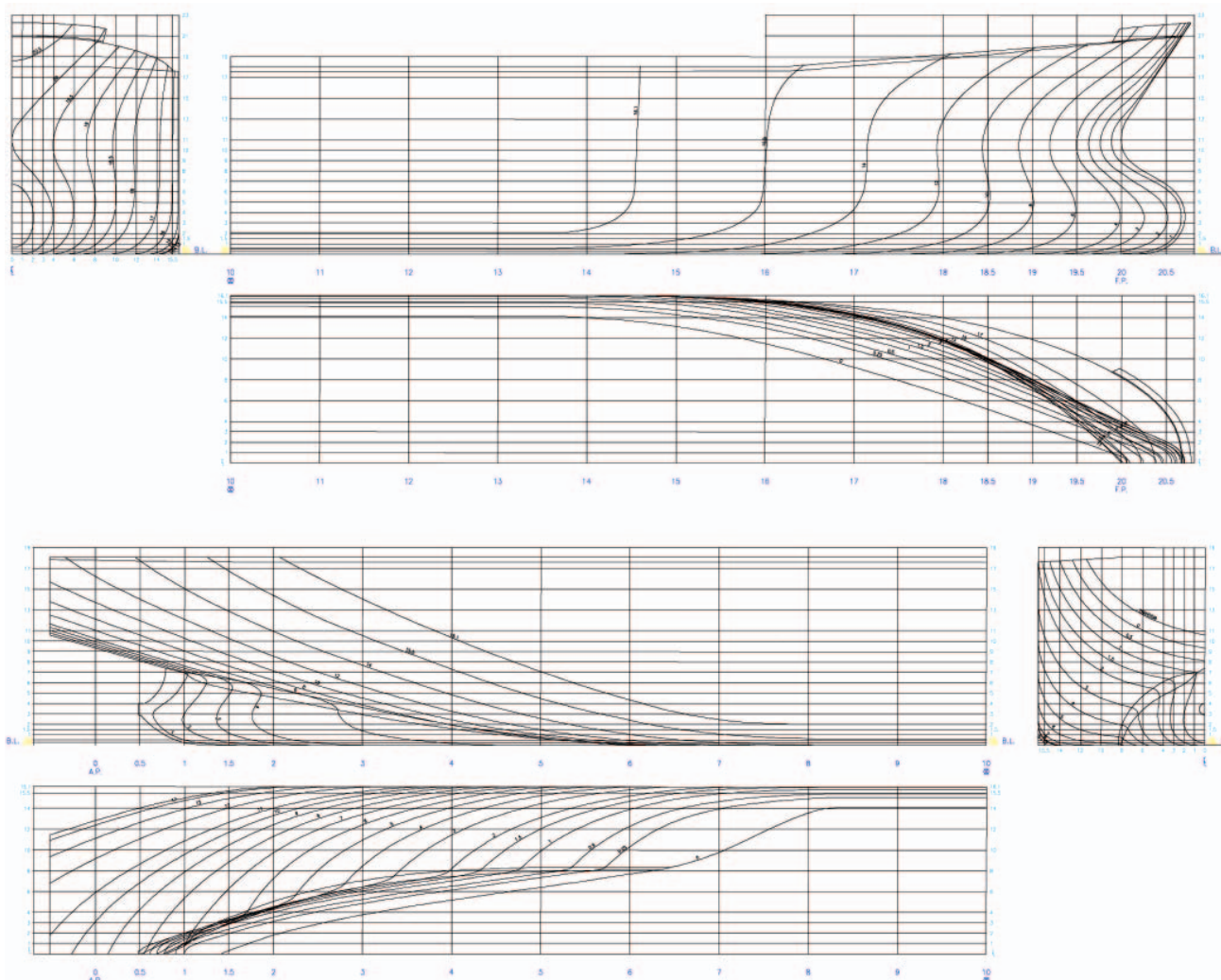


Fig. 1. Body lines of the analyzed hull form of B 573 ship

Tab. 1. Main parameters of B 573 ship in various loading conditions

Length between perpendiculars	L_{PP}	172.00 m	172.00 m	172.00 m
Waterline length	L_{WL}	176.17 m	176.41 m	176.52 m
Hull breadth	B	32.20 m	32.20 m	32.20 m
Draught	T	10.50 m	11.30 m	12.00 m
Volumetric displacement	∇	46540 m ³	50500 m ³	54010 m ³
Wetted surface area	S	7874 m ²	8201 m ²	8477 m ²
Block coefficient	C_B	0.800	0.807	0.813

Prior to actual numerical analyzes a test which consisted in comparing results of resistance calculations made for the initial hull form (Fig. 1) by using CFD method with results of basin model tests [7], was performed. The calculations were conducted for the ship in 1:25 model scale. They were performed by modelling the flow around with the use of RANS equations where turbulence was modeled by means of Reynolds stresses (RSM). Boundary layer was modelled by means of standard functions approximating the flow, with the parameter $y^+ = 50$.

To discretize the domain a non-structural numerical grid (Fig. 2) with prismatic elements in boundary layer was elaborated, which was then converted to that of polyhedral elements (Fig. 3). The non-structural grid was elaborated by using Gambit system and the conversion - by Fluent system.

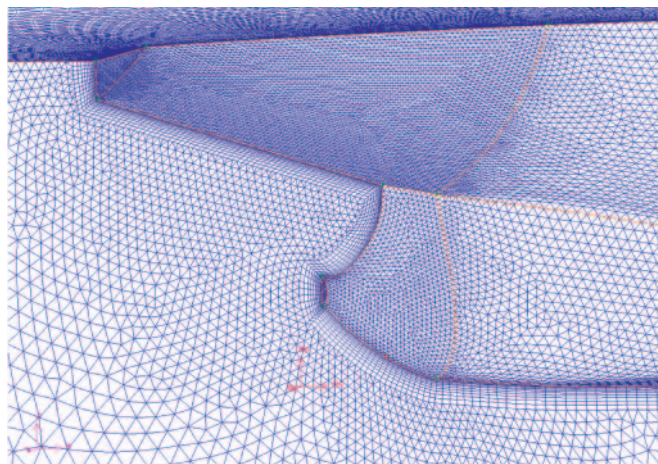


Fig. 2. Non-structured tetrahedral grid

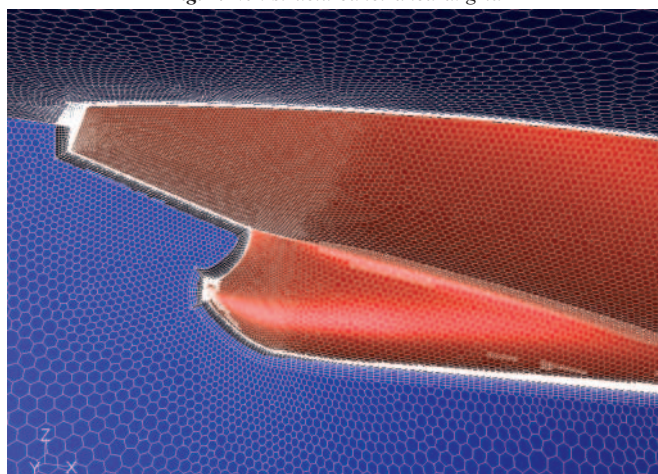


Fig. 3. Polyhedral grid obtained from conversion of non-structured tetrahedral one

Conversion of non-structural grids to polyhedral ones makes it possible to decrease number of grid elements by 3 to 5 times and to improve their parameters, especially the element skewness parameter. The whole number of elements in all variants of calculations for particular draughts was finally contained in the range from 650 to 750 thousand.

In all calculation variants convergence of iteration process was controlled both for residual values of all equations and coefficients of forces generated on the hull. An example convergence run (which was similar for all the tests) is presented in Fig. 4. Iteration tests was terminated when all the remainders (residuals) were below the value of $1e^{-04}$ and resistance coefficient value did not undergo changes any further.

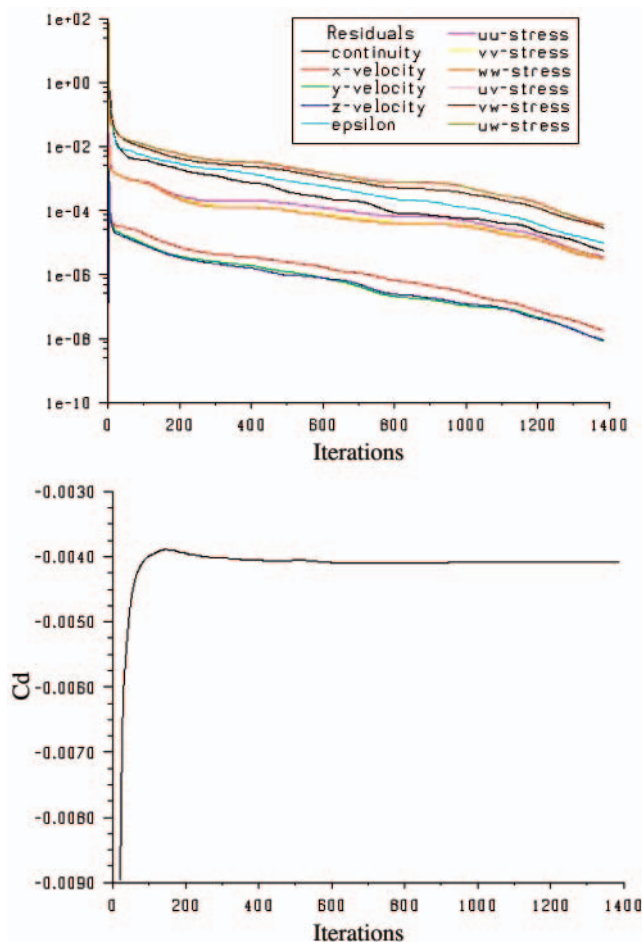


Fig. 4. Diagrams of iteration process convergence of resistance calculations of B573 ship's hull model

Comparison test for resistance calculations

Ship draught $T = 11.3$ [m]
 Water density $\rho = 999.0$ [$\text{kg} \cdot \text{m}^{-3}$]
 Kinematic viscosity $\nu = 1.13896$ [$\text{m}^2 \cdot \text{s}^{-1}$]

The calculations were conducted for three speed values – their results are given in Tab. 2 and Fig. 5.

Tab. 2. Comparison test for resistance

V_s [knots]	V_m [m/s]	Model resistance acc. basin model tests [N]	Model resistance acc. numerical calculations [N]
11.00	1.132	34.795	36.18
14.50	1.492	59.307	61.58
16.00	1.646	76.500	73.5

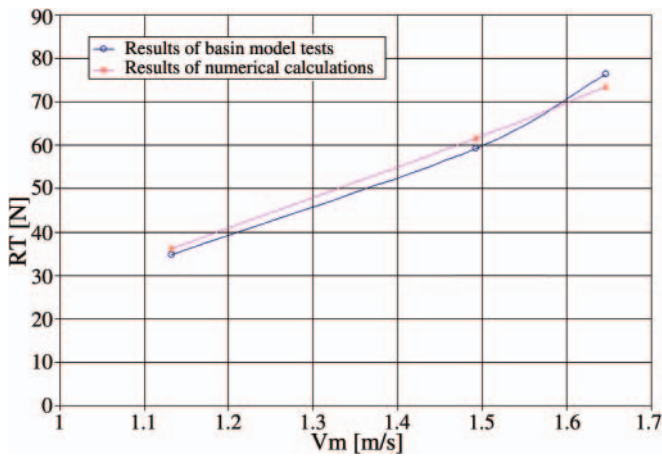


Fig. 5. Model resistance (comparison test)

NUMERICAL RESISTANCE CALCULATIONS FOR MODIFIED HULL VERSIONS OF B 573 SHIP

On the basis of the available hull documentation (hull body lines, Fig. 1) various hull form modifications were prepared. Their scope covered the following (Tab. 3):

- change of the ship's hull block coefficient C_B
- change of the ship's hull prismatic coefficient C_P
- change of location of the longitudinal centre of buoyancy LCB
- manual change of the entire ship's hull form or its stern part only.

Tab. 3. Range of changes of B573 ship hull form

Number of variant	Change of parameter	Parameter
1	-0.01	0.790
2	-0.005	0.795
3	-0.015	0.785
4	+0.01	0.810
5	+0.005	0.805
6	+0.015	0.815
7	-0.01	0.780
8	-0.02	0.770
9	-0.03	0.760
10	+0.01	0.800
11	+0.02	0.810
12	-1% shift fore	47%
13	-2% shift fore	46%
14	-3% shift fore	45%
15	+1% shift aft	49%
16	+2% shift aft	50%
17	+3% shift aft	51%
17	Manual hull form modification of its stern part only	-

The hull form modifications were so performed as to maintain the ship's displacement ∇ constant:

$$\nabla = L \cdot B \cdot T \cdot C_B \quad (1)$$

and the ship's breadth as well. In the case of the analyzed ship the breadth amounted to 32.2 m, hence its enlargement would not be justified from the point of view of the imposed design limitations. While changing the parameters given in particular groups the remaining quantities were left unchanged.

For each of the hull versions new body lines and next numerical computational grids were prepared, and finally calculations of resistance and wake distribution were performed. Example frame sections of modified hull form variants are shown in Fig. 6 ÷ 9.

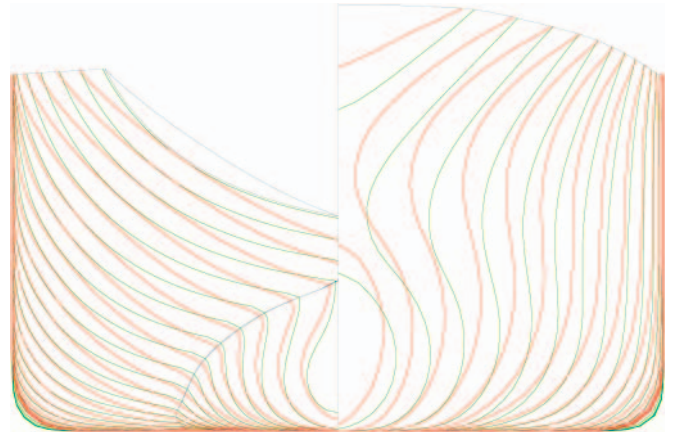


Fig. 6. Variant no.1 – original hull form - marked green; modified hull form – marked red.

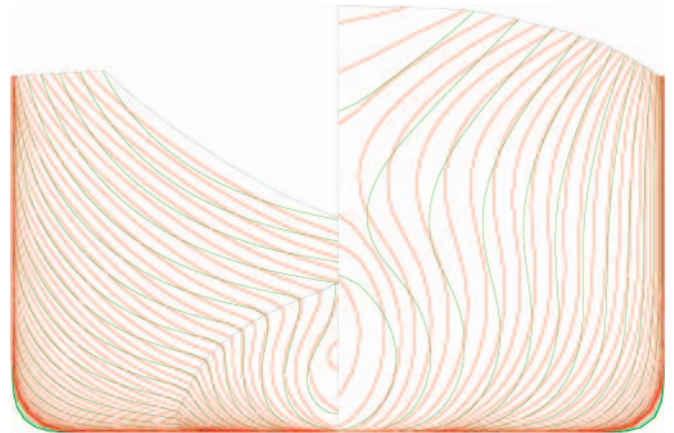


Fig. 7. Variant no.2 – original hull form - marked green; modified hull form – marked red.

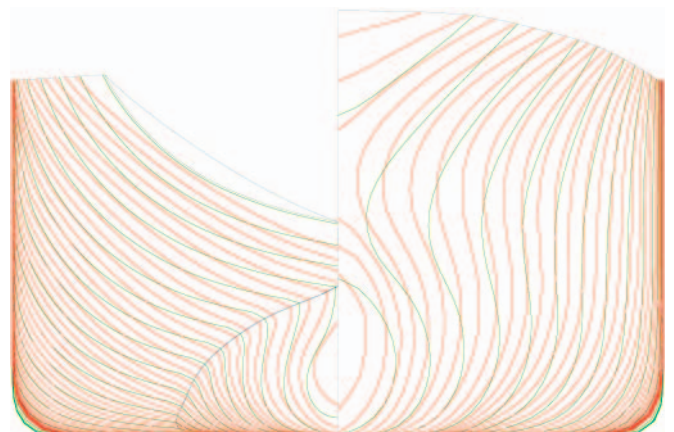


Fig. 8. Variant no.3 – original hull form - marked green; modified hull form – marked red.

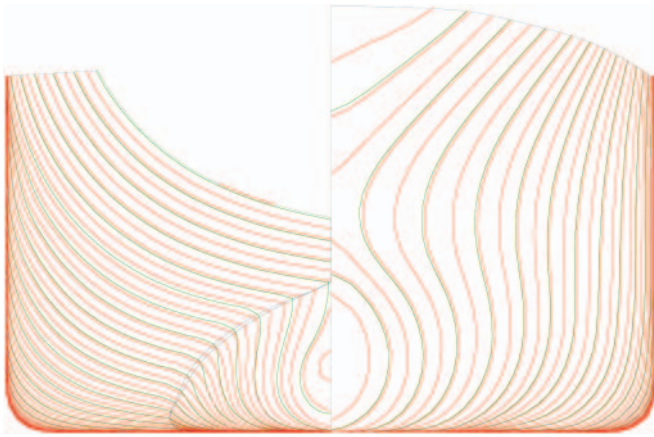


Fig. 9. Variant no.18 – original hull form - marked green; manually modified hull form – marked red.

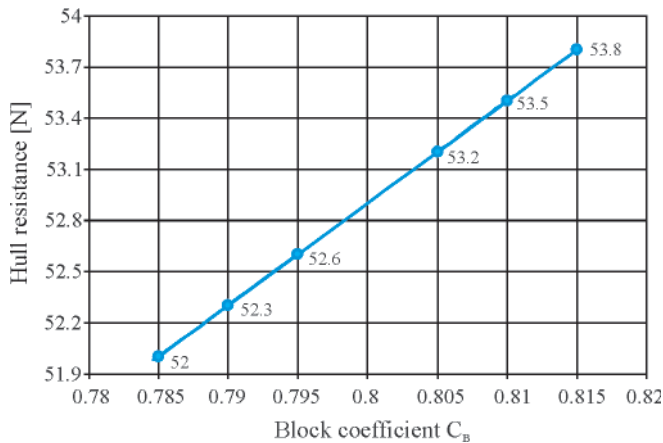


Fig. 10. Calculated hull resistance in fuction of C_B ($V_m=1.492$ m/s)

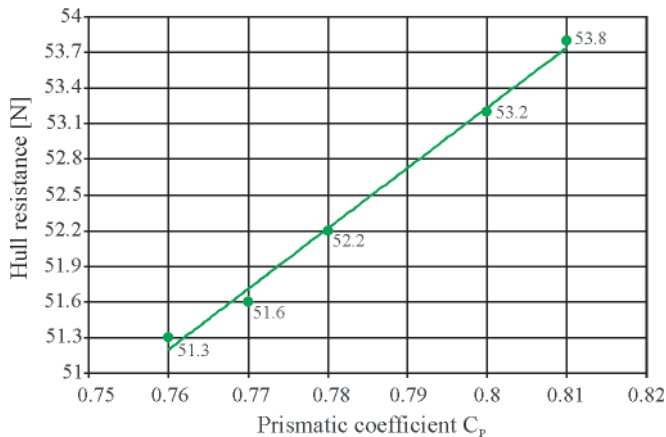


Fig. 11. Calculated hull resistance in fuction of C_P ($V_m=1.492$ m/s)

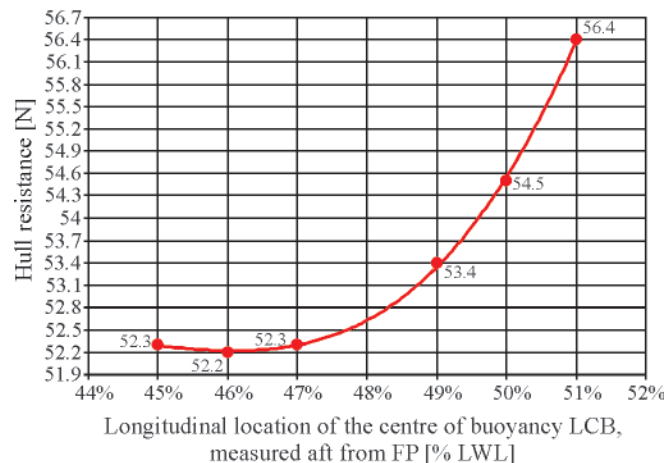


Fig. 12. Calculated hull resistance in fuction of LCB ($V_m=1.492$ m/s)

Tab. 4. Results of numerical resistance calculations for modified form versions of ship hull model ($V_m = 1.492$ m/s)

Number of variant	Modified parameter	Hull model resistance [N]
C_B		
1	0.790	52.3
2	0.795	52.6
3	0.785	52.0
4	0.810	53.5
5	0.805	53.2
6	0.815	53.8
C_P		
7	0.780	52.2
8	0.770	51.6
9	0.760	51.3
10	0.800	53.2
11	0.810	53.8
LCB		
12	47%	52.3
13	46%	52.2
14	45%	52.3
15	49%	53.4
16	50%	54.5
17	51%	56.4
18	Manual modification	52.7

Next resistance calculations were performed for 18 versions of hull form modifications presented in Tab. 2, for the speed $V_m = 1.492$ m/s; their final results are given in Tab. 4. Also, influence of particular modified form parameters of hull model on its resistance to motion is presented in Fig. 10 ÷ 12. Full range of the results obtained from the numerical calculations is contained in the research project's report [10].

CONCLUSIONS DRAWN FROM THE PERFORMED INVESTIGATIONS

- The results of the comparison test (Tab. 2, Fig. 5) reveal certain differences between basin model tests and numerical calculations. They may result form the following reasons:
 - Hull model as well as numerical computational grid has been elaborated on the basis of two-dimensional drawing of body lines. The three-dimensional models based on it may hence differ to each other, in such tests three-dimensional ship hull models should be rather used.
 - The numerical resistance calculations have been performed for hull form model of B 573 ship without propeller, whereas basin model tests have been conducted with the use of a fairwater body substituting propeller cone.
 - Accuracy of numerical calculations may be influenced by a type of computational grid, number of computational domain elements as well as other parameters of CFD method, that should be further investigated.
 - The ship resistance numerical calculations were performed for the selected ship hence it is necessary to examine whether for other hull forms similar relations would be obtained.

- The results obtained from numerical resistance calculations for modified ship hull form versions are not any new relations and such trends are rather obvious. However it is interesting that the numerical method properly reproduces the trends, all the more that the changes of the parameters are relatively small (similar relationships have been also obtained from the approximate method [2] but only for varying global geometrical parameters since the method has not covered geometrical modifications of stern part of ship hull). This may serve as a basis for application of such approach to optimization of ship hull form and improvement of its propulsion efficiency. Especially, the diagram showing the relation between resistance and longitudinal location of buoyancy centre, which suggests existence of a minimum resistance for LCB relative value equal to 46%.

Acknowledgements

Results of the investigations presented in this paper have been financed by Ministry of Science and Higher Education in the frame of the research project no. R10 008 01.

NOMENCLATURE

B	– hull breadth
c_B	– hull block coefficient
c_P	– hull prismatic coefficient
L_{CB}	– longitudinal location of ship centre of buoyancy
L_{PP}	– ship length between perpendiculars
L_{WL}	– ship waterline length
R_T	– ship hull resistance
S	– area of hull wetted surface
T	– ship draught
V_m	– ship model speed
V_s	– ship speed
∇	– volumetric displacement of underwater part of hull
ρ	– water density
ν	– water kinematic viscosity.

BIBLIOGRAPHY

1. Abt C., J.J. Harries S., Heimann J., Winter H.: *From Redesign to Optimal Hull Lines by Means of Parametric Modelling*, COMPIT 2003, Hamburg, May 2003
2. Harries S., Valdenzzi F., Abt C., Viviani U.: *Investigation on Optimisation Strategies for the Hydrodynamic Design of Fast Ferries*, FAST01, Southampton, September 2001
3. Hoekstra M., Raven H.: *A practical approach to constrained hydrodynamic optimization of ships*, NAV 2003, Palermo, June 2003
4. Hollenbach K.U.: *Estimating resistance and propulsion for single-screw and twin-screw ship*. Ship Technology Research 45/2, 1998
5. Holtrop J., Mannen G.G.J.: *An Approximate Power Prediction Method*. ISP, Vol. 29, No. 335, 1982
6. Janson C.E., Larsson L.: *A method for the optimization of ship hulls from a resistance point of view*, 21st Symposium on Naval Hydrodynamics, Trondheim, 1996
7. Jaworski S., Syrocki W.: *Ship B 573: Results of Model Tests-Resistance, Wake Measurements*. Technical Report No RH-95/T-041A, Ship Design and Research Centre, Gdańsk, 1995
8. Maisonneuve J.J., Harries S., Marzi J., Raven H.C., Viviani U., Piippo H.: *Towards Optimal Design of Ship Hull Shapes*, IMDC'03, Athens, May 2003
9. Marzi J.: *Use of CFD methods for hullform optimization in a model basin*, MARNET – CFD Workshop, Haslar, U.K., 2003
10. Szelangiewicz T.: *Numerical research on rudder-propeller-ship stern interaction, aimed at improving propulsion and manoeuvrability qualities of transport ship* (in Polish). Appendix to the final report on realization of the research project no. R 10 008 01, Szczecin, 2009.

CONTACT WITH THE AUTHORS

Tadeusz Szelangiewicz, Prof.
Tomasz Abramowski, Ph. D.
West Pomeranian University of Technology, Szczecin
Faculty of Marine Technology
Al. Piastów 41
71-065 Szczecin, POLAND
e-mail: tadeusz.szelangiewicz@ps.pl

Selected problems on application of steel sandwich panels to marine structures

Janusz Kozak, Assoc. Prof.
Gdańsk University of Technology

ABSTRACT



The paper presents a view on selected problems concerning application of steel sandwich panels to marine structures. Such problems connected with specificity of thin-skin laser-welded structure are varying in topics beginning from micro-scale properties of laser-welded T-joint through the joining of sandwich structures together up to connection and integration of such structures with a classical single-skin structure.

Keywords: laser-welded structures, steel sandwich panels

INTRODUCTION

Sandwich structures are considered as an optimum design for transferring bending loads and can be either metal structures (built of aluminium skins and honeycomb or metal-foam cores) or polymer structures (built of composite skins and polymer-foam cores). The laser welding technique - a new idea which went out from laboratory testing phase - is currently being applied on industrial scale in shipbuilding. Such technique offers new interesting possibilities because application of the laser-welding creates new opportunities of changing the single-skin configuration typical for ship structure into that of two metal shells connected by internal system of joining and supporting elements, see Fig. 1, by application ideas and design

solutions which have been reserved so far for glass-reinforced plastic structures.

Such approach offers significantly higher strength properties of cross section of structures in relation to their weight. However the replacement of the "classical" ship hull design consisted of shell plating supported by perpendicular system of heavy stiffeners by such new structure requires knowledge of its characteristics of strength, corrosion, vibration and fire resistance, and also fatigue strength. Moreover the problem of integration of sandwich structures with "classical" ones has to be solved. It concerns joints between sandwich panels themselves as well as between sandwich panels and single-skin structures, outfitting elements (windows, passages), attachment of equipment like cabling, piping etc.

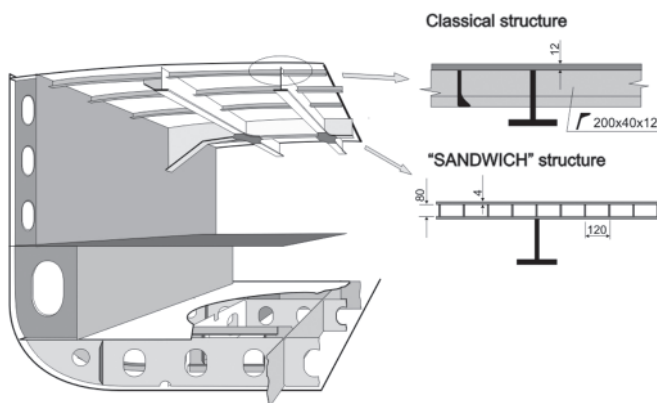


Fig. 1. Example ship deck structure configurations: conventional structure (on the left); I-core-sandwich structure (on the right)

GENERAL IDEA OF SANDWICH STRUCTURES

Among new materials introduced recently into ship structures, the main light-weight materials used on ships are fibre-reinforced-plastic (FRP) composites and aluminium alloys. The FRP is used in both single-skin and sandwich configurations. Aluminium alloys are commonly found in welded stiffened-plate configurations and in the form of extruded sections (both open and closed), but sandwich arrangements are also possible. High strength steels may also be used to reduce weight, although they are not considered usually to be light-weight materials; they may be found in stiffened-plate configurations and, recently, also in certain sandwich configurations. There is increasing use of mixed solutions in which various materials are combined to form a ship or superstructure.

Depending on applied materials and sandwich configuration, the following classes of the structure in question can be found:

- all-metal sandwich structures whose both skins as well as core is metallic,
- semi-steel (hybrid) sandwich structures whose plating is made of a metal but core is non-metallic,
- combined steel-plastic sandwich structures in which only certain components are metallic.

The FRP is a composite material widely applied in ship hull structures as the basis for different kind of laminates, but the question what is maximum size of FRP ship hull remains still open. To compare FRP and metal structures such aspects as manufacturing costs, weight, speed, manoeuvrability, maintaining and repairing costs, possible military aspects as well as utilisation costs have to be taken into account [15].

Another idea of sandwich structure presents the concept of Sandwich Plate System (SPS) in which two steel outer skins are connected by means of BASF Inoac elastomer filler. The elastomer core bonded with the steel, acts as a web and provides continuous support to the faces to preclude local plate buckling, and allows this way to eliminate closely spaced stiffeners, though stiffening plates may be added. The flexural stiffness and strength are tailored as required by using appropriate thickness values of the sandwich elements. Some applications of the SPS such as revitalisation of car decks on ferries or repair of FPSO bottom shell plating, were published. As to the latter example the maximum stresses in the damaged bottom plating were reduced by approximately 50% to satisfy ABS strength requirements, and all hard-point stress concentrations were eliminated [6]. For potential application Limit States Design rules are proposed for innovative bridge decks comprising SPS panels that replace concrete decks [7].

A new hybrid concept of sandwich structures is presented by [13], which consists in combining most of the advantages of metallic and polymer materials while avoiding some of their main disadvantages. For this new concept metal sheets are used at the outer surfaces to maximize rigidity while introducing in between light-weight cores adhesively bonded to keep the whole structure together. Furthermore, composite or wood layers may be used as intermediate layers to improve impact resistance. Potential manufacturing methods for the new structure are based on compression- under- vacuum technique.

Basic type of all-metallic sandwich structures is I-core arrangement which consists of the steel or aluminium panels fabricated as two shell plating of thickness value from 1 to 6 mm each, with distance between them (height) from 40 to 120 mm, stiffened by one-directional system of stiffeners of 40-120 mm span, connected by using laser welding technique applied from outside of shell plates and creating welded joint through the whole thickness of plate. Application of the sandwich structure instead conventional one (Fig.1), can give about 34% weight reduction and about 50% reduction of the manufacturing costs [16].

Steel concrete-filled sandwich structure offers promising properties as it significantly improves strength properties without significant cost increasing. It was also demonstrated that application of low-density covering on outer side of steel sandwich rises resistance to damage resulting from impact transverse load [12].

As bending properties of multilayer thin-skin sandwich structure significantly differ from those of single-shell structure, in the 1950s investigations were initiated on theoretical determination of stiffness matrix of sandwich structure [19,

20]. Latest research in this field provides a bending response theory of web-core sandwich plates, consisting in transforming an originally discrete core into an equivalent homogenous continuum forming a sandwich plate, and following thick-face-plate kinematics by applying analytical formulation to determine equivalent stiffness properties of the plate. The internal forces and displacements are determined by means of the finite element method solution for a given load and boundary conditions. Thereafter, the periodic structure is reconsidered and the internal forces are used for stress prediction based on analytical formulation [17].

EXAMPLES OF APPLICATION OF METAL SANDWICH PANELS TO MARINE STRUCTURES

Metal sandwich panels -due to their particular properties- can be used as structural elements of ship hull smooth, flat surfaces like decks, walls and, in certain cases, side shells, Fig.2.



Fig. 2. Internal superstructure walls made of steel sandwich panels (source: Internet)

Another example of sandwich panel application is a Ro-Ro ship's internal ramp – Fig.3. Such structural part of ship is suitable for panel application hence it remains a matter of interest of designers [22].

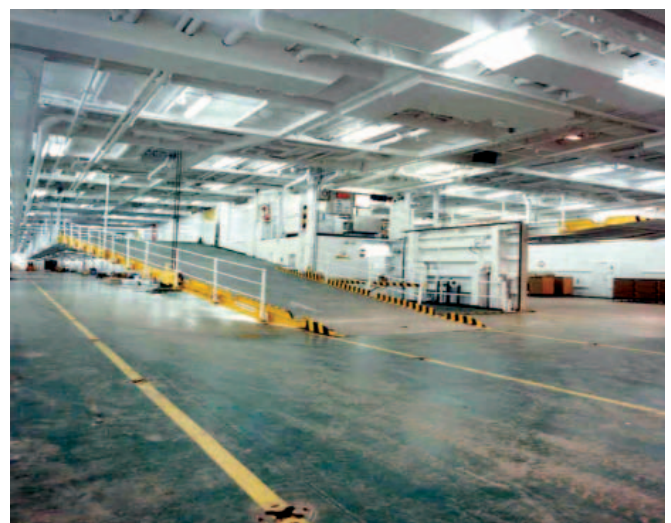


Fig. 3. Ro-Ro ship's internal communication ramp built of steel sandwich panels (source: Internet)

Specific problems related to steel sandwich panels

Modelling laser-welded T-joint

To enable proper modelling of laser-welded steel sandwich panel, a set of methods for generation of its stiffness matrix to reduce amount of model data, is necessary. Meanwhile laser-welded T-joint connecting shell and internal core stiffener, which is present in all steel sandwich panels, significantly differs from conventional MAG-welded fillet joint. Laser-welded joint is formed due to heat generated by light beam acting from outside of shell plate and forming a needle-shape joint from melted metal of joined components. Cross sectional area of such laser weld is significantly smaller than thickness of the joined stiffener. Moreover, regardless of how high quality welding process is, a gap between stiffener and adjacent plate always appears as a result of manufacturing process. A typical cross section of laser-welded T-joint is presented in Fig. 4a where the above mentioned properties are also shown. Additionally, a high gradient of hardness distribution due to high intensity of laser light energy during welding process is observed, which suggests presence of local stress concentration due to structural non-homogeneity (Fig. 4b).

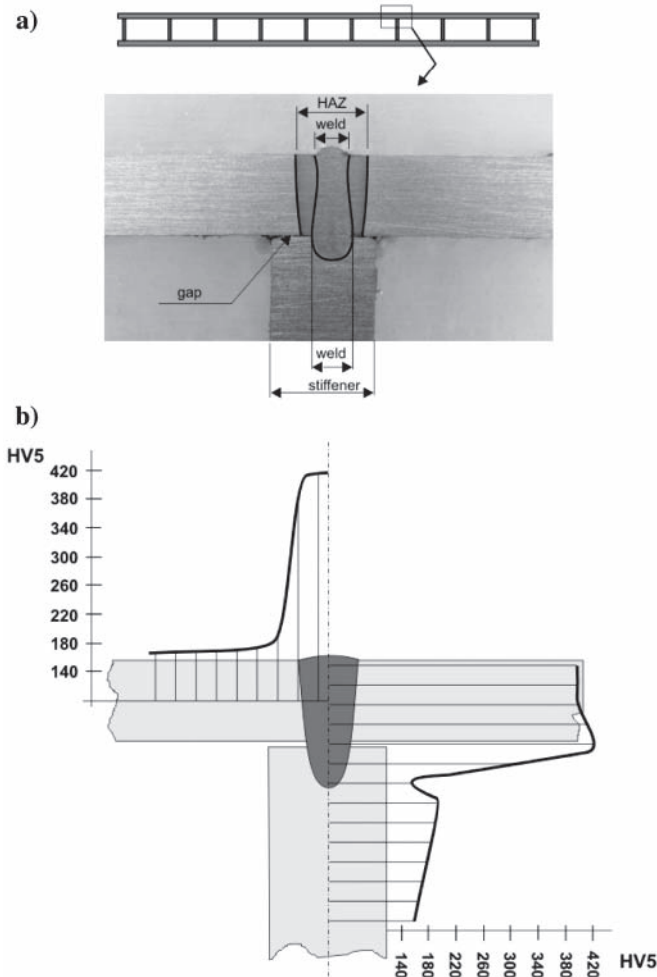


Fig. 4. Properties of laser-welded T-joint: a) geometry of joint, b) distribution of hardness

Such features suggest that the laser-welded T-joint is more sensitive to in-plane bending than „classical” one. As additional effect of the sensibility the contact processes between faces of stiffener and shell plating can occur. The above mentioned properties suggest radically different fatigue properties as compared to classical T-fillet welded joint.

The transverse dimension of the laser-welded T-joint presented in Fig. 4, is equal to 1.2-1.5 mm in stiffener face section, whereas the gap between face of stiffener and shell plate is equal to 0.2 mm. The above mentioned peculiarities lead to conclusion that process of the modelling of such geometry by using the finite element method (FEM) for determination of stress distribution, should be carried out on a significantly higher level of details than for classical welded joints. To obtain more detailed information on deformation of joint, investigations for description of deformation field in a laser-welded joint under bending have been carried out. Results obtained from a laboratory-tested specimen by using the laser extensometer technique (LES) confirmed a complex behaviour of the joint under bending load. Apart from tension strain zone also wide compression strain zone occurs. The occurring contact process is responsible also for the shifting of the neutral axis in weld under bending, Fig. 5 [1, 8].

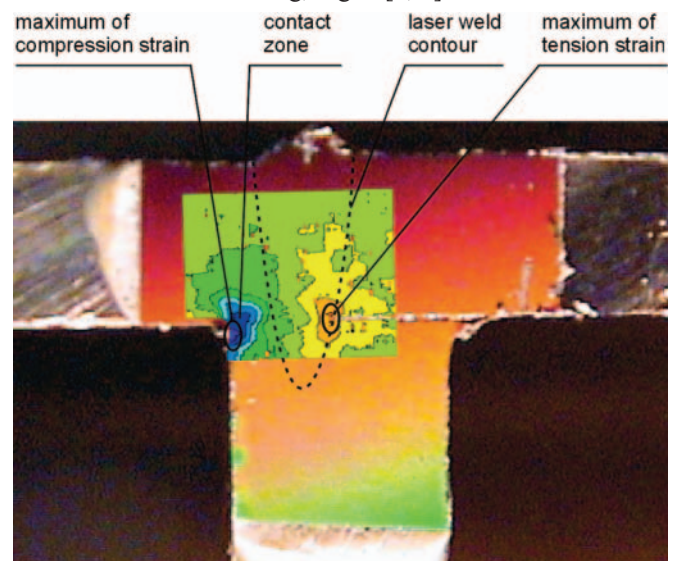


Fig. 5. Strain field in a bended laser-welded joint [1]

Study of the presented strain field distribution shows that due to the contact process the maximum value of compression strain is almost twice higher in relation to that of tension strain [8].

The above mentioned features of the laser-welded T-connection suggest that the proper modelling of its strength behaviour should reflect all the features. The problem leads to studies on the proper modelling of laser weld vicinity with taking into account its stiffness, contact processes as well as material non-homogeneity. Fig. 6 presents the FEM model reflecting the features in question for the joint presented in Fig. 4a.

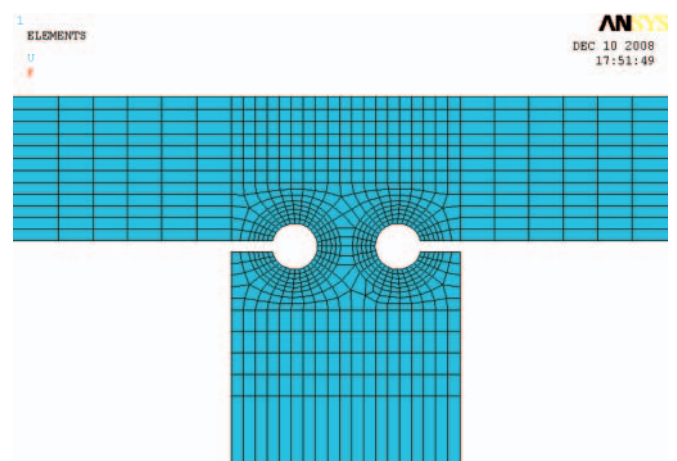


Fig. 6. FEM model of the laser-welded joint [14]

Joins of sandwich structure

Connection of the sandwich structure to single-skin structure is one of the important problems to be solved when a sandwich solution has to be applied. In such case the following classes of the problems may be distinguished:

- connection of composite structure to steel single - skin one
- joining steel sandwich panels together
- connection of steel sandwich structure to steel single - skin one
- three dimensional connections.

The use of polymer composites for naval structures is becoming more and more common, particularly due to potential weight savings. It requires to elaborate various kinds of connections between composite structure and steel hull structure. Such connections should be watertight, sufficiently resistant to failure, and, modular panel assembly should be used to make composite-to-metal connection possible. A few different approaches to solving the problem have been presented recently [2, 3]. Another group of problems is created by the connection between composite panels and supporting steel frames [5].

For all-steel sandwich structure internal joints are necessary because of limited sizes of actually produced panels due to limits of manufacturing lines. The main problem is to maintain continuity of internal stiffener – see Fig. 7. - but appropriate stiffness, water-tightness, manufacturing easiness and low post-welding distortions are also strictly required.

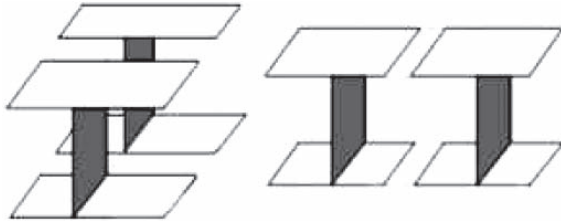


Fig. 7. Scheme of the internal-longitudinal and transverse - joining of metal panels

Possibility of solving a given connection problem depends upon a particular case, but optimisation of a given design from the point of view of stress concentration, weight or manufacturing process is still a subject of research.

For the panel-to-panel connections many proposals can be found depending on given assumptions and limitations. A few possible solutions are presented in Fig. 8.

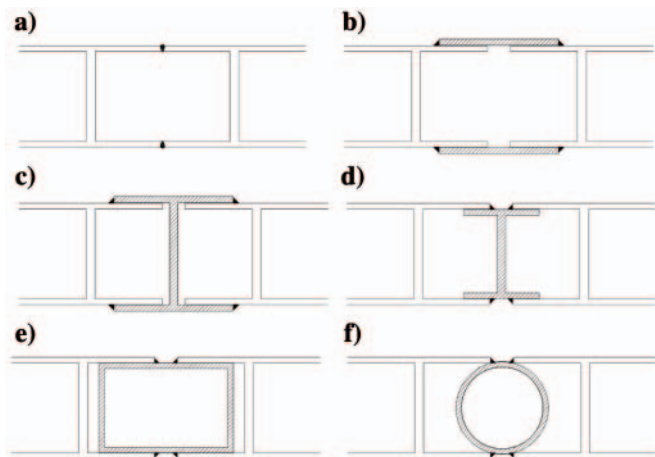


Fig. 8. Selected proposals for panel-to-panel joints [14]

To find the best design as well as optimum geometrical configuration appropriate optimisation procedure is required.

As a target function minimum value of weight or stress concentration factor can be assumed. In Fig. 9 the deformed model of the joint as given in Fig.8b, with indicated von-Mises-stress distribution for the optimum geometrical parameters, is presented.

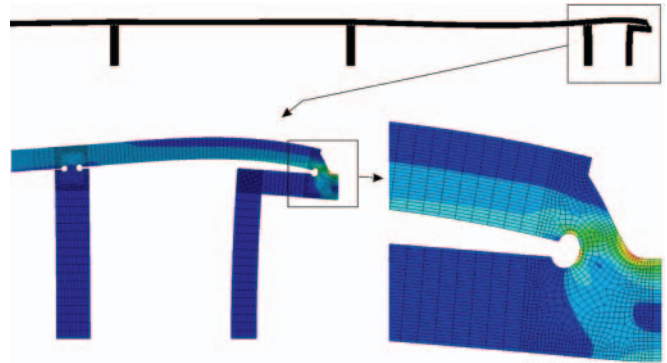


Fig. 9. Deformed model of the joint as given in Fig.8b, with indicated von-Mises-stress distribution for the optimum geometrical parameters [14]

In the case of angular steel sandwich connection the problem of selection of proper geometry and later – its sizing and then optimisation of the applied design – is additionally complicated by influence of relationship between bending moment and shear force acting in joint area; the obtained results are strongly influenced by this factor [18, 21]. For the angular connection, apart from its strength properties, manufacturing process is of importance. In Fig.10. two proposals for such joint are presented.

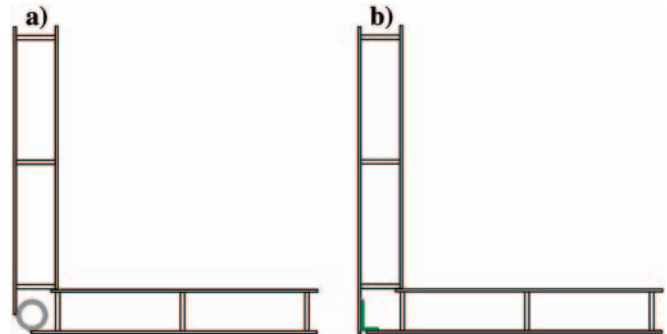


Fig. 10. Selected proposals for angular panel-to-panel joints

For the geometry presented in Fig. 10.b, calculations have been carried out to obtain location and value of the geometric stress concentration factor. The joint deformed under bending moment is presented in Fig. 11, and location of potentially high-stressed area of the joint is shown in Fig. 12.

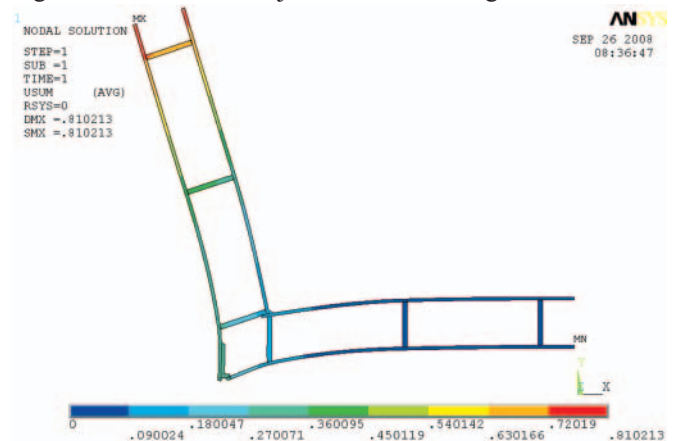


Fig. 11. Angular joint deformed under in-plane bending moment [18]

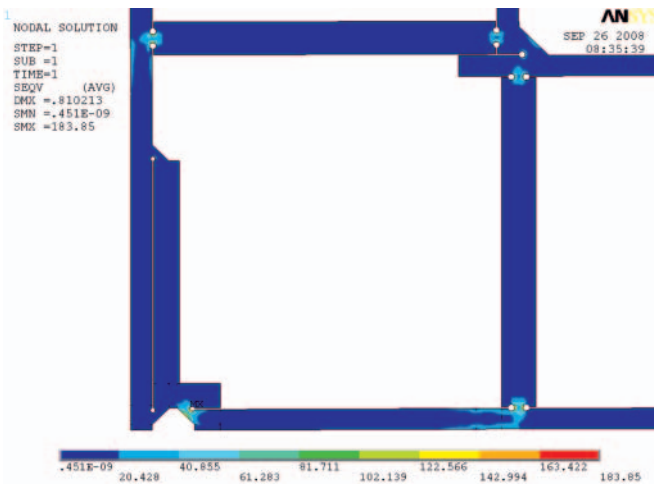


Fig. 12. Detail of high-stressed areas in the joint shown in Fig. 11 [18]

Another problem arises when three sandwich panels have to be mutually connected, for instance, while assembling deck with transverse wall structure – as shown in Fig. 2. Such T-shape connection can be made in a wide variety of geometric forms – depending on strength requirements and manufacturing limitations. Example proposals of such connection are shown in Fig. 13; and example results of calculation of the geometric stress concentration factor are presented in Fig. 14 and Fig. 15.

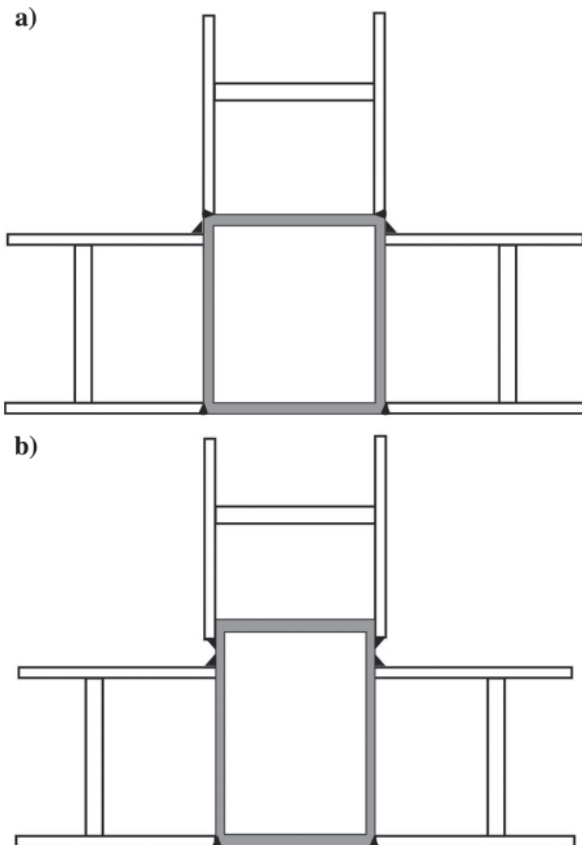


Fig. 13. Proposals for T-connection of sandwich panels [21]

Optimisation of panel structure

To perform optimisation of the whole structure containing both panel and supporting grillage is common problem when collaboration between stiffeners and panel is necessary. The below presented example was developed on occasion of redesign of a Ro-Ro/car carrier where it was decided that

the fixed car decks no. 7 through no.10 had to be made of steel sandwich panels instead of conventional stiffened ones, which required the sandwich deck load-carrying structure to be optimised. The optimisation was carried out in the following steps:

- optimization of a prototype structure with equivalent beam model for transverses, whereas girders and sandwich panels were modelled as masses;
- optimization of fine models of girder and transverse beam (new beam scantlings - height and width assumed fixed);
- re-optimization of a superstructure module with new scantlings of transverses and under smaller load resulting from lighter girders [22].

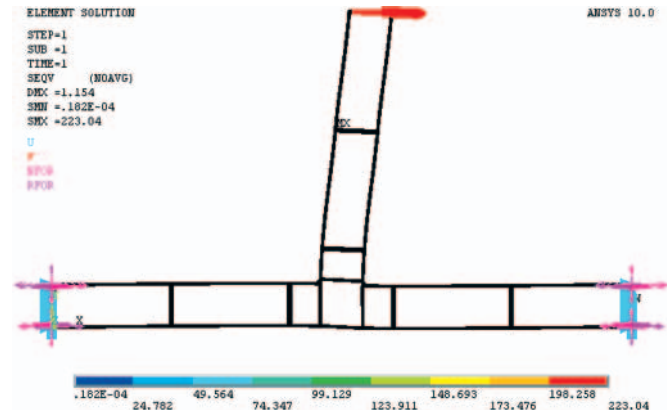


Fig. 14. Deformed FEM model of the joint shown in Fig. 13b [21]

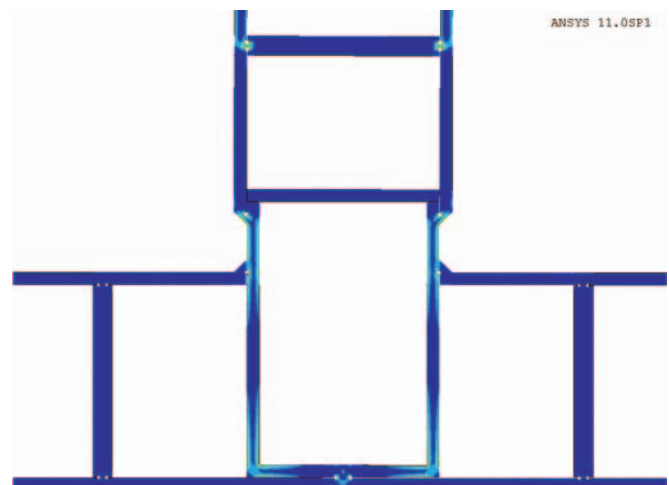


Fig. 15. Detail of high-stressed areas found in the joint shown in Fig. 13b [21]

Flow chart of such procedure is presented in Fig. 16.

AREA OF RESEARCH ON APPLICATION OF STEEL SANDWICH PANELS TO SHIP STRUCTURES

Possible application of multilayer sandwich panels to hull construction opens prospects for a new generation of ship hull structures. One may say that new philosophy of ship hull design arises. However, before panel structures could be applied, one has to be aware of principles of their behaviour in regions crucial for hull structural safety, namely:

- their mechanical properties under long-term static and variable load, theoretical background for occurring phenomena and principles for their modelling
- progress of corrosion processes in sandwich panels containing metal parts and its influence on their mechanical properties and serviceability

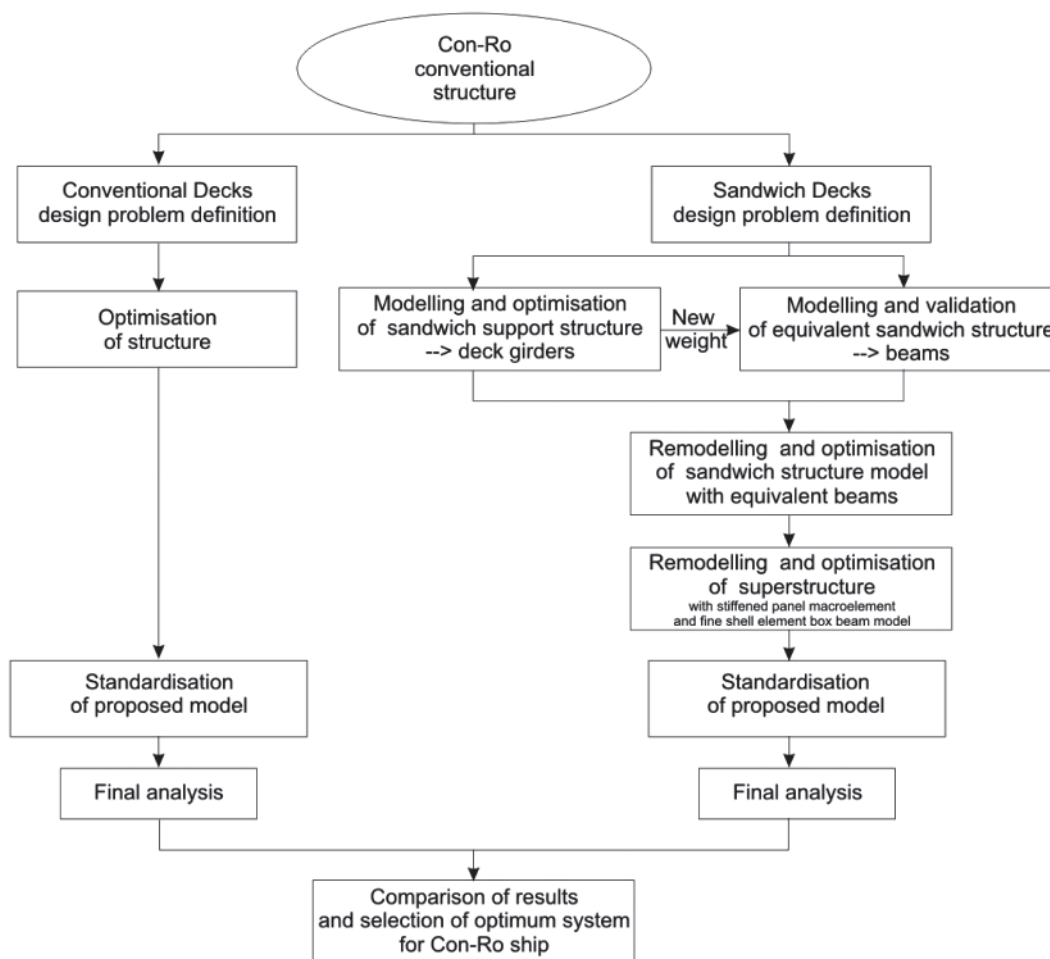


Fig. 16. Flow chart of optimisation procedure of sandwich structure for Ro-Ro car deck [22]

- their vibro-acoustic properties and background for their modelling and forming
- their mechanical properties in elevated and higher temperatures.

Apart from the mechanical characteristics, are also important problems related to manufacturing sandwich panels and mounting them into hull body, such as:

- quality checking procedure of laser welds during manufacturing
- manufacturing tolerances for metal sandwich panels
- strength calculation procedures for joints between sandwich panels themselves as well as between the sandwich panels and classical single-skin structures, including also fatigue life assessment
- design of panel details like passages for cables and pipes, foundations, openings etc.
- assembly procedure for larger structures
- repair procedures
- post-usage utilisation of panels.

FINAL REMARKS

- The above mentioned problems and many other ones have to be solved to prove safe performance of sandwich consisting structures both in normal and extreme conditions.
- It is necessary to elaborate requirements for application of sandwich structures, written in the form of rules and/or recommended practices, similar to those used for single-skin steel structures. Such rules concerning strictly sandwich structures have not been introduced so far.

- Noteworthy is also the fact that the introducing of sandwich panels into ship structures would change specificity of ship production. Today character of shipyards would be transformed from the manufacturing of steel structures to the assembling of tailored panels produced by highly specialised enterprises and delivered ready for assembling. Such approach would lead to simplification of ship prefabrication processes, reduction of distortions of structures and their assembly time as well as to improvement of manufacturing accuracy.

BIBLIOGRAPHY

1. Boroński D., Kozak J.: *Research on deformations of laser welded joint of a steel sandwich structure model*. Polish Maritime Research, No.2, 2004
2. Boyd S.W., Blake J.I.R., Sheno R.A., Mawella J.: *Optimisation of steel-composite connections for structural marine applications*. Composites: Part B 39 (2008)
3. Clifford S.M., Manger C.I.C., Clyne T.W.: *Characterisation of a glass-fibre reinforced vinylester to steel joint for use between a naval GRP superstructure and a steel hull*. Composite Structures, 57 (2002)
4. Internet source: <http://sandwich.balport.com>; <http://www.i-core.com>
5. Kabche J.P., Caccese V., Berube K.A.: *Structural response of a hybrid composite-to-metal bolted connection under uniform pressure loading*. Composite Structures 78 (2007)
6. Kennedy S.J., Bond J., Braun D., Noble P.G., Forsyth D.J.: *An Innovative "No Hot Work" Approach to Hull Repair on In-Service FPSOs Using Sandwich Plate System Overlay*. 2003 Offshore Technology Conference, Houston, Texas, U.S.A., 5–8 May 2003

7. Kennedy D.J.L., Ferro A., Dorton R.A.: *Tentative Design Rules for Innovative Bridge Decks Comprising Sandwich Plate System Panel*. 2005 Annual Conference of the Transportation Association of Canada, Calgary
8. Kozak J.: *Strength Tests of Steel Sandwich Panel*. Schiffbautechnische Gesellschaft, e.V. Seehafen_Verlag, PRADS 2004
9. Kozak J.: *Problems of Assessing Strength Properties of Double Shell, Steel Sandwich Panels*. Gdansk University of Technology, Monograph no.65, Gdansk, 2005
10. Kozak J.: *Problems of strength modeling of steel sandwich panels under in-plane load*. Polish Maritime Research, S1/2006
11. Kozak J.: *Fatigue life of steel, laser-welded panels*. Polish Maritime Research, S1/2006
12. Kujala P., Klanac A.: *Analytical and Numerical Analyses of All Steel Sandwich Panels Under Uniform Pressure Load*. Design 2002, Vol. 2, Dubrovnik, 2002
13. Mamalis A.G., Spentzas K.N., Pantelelis N.G., Manolakos D.E., Ioannidis M.B.: *A new hybrid concept for sandwich structures*. Composite Structures 83 (2008)
14. Niklas K.: *Search for optimum geometry of selected steel sandwich panel joints*. Polish Maritime Research, No. 2/2008
15. Noury P., Hayman B., McGeorge D., Weitzenbock J.: *Lightweight Construction for Advanced Shipbuilding – Recent Development*. DNV internal report, 2002
16. Roland F., Metschkow B.: *Laser Sandwich Panels for Shipbuilding and Structural Steel Engineering*. Meyer Werft, Papenburg, 1997
17. Romanoff J., Varsta P.: *Bending response of web-core sandwich plates*. Composite Structures 81 (2007)
18. Samluk J.: *Numerical analysis of angular sandwich-sandwich panel connection*. M.Sc. Thesis, Gdansk University Technology, Faculty of Ocean Engineering and Ship Technology, 2008, unpublished
19. Tat-Ching Fung et al.: *Shear Stiffness for C-core Sandwich Panels*. Journal of Structural Engineering, August 1996
20. Lok T.S., Cheng O.H.: *Elastic Stiffness Properties and Behaviour of Truss-core Sandwich Panels*. Journal of Structural Engineering, May 2000
21. Zaremba M.: *Analysis of the concentration coefficients in T-connections of the sandwich panels*. M.Sc. Thesis, Gdansk University Technology, Faculty of Ocean Engineering and Ship Technology, 2008, unpublished
22. Zanic V., Andric J., Stipcevic M., Prebeg P., Hadzic N.: *Structural Optimization of a Sandwich Car Deck Structure For Ro/Ro Car Carrier from Uljanik Shipyard*. The 18th Symposium on Theory and Practice of Shipbuilding – SORTA 2008. Pula, 16-18 October 2008.

CONTACT WITH THE AUTHOR

Janusz Kozak, Assoc. Prof.
Faculty of Ocean Engineering
and Ship Technology,
Gdańsk University of Technology
Narutowicza 11/12
80-952 Gdańsk, POLAND
e-mail: kozak@pg.gda.pl

The operating field of a hydrostatic drive system parameters of the energy efficiency investigations of pumps and hydraulic motors

Zygmunt Paszota, Prof.
Gdansk University of Technology

ABSTRACT



The operating field of hydrostatic drive system is presented. Subdivision of the hydraulic motor and pump work parameters into parameters independent of and dependent on the operation of displacement machines and the system is justified. A research project is proposed aimed at development of methods determining the energy characteristics of pumps and rotational hydraulic motors as well as modified methods of determining the energy characteristics of hydrostatic drive systems with selected structures of hydraulic motor speed control. The paper is an extended version of reference [11].

Keywords: hydrostatic drive and control; pumps; hydraulic motors; Sankey diagram; energy efficiency; laboratory and simulation investigations

INTRODUCTION

The working machines with hydrostatic drive and control and also with hydraulic servomechanisms are, due to their drive and control characteristics, very popular in the world-wide economy. However, designers of those machines, manufacturers of the pumps, hydraulic motors and hydrostatic drive systems used in the machines do not have at their disposal a simulation tool for precise determination of their energy behaviour in the entire field of the change of parameters and operating conditions. That makes it impossible to evaluate the drive energy efficiency at an arbitrary point of the operating field and to search for energy saving solutions.

The existing state of affairs is an effect of common views on the way of conducting of laboratory tests of pumps and hydraulic motors used in the hydrostatic drives and control systems and on the method of determining the energy losses in them. That method is an outcome of the traditional reading the energy balance of a hydrostatic drive system illustrated by the Sankey diagram.

The Sankey diagram informs, in relation to the energy balance of a drive system, that the width of the input power stream is equal to the combined width of the output power streams.

In the case of the pump, hydraulic motor and hydrostatic drive system energy balance, the Sankey diagram suggests a situation where the power stream of energy losses should be deducted from the input power stream. However, in the case of a hydrostatic drive system, in its operating field (Fig. 1), i.e. in the hydraulic motor $0 \leq \overline{\omega}_M < \overline{\omega}_{Mmax}$ range of speed coefficient and the $0 \leq \overline{M}_M < \overline{M}_{Mmax}$ range of load coefficient,

the power stream of energy losses should be added to the output power stream, because it is the output (and not input) power parameters that decide about the power of losses.

Only the upper limits $\overline{\omega}_{Mmax}$ and \overline{M}_{Mmax} , describing the hydraulic motor operating field in the hydrostatic drive system (limits influencing the maximum achievable drive output power), are defined by the maximum pump working parameters. They are a result of the theoretical (maximum in the variable capacity pump) capacity q_{pt} per one pump shaft revolution and of the pump shaft rotational speed n_p (dependent in turn on the pump driving electric motor or internal combustion engine characteristics) and also of the nominal pressure p_n of the system (maximum pressure of the continuous system operation) determined in the pump discharge conduit. Besides, they depend on the used structure of the hydraulic motor speed control and on the losses in the system elements. Therefore, the upper limits of hydraulic motor operating field are different in systems with different motor speed control structures.

The simulation methods of determining, by means of mathematical models and computer programs, of the power of losses, energy efficiency and operation field of the hydrostatic drive and control systems of machines are a way to the precise qualitative and quantitative evaluation of the energy behaviour of those systems. The key question is proper selection of the parameters deciding about the system energy behaviour.

The simulation methods allow to investigate and compare the energy saving system solutions and also precise and simple evaluation of the quality of used pumps and hydraulic motors, motor speed control structures, impact of the viscosity and type of working liquid (hydraulic oil, oil-water emulsion, water).

The computer simulation of hydrostatic drive energy behaviour is limited because there are no laboratory methods for determination of pump and hydraulic motor energy characteristics allowing to calculate the respective energy loss coefficients. It is possible only in the situation when the energy losses (and the loss coefficients describing them) are determined as a function of the parameters that they directly depend on.

In a hydrostatic drive system, the power in the power stream increases in the opposite direction to the direction of power stream because of the need to overcome the power of energy losses. Presentation of the power of energy losses in the system must be constructed in the direction from the rotational hydraulic motor shaft or linear motor piston rod to the pump shaft.

In the references [1 – 4] it is shown that the so far practiced presentation of the results of laboratory tests of rotational hydraulic motor losses and energy efficiency as a function of parameters dependent on those losses should be abandoned.

References [5 – 10] present and analyse the areas of power of energy losses in the hydraulic system elements with different rotational hydraulic motor speed control structures. Those considerations allow to understand the roles deciding of the power of losses corresponding to the current motor work parameters required by the hydraulic motor driven device, i.e. the motor load M_M and speed ω_M (n_M). Those considerations allow to draw conclusions about the conditions of achieving high energy efficiency η of a selected structure system. It is also possible to compare the power of losses due to the used hydraulic motor speed control structure. The power P_{pc} consumed by the pump from its driving electric (or internal combustion) motor is the power necessary for providing the useful power $P_{Mu} = M_M \omega_M$ required of the hydraulic motor by the driven device.

In references [7] and [9] a diagram is proposed and explained presenting the direction of increase of power stream flowing from the pump shaft to the hydraulic motor shaft or piston rod, but increasing from the hydraulic motor shaft or piston rod to the pump shaft. The increase of power in the power stream is caused by the necessity of compensating the power of energy losses in the hydrostatic drive and control system elements. The pump shaft power is a function (sum) of the hydraulic motor shaft or piston rod power and power of losses in the system elements. The proposed diagram replaces the Sankey diagram.

INDEPENDENT AND DEPENDENT PARAMETERS OF HYDRAULIC MOTOR AND PUMP OPERATION

The work of a rotational or linear hydraulic motor as an element of hydrostatic drive and control system, directly connected with the driven machine (device) must provide parameters required by the driven machine (speed ω_M (n_M) of the shaft or v_M of the piston rod and shaft load M_M or piston rod load F_M) and also ensure the required machine movement direction.

The mechanical parameters of a motor (speed ω_M (n_M) or v_M and also load M_M or F_M) change in the range from zero to maximum values ω_{Mmax} (n_{Mmax}) or v_{Mmax} , M_{Mmax} or F_{Mmax} .

The required current speed ω_M (n_M) or v_M and required current load M_M or F_M of the driven machine are an effect of its work cycle and the work task. The current driven machine speed and load values are independent of the type and structure of that machine driving system control (e.g. an electrical or hydrostatic system).

The current speed and current load of a hydrostatic system driven machine have a direct or indirect impact on the mechanical, volumetric and pressure losses in the hydraulic motor, pump and other system elements, a system with determined motor speed control structure. The losses are also an effect of the viscosity or kind of the used working liquid (hydraulic oil, oil-water emulsion, water).

The current speed ω_M (n_M) or v_M and current load M_M or F_M of the driven machine influence, in consequence, the current hydraulic motor absorption capacity Q_M and pressure decrease Δp_M and also (depending on the used motor speed control structure) the current pump capacity Q_p and discharge pressure p_{p2} .

If in effect of the increasing, required by the driven machine (device) hydraulic motor speed ω_M (n_M) or v_M , as well as in effect of the increasing, required by the driven machine motor load M_M or F_M , and also in effect of the mechanical, volumetric and pressure losses of the hydrostatic drive system elements, the maximum drive system capacity (determined by the maximum pump capacity Q_{pmax} or maximum pump discharge conduit pressure p_{p2max} limited to the system nominal pressure p_n) is fully used, then further increase of ω_M (n_M) or v_M as well as M_M or F_M will not be possible.

Maximum pump capacity Q_{pmax} is smaller than its theoretical capacity Q_{pt} . The pump theoretical capacity Q_{pt} is a product of the theoretical capacity q_{pt} per one pump shaft revolution and the unloaded pump shaft speed n_{p0} . The pump Q_{pmax} capacity, however, results from the loaded pump speed n_p lower than the speed n_{p0} , and from volumetric losses in the pump.

The system nominal pressure p_n is a maximum permissible continuous operation pressure p_{p2max} determined in the pump discharge conduit.

The maximum speed values ω_{Mmax} (n_{Mmax}) or v_{Mmax} as well as the maximum load values M_{Mmax} or F_{Mmax} of the hydraulic motor used in a hydrostatic drive system are limited by the maximum pump capacity Q_{pmax} or by the system (pump) nominal pressure p_n and also by the corresponding mechanical, volumetric and pressure losses in the remaining system elements, the losses being also an effect of viscosity or the kind of working liquid used. Therefore, the ω_{Mmax} (n_{Mmax}) or v_{Mmax} , M_{Mmax} or F_{Mmax} values are dependent variables.

The current mechanical operating parameters of the hydraulic motor used in a hydrostatic drive system (current motor speed ω_M (n_M) or v_M and current motor load M_M or F_M) are independent values in the motor, deciding of the motor losses and of the hydraulic parameters (the current motor absorbing capacity Q_M and current pressure decrease Δp_M also depending on the motor mechanical, volumetric and pressure losses). The current motor absorbing capacity Q_M and current pressure decrease Δp_M are dependent variables in the motor.

In the hydraulic motor (hydrostatic drive system) operating field ($0 \leq \omega_M$ (n_M) $< \omega_{Mmax}$ (n_{Mmax}), $0 \leq M_M < M_{Mmax}$) or ($0 \leq v_M < v_{Mmax}$, $0 \leq F_M < F_{Mmax}$), the pressure and flow intensities in the system and also the energy losses in the motor, in the pump and in the whole system, power of energy losses and energy efficiencies of the system elements should be considered the functions of the current speed ω_M (n_M) or v_M and the current load M_M or F_M required by the system driven machine (device). Also the torque M_p that the pump loads the driving (electric or internal combustion) motor and the speed n_p that the motor drives the pump with should be considered the functions of the current speed and the current load required by the system driven machine.

The decrease of speed n_p that the electric or internal combustion motor drives the pump with is connected with the increase of torque M_p that the pump loads the motor with. The

decrease of speed depends on the operating characteristics of the motor, which is not a component of the hydrostatic drive system. Therefore, the **pump driving speed n_p should be treated as a parameter independent of the system (of the pump)**.

NON-DIMENSIONAL COEFFICIENTS OF THE HYDRAULIC MOTOR PARAMETERS, COEFFICIENTS OF ENERGY LOSSES IN THE SYSTEM ELEMENTS

The energy efficiency of the hydraulic drive system and its elements is described by mathematical models as functions of the hydraulic motor hydrostatic drive system speed coefficient $\bar{\omega}_M$ and hydraulic load coefficient \bar{M}_M .

The current angular speed ω_M (rotational speed n_M) required of a rotational motor or the linear speed v_M required of a linear motor, operating in a hydrostatic drive system, are replaced in the energy efficiency mathematical models by the motor speed non-dimensional coefficient $\bar{\omega}_M$:

$$\bar{\omega}_M = \frac{\omega_M}{\omega_{Mt}} = \frac{n_M}{n_{Mt}} = \frac{\omega_M q_{Mt}}{2\Pi Q_{Pt}} = \frac{n_M q_{Mt}}{Q_{Pt}}$$

or

$$\bar{\omega}_M = \frac{v_M}{v_{Mt}} = \frac{v_M S_{M1}}{Q_{Pt}}$$

The rotational hydraulic motor speed coefficient $\bar{\omega}_M$ is a ratio of the current angular speed ω_M (rotational speed n_M), required of the motor by driven machine, to:

theoretical angular speed

$$\omega_{Mt} = \frac{2\Pi Q_{Pt}}{q_{Mt}}$$

theoretical rotational speed

$$n_{Mt} = \frac{Q_{Pt}}{q_{Mt}}$$

which would correspond with the theoretical capacity Q_{Pt} of the motor driving pump and with the theoretical motor absorbing capacity q_{Mt} per one shaft revolution. The speed ω_{Mt} (n_{Mt}) would be achievable on the condition, that there are no volumetric losses in the hydrostatic drive system (including the pump and the hydraulic motor) and the pump is driven by an (electric or internal combustion) motor operating with constant rotational speed $n_p = n_{p0}$ independent of its load.

The theoretical angular speed ω_{Mt} (rotational speed n_{Mt}) of a rotational motor is treated as a constant reference value for the motor current angular speed ω_M (rotational speed n_M).

The linear hydraulic motor speed coefficient $\bar{\omega}_M$ is a ratio of the current linear speed v_M , required of the motor by driven machine, to:

theoretical linear speed

$$v_{Mt} = \frac{Q_{Pt}}{S_{M1}}$$

which would correspond with the theoretical capacity Q_{Pt} of the motor driving pump and with effective area S_{M1} of the motor piston in the inlet chamber. The speed v_{Mt} would be achievable on the condition, that there are no volumetric losses

in the hydrostatic drive system (including the pump and the hydraulic motor) and the pump is driven by an (electric or internal combustion) motor operating with constant rotational speed $n_p = n_{p0}$ independent of its load.

The theoretical linear speed v_{Mt} of a linear motor is treated as a constant reference value for the current motor linear speed v_M .

The current torque M_M required of a rotational motor or current force F_M required of a linear motor, operating in a hydrostatic drive system, are replaced by the motor load non-dimensional coefficient \bar{M}_M :

$$\bar{M}_M = \frac{M_M}{M_{Mt}} = \frac{2\Pi M_M}{q_{Mt} p_n}$$

or

$$\bar{M}_M = \frac{F_M}{F_{Mt}} = \frac{F_M}{S_{M1} p_n}$$

The rotational hydraulic motor load coefficient \bar{M}_M is a ratio of the current torque M_M , required of the motor by driven machine, to:

theoretical torque

$$M_{Mt} = \frac{q_{Mt} p_n}{2\Pi}$$

which would correspond with the theoretical absorbing capacity q_{Mt} per one motor shaft revolution and with the hydrostatic system nominal pressure p_n . The torque M_{Mt} would be achievable on the condition that there are no mechanical or pressure losses in the hydraulic motor and in the remaining system elements (except the pump) and the pressure p_{p2max} in the pump discharge conduit is equal to the system nominal pressure p_n .

The rotational motor theoretical torque M_{Mt} is treated as a constant reference value for the current motor torque M_M .

The linear hydraulic motor load coefficient \bar{M}_M is a ratio of the current force F_M , required of the motor by driven machine, to:

theoretical force

$$F_{Mt} = S_{M1} p_n$$

which would correspond with the effective area S_{M1} of the motor piston in its inlet chamber and with the system nominal pressure p_n . The force F_{Mt} would be achievable on the condition that there are no mechanical or pressure losses in the hydraulic motor and in the remaining system elements (except the pump) and the pressure p_{p2max} in the pump discharge conduit is equal to the system nominal pressure p_n .

The linear motor theoretical force F_{Mt} is treated as a constant reference value for the current motor force F_M .

The mechanical, volumetric and pressure losses in a hydraulic motor, pump and in the remaining hydrostatic drive system elements are described in the mathematical models of the losses, power of losses and energy efficiency by the coefficients k_i – relations to the values connected with the values of the hydrostatic drive system characteristic parameters:

- theoretical capacity q_{Pt} per one pump shaft revolution
- theoretical absorbing capacity q_{Mt} per one rotational hydraulic motor revolution or effective piston area S_{M1} in the linear motor inlet chamber
- theoretical pump capacity Q_{Pt}
- system nominal pressure p_n .

The basis of energy evaluation of the particular design solutions and size of the volumetric machines is a catalogue of the coefficients k_i of energy losses in various types of pumps and hydraulic motors used in the hydrostatic drive systems, operating with different levels of pump theoretical capacity Q_{pt} and system nominal pressure p_n , with the working liquid reference viscosity ν_n .

THE MOTOR OPERATING FIELD IN A HYDROSTATIC DRIVE SYSTEM

Figure 1 presents the operating field of a rotational or linear hydraulic motor in a hydrostatic drive system. The operating field is determined in the plane of motor mechanical parameters, i.e. speed coefficient $\bar{\omega}_M$ and load coefficient \bar{M}_M , independent of the motor and of the system.

The limit values $\bar{\omega}_{Mmax} = f(\bar{M}_M)$ or $\bar{M}_{Mmax} = f(\bar{\omega}_M)$ of the hydraulic motor operating field are determined by the maximum motor feed capability in the hydrostatic drive system. The values $\bar{\omega}_{Mmax}$ and \bar{M}_{Mmax} are dependent on the motor and on the system losses.

The maximum motor absorbing capacity Q_{Mmax} , achieved in the system by the applied motor speed control

structure, should be equal or close to the instantaneous maximum pump capacity Q_{pmax} (resulting from the theoretical capacity Q_{pt} , decrease of the pump shaft rotational speed n_p and the intensity of pump volumetric losses Q_{pv}).

The maximum possible motor pressure decrease Δp_{Mmax} should be equal or close to the system nominal pressure p_n determined in the pump discharge conduit, reduced by the pressure losses Δp_c in the system conduit. (In the motor series throttling speed control structure, the maximum slot area of the throttling valve, proportional directional valve or servo-valve should allow to minimize the pressure decrease $\Delta p_{DE|Q_{Mmax}}$ with the set $Q_{Mmax} \approx Q_{pmax}$).

Therefore, the limit values $\bar{\omega}_{Mmax}$ of the hydraulic motor speed coefficient are a function of the current motor load coefficient \bar{M}_M , coefficients k_i of the volumetric losses in the hydrostatic system elements (including coefficient k_2 of the pump shaft rotational speed decrease Δn_p) and a function of the ratio of working liquid viscosity ν to the reference viscosity $\nu_n - \nu/\nu_n$.

On the other hand, the limit values \bar{M}_{Mmax} of the hydraulic motor load coefficient are a function of the current motor speed coefficient $\bar{\omega}_M$, coefficients k_i of the mechanical and pressure losses in hydrostatic system elements and a function of the ratio of working liquid viscosity ν to the reference viscosity ν_n .

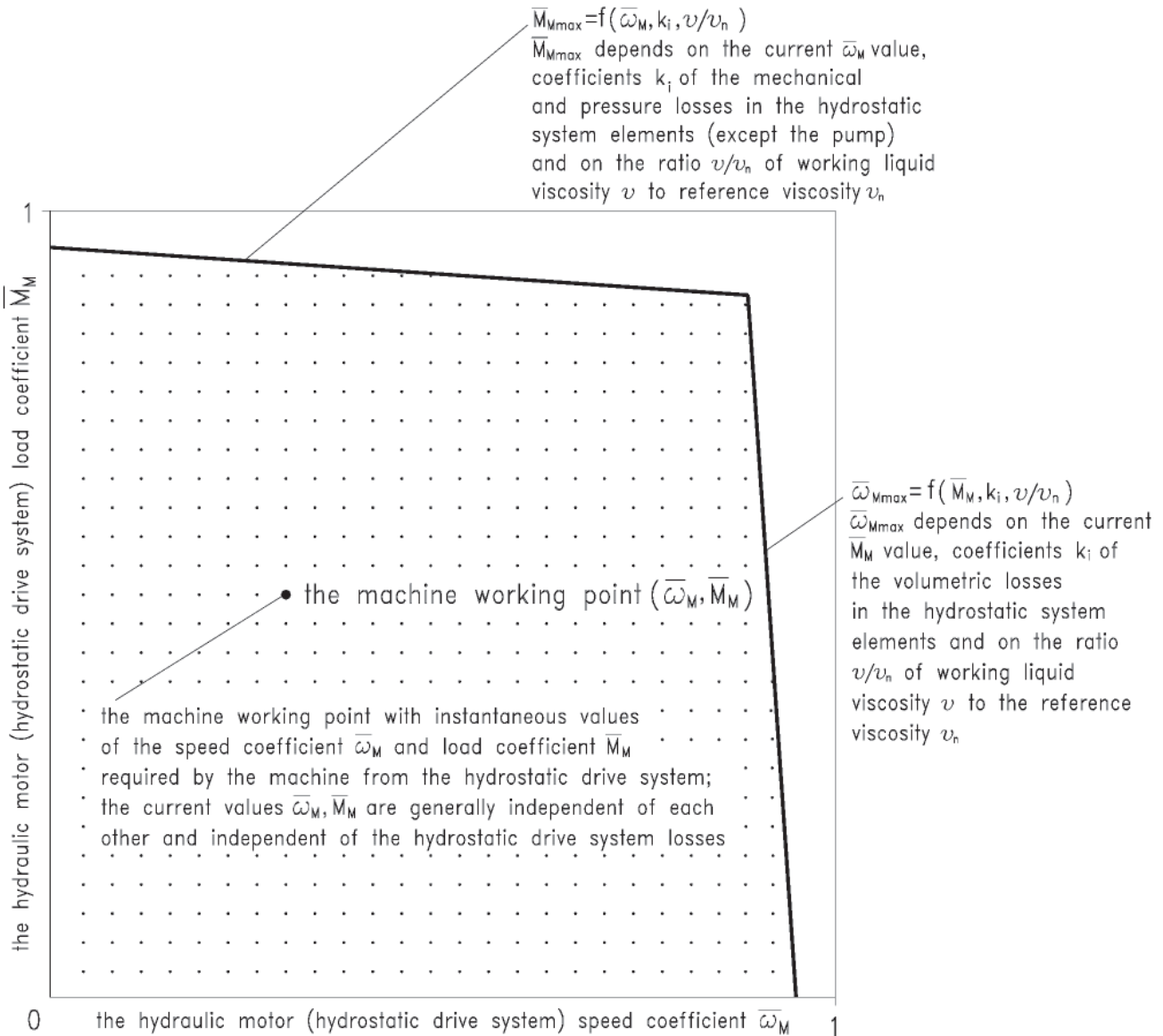


Fig. 1. The range of hydraulic motor speed coefficient $\bar{\omega}_M$ and load coefficient \bar{M}_M ($0 \leq \bar{\omega}_M < \bar{\omega}_{Mmax}$, $0 \leq \bar{M}_M < \bar{M}_{Mmax}$) in a machine hydrostatic drive and control system

THE INVESTIGATIONS OF THE HYDRAULIC MOTOR AND PUMP IN A DRIVE SYSTEM

In a hydraulic motor and hydrostatic drive system operating field ($0 \leq \overline{\omega}_M < \overline{\omega}_{Mmax}$, $0 \leq \overline{M}_M < \overline{M}_{Mmax}$), the losses, power of losses and energy efficiency of the various motor versions, operating:

- in a drive system with different speed control structures
- with different pump theoretical capacity Q_{pt}
- with different system nominal pressures p_n
- with different working liquid viscosity ν ,

should be determined (and compared) as a function of mechanical parameters required by the driven machine, i.e. as a function of the motor speed coefficient $\overline{\omega}_M$ and load coefficient \overline{M}_M and also as a function of the ratio of working liquid viscosity ν to the reference viscosity ν_n . The motor operating field ($0 \leq \overline{\omega}_M < \overline{\omega}_{Mmax}$, $0 \leq \overline{M}_M < \overline{M}_{Mmax}$) or the function $\overline{\omega}_{Mmax} = f(\overline{M}_M)$, $\overline{M}_{Mmax} = f(\overline{\omega}_M)$ should also be determined (and compared).

In a hydraulic motor and hydrostatic drive system operating field ($0 \leq \overline{\omega}_M < \overline{\omega}_{Mmax}$, $0 \leq \overline{M}_M < \overline{M}_{Mmax}$), the losses, power of losses and energy efficiency of the various pump versions, with constant or variable capacity, operating:

- in a drive system with different speed control structures,
- with different pump theoretical capacity Q_{pt}
- with different system nominal pressures p_n
- with different working liquid viscosity ν ,

should be determined (and compared) as a function of the pump capacity coefficient $\overline{Q}_P = Q_P/Q_{pt}$ and a function of the pump discharge pressure coefficient $\overline{p}_{P2} = p_{P2}/p_n$ resulting from the current values of mechanical parameters required by the hydrostatic system driven machine, i.e. the hydraulic motor speed coefficient $\overline{\omega}_M$ and load coefficient \overline{M}_M and also as a function of the ratio of working liquid viscosity ν to the reference viscosity ν_n . The current pump operation coefficients \overline{Q}_P and \overline{p}_{P2} are determined by the current hydraulic motor coefficients $\overline{\omega}_M$ and \overline{M}_M and also by the energy losses in the motor, in the conduits and the losses resulting from the used motor speed control structure.

THE INVESTIGATIONS OF A PUMP IN THE CONDITIONS INDEPENDENT OF THE DRIVE SYSTEM (INVESTIGATIONS OF AN ISOLATED PUMP)

Investigations of the losses, power of losses and energy efficiency of a pump, together with evaluation of the coefficients k_i of the pump losses, are carried out in the conditions independent of the hydrostatic drive system.

- **During the investigation of a constant capacity ($q_{pt} = cte$) pump** (an isolated pump investigated independently of a drive system), **the losses, power of losses and energy efficiency should be evaluated (and compared) as a function of the discharge pressure coefficient $\overline{p}_{P2} = p_{P2}/p_n$, changing in the $0 \leq \overline{p}_{P2} \leq 1$ range.** The pump capacity coefficient \overline{Q}_P should be also evaluated (and compared) as a function of the \overline{p}_{P2} and the ratio ν/ν_n of the working liquid viscosity ν to the reference viscosity ν_n . **In the constant capacity pump ($q_{pt} = cte$), the current discharge conduit pressure p_{P2} is an independent value,** deciding of the pump losses and the current pump capacity Q_P and of the pump shaft torque M_P . **Also the pump driving motor speed n_P , deciding of the current pump capacity Q_P , is a value independent of the pump.**

In a constant capacity pump ($q_{pt} = cte$), the current pump capacity Q_P and the pump shaft torque M_P are dependent values in the pump.

- **During the investigation of a variable capacity pump ($0 \leq q_{pgv} \leq q_{pt}$)** (an isolated pump investigated independently of a drive system), **the losses, power of losses and energy efficiency should be evaluated as a function of the pump capacity coefficient $\overline{Q}_P = Q_P/Q_{pt}$ and as a function of the pump discharge pressure coefficient $\overline{p}_{P2} = p_{P2}/p_n$, changing in the $0 \leq \overline{p}_{P2} \leq 1$ range.** The pump maximum capacity Q_{Pmax} coefficient should be also evaluated (and compared) as a function of the \overline{p}_{P2} coefficient and of the ratio ν/ν_n of the working liquid viscosity ν to the reference viscosity ν_n .

In a variable capacity pump ($0 \leq q_{pgv} \leq q_{pt}$), the current pump capacity Q_P and the discharge conduit pressure p_{P2} are independent values deciding of the pump losses, the current capacity q_{pgv} per one pump shaft revolution (the current $b_P = q_{pgv}/q_{pt}$ coefficient) and of the pump shaft torque M_P . **Also the pump driving motor speed n_P is a value independent of the pump.**

In a variable capacity pump, the current pump capacity q_{pgv} per one pump shaft revolution (the current $b_P = q_{pgv}/q_{pt}$ coefficient) **and the pump shaft torque M_P are dependent values in the pump.**

CONCLUSIONS

- The diagram proposed in [7] and [9], presenting the direction of increase of the power stream in a hydrostatic drive system (replacing the Sankey diagram), the power flowing from the pump shaft to the hydraulic motor shaft or piston rod, but increasing from the hydraulic motor shaft or piston rod to the pump shaft, makes one understand the subdivision of the hydraulic motor and pump work parameters into the parameters independent of and dependent on the energy losses in those machines.
- The graphical presentation of subdivision of the hydraulic motor and the system (in consequence, also the pump) work parameters into the parameters independent of and dependent on the hydrostatic drive system losses is the system operating field presented in the hydraulic motor speed coefficient $\overline{\omega}_M$ and load coefficient \overline{M}_M coordinates (Fig. 1).
- Mathematical models, describing the system losses and energy efficiency as a function of parameters independent of the losses, should be based on the defined k_i coefficients of the hydraulic motor, pump and conduits, and also of the motor speed throttling control assembly, mechanical, volumetric and pressure losses.
- The values of k_i coefficients of the hydraulic motor and pump mechanical, volumetric and pressure losses should be a basis for evaluation of the motor and pump design solutions. The values of k_i coefficients of the losses should be determined nominal pressure p_n levels of the system where the hydraulic motor and pump are used and also in the full range of the working liquid kinematic viscosity.
- The simulation determination of the pump, rotational hydraulic motor and hydrostatic drive system energy efficiency will be enabled by development of the laboratory methods of determination of the pump and hydraulic motor energy characteristics as well as of the modified methods of determination of energy characteristics of the hydrostatic drive systems with selected motor speed control structures. That simulation technique of determining the energy efficiency will be a work tool of the drive system designer.

It will allow to search for energy saving solutions of pumps and hydraulic motors and also for the analysis of energy saving hydrostatic drive and control systems.

- It is suggested to open a research project aimed at considerable reduction of the scope of pump, rotational hydraulic motor and hydrostatic drive system energy efficiency laboratory investigations. The aim is to be achieved by replacing the so far executed full laboratory investigations by simpler tests determining only the k_1 coefficients of losses in the system elements. The coefficients k_1 are then used in the mathematical models and in simulation computer programs for the pump, hydraulic motor and hydrostatic drive system energy efficiency calculations. The mathematical models should take into account and describe the physical phenomena and power of losses, determine the pump, hydraulic motor and hydrostatic drive system operating field and the energy efficiency at any point of that field. They also should allow to evaluate the relative value of power of losses in the pump, hydraulic motor or drive system during the unloaded pump, unloaded hydraulic motor or unloaded drive system operation.

BIBLIOGRAPHY

1. Paszota Z.: *Power of energy losses in the hydrostatic drive system elements – definitions, relations, range of changes, energy efficiencies. Part I – Hydraulic motor.* Chapter in the monograph: „*Research, design, production and operation of hydraulic systems*” (in Polish), Andrzej Meder and Adam Klich editors. „Cylinder” Library. Komag Mining Mechanisation Centre, Gliwice 2007
2. Paszota Z.: *Power of energy losses in the hydrostatic drive system elements – definitions, relations, range of changes, energy efficiencies. Part II – Conduits, throttling control assembly, pump.* Chapter in the monograph: „*Research, design, production and operation of hydraulic systems*” (in Polish), Andrzej Meder and Adam Klich editors. „Cylinder” Library. Komag Mining Mechanisation Centre, Gliwice 2007
3. Paszota Z.: *Power of energy losses in the hydrostatic drive system elements – definitions, relations, range of changes, energy efficiencies. Part I – Hydraulic motor.* (in Polish) Napędy i sterowanie, scientific monthly, No 11 (103), November 2007
4. Paszota Z.: *Power of energy losses in the hydrostatic drive system elements – definitions, relations, range of changes, energy efficiencies. Part II – Conduits, throttling control assembly, pump* (in Polish), Napędy i sterowanie, scientific monthly, No 12 (104), December 2007
5. Paszota Z.: *Graphical presentation of the power of energy losses and power developed in the elements of hydrostatic drive and control system. Part I – Rotational hydraulic motor speed series throttling control systems.* Chapter in the monograph: „*Research, design, production and operation of hydraulic systems*” (in Polish), Adam Klich, Edward Palczak and Andrzej Meder editors. „Cylinder” Library. Komag Mining Mechanisation Centre, Gliwice 2008
6. Paszota Z.: *Graphical presentation of the power of energy losses and power developed in the elements of hydrostatic drive and control system. Part II – Rotational hydraulic motor speed parallel throttling control and volumetric control systems.* Chapter in the monograph: „*Research, design, production and operation of hydraulic systems*” (in Polish), Adam Klich, Edward Palczak and Andrzej Meder editors. „Cylinder” Library. Komag Mining Mechanisation Centre, Gliwice 2008
7. Paszota Z.: *Direction of increase of power stream in the hydrostatic drive and control system. Graphical presentation of the power of energy losses and power developed in the elements of hydrostatic drive and control system. Part I – Rotational hydraulic motor speed series throttling control systems.* (in Polish), Napędy i sterowanie, scientific monthly, No 10 (114), October 2008
8. Paszota Z.: *Direction of increase of power stream in the hydrostatic drive and control system. Graphical presentation of the power of energy losses and power developed in the elements of hydrostatic drive and control system. Part II – Rotational hydraulic motor speed parallel throttling control and volumetric control systems.* (in Polish), Napędy i sterowanie, scientific monthly, No 11 (115), November 2008
9. Paszota Z.: *Graphical presentation of the power of energy losses and power developed in the elements of hydrostatic drive and control system. Part I – Rotational hydraulic motor speed series throttling control systems.* Polish Maritime Research 03/2008
10. Paszota Z.: *Graphical presentation of the power of energy losses and power developed in the elements of hydrostatic drive and control system. Part II – Rotational hydraulic motor speed parallel throttling control and volumetric control systems.* Polish Maritime Research 04/2008
11. Paszota Z.: *The operating field of a hydrostatic drive system.* Chapter in the monograph: „*Research, design, production and operation of hydraulic systems*” (in Polish), Adam Klich, Antoni Kozieł and Edward Palczak editors. „Cylinder” Library. Komag Mining Mechanisation Centre, Gliwice 2009

CONTACT WITH THE AUTHOR

Prof. Zygmunt Paszota
Faculty of Ocean Engineering
and Ship Technology
Gdansk University of Technology
Narutowicza 11/12
80-233 Gdansk, POLAND
e-mail: zpaszota@pg.gda.pl

Problems of the starting and operating of hydraulic components and systems in low ambient temperature

Part III

Methods of determining parameters for correct start-ups of hydraulic components and systems in low ambient temperatures

Ryszard Jasiński, Ph. D.
Gdansk University of Technology

ABSTRACT



More and more intensive technology development makes it possible to produce modern hydraulically driven devices which secure high reliability of operation in various conditions. To design such devices, investigations are performed, including experimental tests, which are very expensive and time consuming. In the design process of a new hydraulically driven machine or system, designers frequently have to solve problems concerning its operation in different weather conditions, for instance in low ambient temperatures. Due to the complexity of the phenomena of concern, the serviceability of the designed hydraulic component or system in those conditions is most frequently assessed based on numerical calculations, much cheaper than the experiments. The article presents three methods: experimental, analytical, and that based on computer simulation, applied for assessing the serviceability of cold hydraulic components supplied with hot working medium being a source of a so-called thermal shock.

Keywords: hydraulic machines, hydraulic drives, diagnostics, hydraulic systems

INTRODUCTION [4, 5]

Two articles entitled “Problems of the starting and operating of hydraulic components and systems in low ambient temperature”, which were published in Polish Maritime Research No. 4/2008 and 1/2009, presented the results of experimental investigations of hydraulic components and systems in the abovementioned conditions. Basic parameters which affect the correct start-up of a hydraulic component in thermal shock conditions were defined. These parameters include: the flow rate Q of the working medium (most frequently oil), the oil temperature T_{ol} and the initial temperature of the component T_{ot} which most frequently corresponds to the ambient temperature.

In the experimental investigations the time-histories of flow rates and oil pressures at component inlet and outlet were recorded. Based on these data the operation of the examined component was analysed, and conclusions were made about its correctness.

An important factor affecting the serviceability of the components in negative-temperature conditions is its structural properties. Numerous phenomena take place during the component start-up in thermal shock conditions. Among them, the factor which most affects the faultless operation of the component is the changes in the dimensions of axial and radial clearances between the cooperating elements. Methods which make it

possible to determine the areas of correct and incorrect operation of the hydraulic component during its start-up in thermal shock conditions base on analysis of changes of the effective clearance during the transient process of component elements heating.

Determining parameters of correct start-up of the component based on the results of experimental investigations (recorded time-histories of oil pressures and flow rate) is expensive and time consuming. The areas of correct start-up parameters can be assessed not only from experimental investigations, which may lead to component damage, but also using numerical methods, which are recommended as cheaper and faster.

THERMAL PROCESSES IN COLD HYDRAULIC SYSTEM COMPONENTS DURING THEIR START-UPS IN THERMAL SHOCK CONDITIONS

The start-up of a cold hydraulic component supplied with the working medium, usually the mineral oil of higher temperature, is a source of unsteady heat flow $\dot{\Phi}_c$ from the oil to component elements. The temperature of the component elements will change to reach a new steady-state level, as the system (component) response to the input signal in the form of a flow rate jump of the hot oil having the temperature T_{ol} (Fig. 1). During this time the component will absorb some portion of heat, arriving at a new internal energy level.

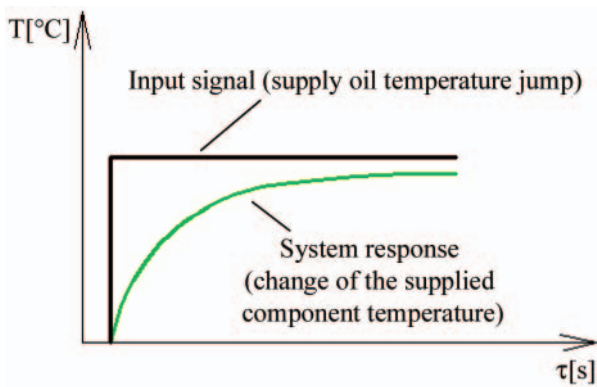


Fig. 1. System response (component temperature) to the set input signal in the form of a flow rate jump of the hot oil having the temperature T_{oi}

The hydraulic system consists of a number of components having different functions. Three basic groups of components, differing by the structure, can be named, which are: supply, control, and executing components.

The article presents thermal balances for two systems of hydraulic components, typical from the point of view of the examined problem, which are pumps and spool valves.

THERMAL BALANCE OF A HYDRAULIC PUMP IN THERMAL SHOCK CONDITIONS

It was assumed in the pump heating model that external leakage flows are absent, i.e. the mass flow rates of the working medium at the pump inlet and outlet are equal to each other:

$$\dot{m}_1 = \dot{m}_2 \quad (1)$$

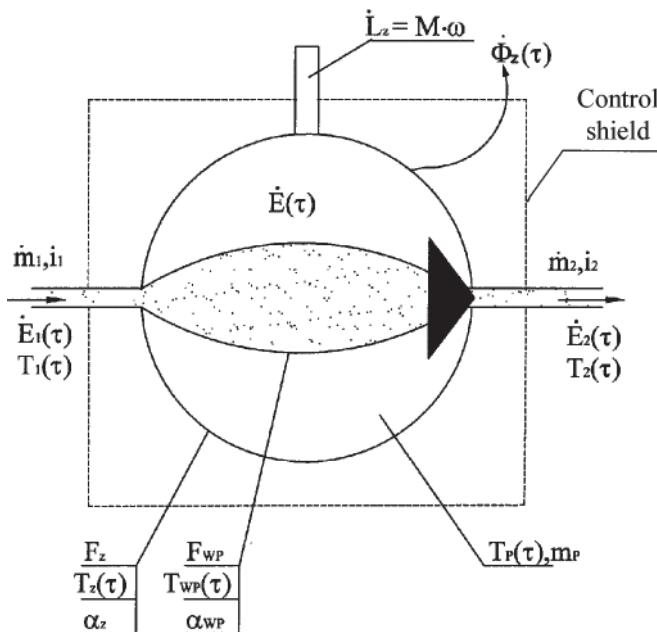


Fig. 2. Parameters used for determining energy balance in hydraulic pump

According to the first law of thermodynamics, the energy E_1 delivered to the hydraulic pump during its start-up is the sum of the energy extracted from the system E_2 and the system energy increase ΔE :

$$E_1 = E_2 + \Delta E \quad (2)$$

The energy delivered with the working medium flowing through the pump and that extracted from the pump in time $d\tau$ (Fig. 2) consist of:

- work done for delivering and extracting the elementary mass flow rate flux $dm = \dot{m} d\tau$ of the fluid having the specific volume v and pressure p , i.e.:

$$dL = p \cdot v \cdot dm \quad (3)$$

- internal energy:

$$dU = dm \cdot u \quad (4)$$

- kinetic energy:

$$dE_k = dm \cdot \frac{w^2}{2} \quad (5)$$

where:

w – average fluid flow velocity

- potential energy:

$$dE_p = dm \cdot g \cdot h \quad (6)$$

where:

h – height of the position of the elementary mass of fluid with respect to the reference level.

In the elementary time $d\tau$ the external work dL_z is delivered to the machine, and the heat $d\Phi_z$ is extracted from it to the environment. The internal energy of the pump changes by dE .

Using the balance form of the first law of thermodynamics we arrive at the equation:

$$dm_1(u_1 + p_1 \cdot v_1 + \frac{w_1^2}{2} + g \cdot h_1) + dL_z = \quad (7)$$

$$= dE + d\Phi_z + dm_2(u_2 + p_2 \cdot v_2 + \frac{w_2^2}{2} + g \cdot h_2)$$

Components and differences of the kinetic energy, which depends on the flow velocities: w_1 on the suction side of the pump and w_2 on its pressure side, are negligibly small compared to other terms in Equation (7). Moreover, the positions of the inlet and outlet connectors are most frequently on similar levels, $h_1 \approx h_2$. Taking that into account, the energy balance equation can be simplified by eliminating the potential energy from it, as its differences are close to zero. After these simplifications Equation (7) can be written as:

$$dm_1(u_1 + p_1 \cdot v_1) + dL_z = \quad (8)$$

$$= dE + d\Phi_z + dm_2(u_2 + p_2 \cdot v_2)$$

After introducing the enthalpy, defined as $i = u + p \cdot v$, to Equation (8) we arrive at:

$$\dot{m}_1 \cdot i_1(\tau) + \dot{L}_z(\tau) = \dot{E}(\tau) + \dot{\Phi}_z(\tau) + \dot{m}_2 \cdot i_2(\tau) \quad (9)$$

where:

$i_1(\tau), i_2(\tau)$ – enthalpy of the fluid at inlet and outlet of the control shield.

The hydraulic pump consists of two groups of elements, which are mobile and fixed elements. The simplified scheme of the pump, (Fig. 3), presents the flow of energy fluxes affecting the process of heating of pump elements.

The difference in energy fluxes: $\dot{E}_1(\tau)$ at pump inlet and $\dot{E}_2(\tau)$ at pump outlet depends on:

- thermal energy flux, $\dot{\Phi}_z(\tau)$, flowing from the outer pump surface to the environment. This quantity is defined by the equation:

$$\dot{\Phi}_z(\tau) = \alpha_z \cdot F_z \cdot (T_z(\tau) - T_{ot}) \quad (10)$$

where:

α_z – heat transfer coefficient between the outer pump surface F_z and the environment

$T_z(\tau)$ – average temperature of the outer pump surface

T_{ot} – ambient temperature.

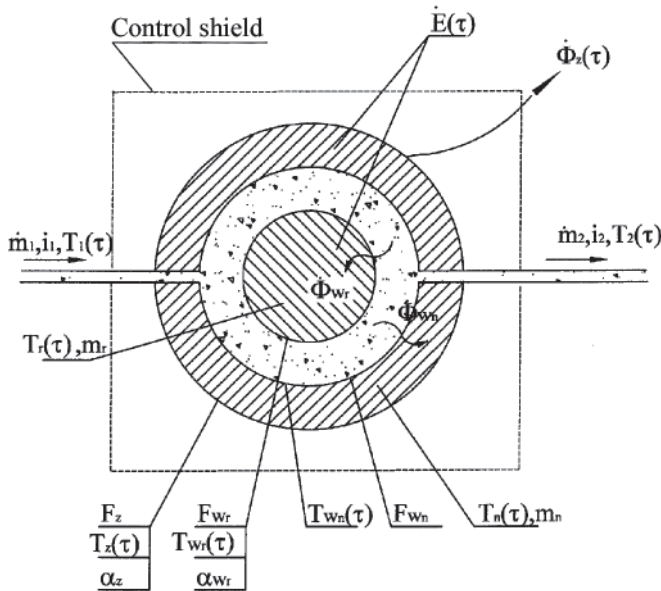


Fig. 3. Model of cold pump heating by the flowing hot fluid

- flux of thermal energy which increases the internal energy of the oil in closed pump chambers and the thermal energy of pump elements:

$$\dot{E}(\tau) = \dot{E}_{Z_{ol}}(\tau) + \dot{E}_p(\tau) \quad (11)$$

$\dot{E}_{Z_{ol}}(\tau)$ – flux of thermal energy that increases the internal energy of the oil in closed pump chambers:

$$\dot{E}_{Z_{ol}}(\tau) = V \cdot \rho_{ol} \cdot c_{ol} \frac{dT_{Z_{ol}}}{d\tau} \quad (12)$$

where:

- V – total volume of pump chambers and passages
- ρ_{ol} – oil density
- c_{ol} – specific heat of oil

$\dot{E}_p(\tau)$ – flux of thermal energy that increases the thermal internal energy of structural pump elements:

$$\dot{E}_p(\tau) = \sum_{i=1}^n m_i \cdot c_i \cdot \frac{dT_i}{d\tau} \quad (13)$$

where:

- m_i – mass of the i -th pump element
- c_i – specific heat of the material of the i -th pump element
- T_i – average temperature of the i -th pump element.

- mechanical power delivered to the pump:

$$\dot{L}_Z(\tau) = \omega(\tau) \cdot M(\tau) \quad (14)$$

Part of the energy $L_Z(\tau)$ delivered to the pump is converted to heat as a result of energy losses caused by leakage flows, flow resistance, and friction. We can assume that the heat generated as a result of pump losses is totally absorbed by the oil.

The flux $\dot{\Phi}_\alpha(\tau)$ of the thermal energy flowing from the oil to the outer pump surface is equal to the flux $\dot{E}(\tau)$ of the thermal energy which increases the internal energy of pump elements and the flux $\dot{\Phi}_z(\tau)$ of the thermal energy flowing from the outer pump surface to the environment:

$$\dot{\Phi}_\alpha(\tau) = \dot{E}(\tau) + \dot{\Phi}_z(\tau) \quad (15)$$

The flux of the thermal energy flowing from the oil to pump elements is equal to:

$$\dot{\Phi}_\alpha(\tau) = F_{WP} \cdot \alpha_{WP} \cdot [T_{ol} - T_{WP}(\tau)] \quad (16)$$

where:

- F_{WP} – heat exchange area between the flowing oil and the pump
- α_{WP} – heat transfer coefficient between oil and pump
- T_{ol} – average oil temperature in the pump
- $T_{WP}(\tau)$ – average temperature of the heat exchange surface between the flowing oil and the pump.

The flux $\dot{\Phi}_\alpha(\tau)$ of thermal energy flowing from the oil to mobile elements $\dot{\Phi}_{Wr}(\tau)$ and fixed elements $\dot{\Phi}_{Wn}(\tau)$ of the pump is equal to:

$$\dot{\Phi}_\alpha(\tau) = \dot{\Phi}_{Wr}(\tau) + \dot{\Phi}_{Wn}(\tau) \quad (17)$$

$$\dot{\Phi}_\alpha(\tau) = \sum_{j=1}^m F_{W_{rj}} \cdot \alpha_{W_{rj}} \cdot [T_{ol} - T_{W_{rj}}(\tau)] + \quad (18)$$

$$+ \sum_{k=1}^z F_{W_{nk}} \cdot \alpha_{W_{nk}} \cdot [T_{ol} - T_{W_{nk}}(\tau)]$$

where:

- r – index defining the mobile element
- n – index defining the fixed element
- m – number of surfaces of mobile elements
- z – number of surfaces of fixed elements.

THERMAL BALANCE OF THE COLD CLASSICAL AND PROPORTIONAL SPOOL VALVE, AND THE HYDRAULIC SERVOVALVE DURING SYSTEM START-UP IN THERMAL SHOCK CONDITIONS

In the spool valves which are most frequently used in hydraulic systems the oil flows through channels connected with the pump 1, executing components 2 and 3, and the outlet to the tank 4 (Fig. 4). During the system start-up in thermal shock conditions, when the hot working medium suddenly flows through the cold valve, the increase of the internal energy of the valve is observed.

The thermal balance for the hydraulic valve with the oil flowing inside (Fig. 4) can be described using the equations in which the energy fluxes of the medium flowing in $\dot{E}_1(\tau) + \dot{E}_3(\tau)$ and out $\dot{E}_2(\tau) + \dot{E}_4(\tau)$ are taken into account:

$$\begin{aligned} & dm_1(u_1 + p_1 \cdot v_1 + \frac{w_1^2}{2} + g \cdot h_1) + \\ & + dm_3(u_3 + p_3 \cdot v_3 + \frac{w_3^2}{2} + g \cdot h_3) = \\ & = dE + d\Phi_Z + dm_2(u_2 + p_2 \cdot v_2 + \frac{w_2^2}{2} + g \cdot h_2) + \\ & + dm_4(u_4 + p_4 \cdot v_4 + \frac{w_4^2}{2} + g \cdot h_4) \end{aligned} \quad (19)$$

Let us assume that the heights of the valve ports are $h_1 \approx h_2 \approx h_3 \approx h_4$, and the flow velocities are $w_1 \approx w_2 \approx w_3 \approx w_4$. After introducing the enthalpy according to the definition $i = u + p \cdot v$ to Equation (19) we arrive at:

$$\begin{aligned} & (\dot{m}_1 \cdot i_1 + \dot{m}_3 \cdot i_3) \cdot d\tau = \\ & = (\dot{m}_2 \cdot i_2 + \dot{m}_4 \cdot i_4) \cdot d\tau + dE + \dot{\Phi}_Z \cdot d\tau \end{aligned} \quad (20)$$

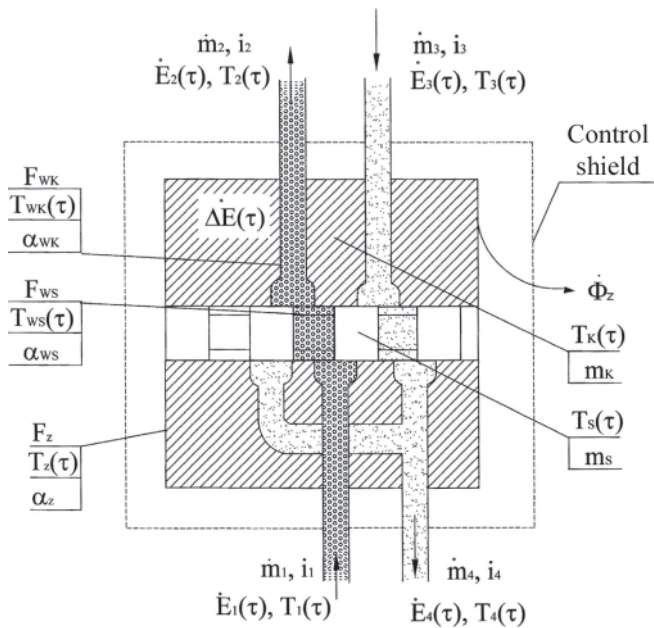


Fig. 4. Model of thermal energy flow from the hot oil to spool valve elements: $E_1(\tau)$ - flux of energy flowing into spool valve channel P; $E_2(\tau)$ - flux of energy flowing out of spool valve channel A; $E_3(\tau)$ - flux of energy flowing into spool valve channel B; $E_4(\tau)$ - flux of energy flowing out of spool valve channel T; Φ_z - flux of energy passed to the environment; \dot{m}_1, \dot{m}_3 - mass flux of oil flowing into the spool valve; \dot{m}_2, \dot{m}_4 - mass flux of oil flowing out of the spool valve; $T_1(\tau), T_3(\tau)$ - oil temperature at inlet; $T_2(\tau), T_4(\tau)$ - oil temperature at outlet; i_1, i_3 - inlet enthalpy of the fluid; i_2, i_4 - outlet enthalpy of the fluid; $T_s(\tau)$ - temperature of the spool; $T_{ws}(\tau)$ - temperature of the spool surface being in contact with the flowing oil; F_{ws} - heat exchange surface between oil and spool; α_{ws} - heat transfer coefficient between the oil and the spool surface; $T_{wk}(\tau)$ - temperature of the inner housing surface; F_{wk} - heat exchange surface between the oil and the housing; α_{wk} - heat transfer coefficient between the oil and the surface of housing; α_z - heat transfer coefficient between the outer surface and the environment

If we assume that the temperature difference between the outer surface and the environment is close to zero in the initial system start-up stage, then the flux of energy flowing from the outer valve surface to the environment becomes also close to zero:

$$\dot{\Phi}_z(\tau) = \alpha_z \cdot F_z \cdot (T_z(\tau) - T_{ot}) \approx 0 \quad (21)$$

With the relation (21) being taken into account in Equation (20), the increase of the internal energy dE of the spool valve elements is given by the equation:

$$dE = (\dot{m}_1 \cdot i_1 + \dot{m}_3 \cdot i_3) d\tau - (\dot{m}_2 \cdot i_2 + \dot{m}_4 \cdot i_4) d\tau \quad (22)$$

Assuming that the mass flow fluxes $\dot{m}_1 = \dot{m}_2$ and $\dot{m}_3 = \dot{m}_4$, Equation (22) can be written in the form:

$$dE = \dot{m}_1(i_1 - i_2)d\tau + \dot{m}_3(i_3 - i_4)d\tau = \dot{\Phi}_\alpha d\tau \quad (23)$$

The increase of the internal energy of spool valve elements (spool and casing) depends on the working medium enthalpy differences between channels 1 and 2, and between channels 3 and 4.

The flux of the thermal energy flowing from the oil to spool valve elements is equal to:

$$\begin{aligned} \dot{\Phi}_\alpha(\tau) = & \alpha_{wk} \cdot F_{wk} \cdot [T_{ol} - T_{wk}(\tau)] + \\ & + \alpha_{ws} \cdot F_{ws} \cdot [T_{ol} - T_{ws}(\tau)] \end{aligned} \quad (24)$$

METHODS FOR DETERMINING CLEARANCES BETWEEN COOPERATING HYDRAULIC COMPONENT ELEMENTS IN THERMAL SHOCK CONDITIONS

Changes in the effective clearance between the cooperating hydraulic component elements during the start-up depend on a number of factors, including: assembly clearance, load of the component, ambient temperature, oil temperature and flow rate.

If the effective clearance values calculated for the start-up of the hydraulic component in thermal shock conditions are positive ($l_e > 0$), we can conclude that the component will work faultlessly in those conditions.

Methods which make it possible to determine component serviceability (calculate clearances between the cooperating elements) are given in Fig. 5. These methods include experimental, analytical, and computer simulation based methods.

Experimental method

The experimental method of determining effective clearance changes between the cooperating hydraulic component elements during the process of component heating requires a number of series of experimental tests for a given component structure scale. The hydraulic components must be prepared for investigations in thermal shock conditions, including possible measurements of temperatures of their elements and the oil temperature. Temperature sensors are to be placed in both the fixed and mobile elements of the component. If the temperature of the mobile elements of the examined component cannot be measured, model investigations of the process of their heating are to be done.

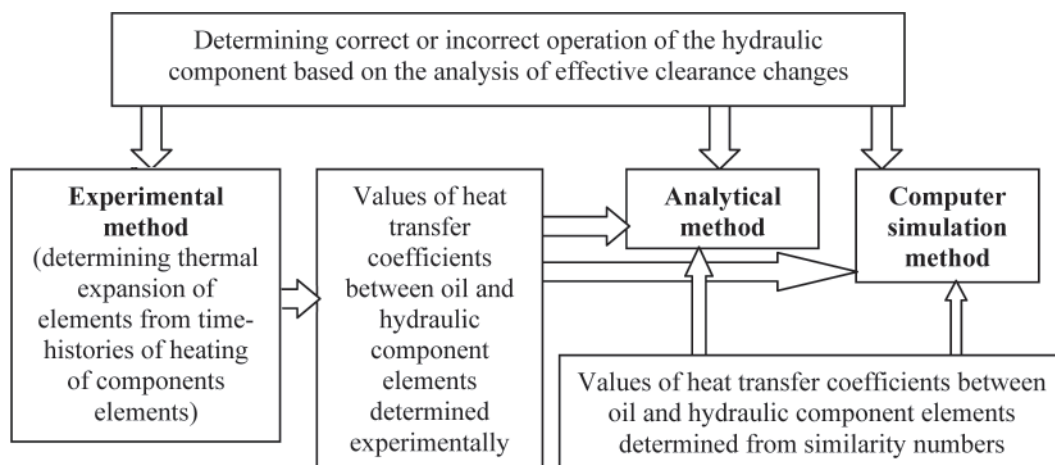


Fig. 5. Methods of determining effective clearance

The experimental investigations of the hydraulic component in thermal shock conditions for selected start-up parameters (flow rate, ambient temperature, and oil temperature) and the initial clearance, will produce the time-histories of temperatures of hydraulic component elements, pressures and flow rates. The collected data, which include the time-histories of temperatures of elements and assembly clearances, will make the basis for determining the correct operation area depending on the initial temperature difference between the oil and the hydraulic component, and the temperature differences between the cooperating component elements.

The effective clearance l_e between the cooperating elements of not loaded component depends on the assembly clearance l_m and the thermal expansion difference Δl_t :

$$l_e = l_m - \Delta l_t \quad (25)$$

When the seizure of the mobile elements in the fixed elements takes place, the effective clearance [3, 4, 5] is equal to zero ($l_e = 0$).

After introducing the equations which describe the thermal expansion differences Δl_t of the hydraulic component elements we get:

$$l_m - \beta_r \cdot h_r \cdot (T_r - T_0) + \beta_n \cdot h_n \cdot (T_n - T_0) = 0 \quad (26)$$

where:

β_r, β_n – linear thermal expansion coefficient of the mobile element (r) and fixed element (n)

h_r, h_n – height of the mobile element, height of the opening in the fixed element

T_r, T_n – average temperature of the mobile element and fixed element, respectively

T_0 – temperature of the element height measurement

After further transformations of Equation 26 a formula is obtained which describes the temperature of the mobile element, at which the effective clearance disappears:

$$T_r = \frac{\beta_n \cdot h_n \cdot T_n + \frac{l_m + \beta_r \cdot h_r \cdot T_0 - \beta_n \cdot h_n \cdot T_0}{\beta_r \cdot h_r}}{\beta_r \cdot h_r} \quad (27)$$

Assuming that the component elements are made of materials revealing similar values of linear thermal expansion coefficients,

($\frac{\beta_n \cdot h_n}{\beta_r \cdot h_r} \cong 1$), Equation 27 can be written as:

$$T_r = T_n + B \quad (28)$$

where:

$$B = \frac{l_m}{\beta_r \cdot h_r}$$

Equation 28 can be used for determining the temperature difference between the mobile element and the fixed elements, at which the effective clearance disappears, i.e. when $l_m = \Delta l_t$:

$$T_r - T_n = \Delta T_{r-n} = B \quad (29)$$

In Equation 25 the temperature difference between the mobile element and the fixed elements depends most of all on the assembly clearance l_m . The smaller the assembly clearance, the smaller the permissible temperature difference between the mobile and fixed elements cooperating with each other at which the effective clearance disappears.

In order to determine the temperature difference ΔT_{ol-ot} between the hot oil and the cold component, the following set of equations is to be solved:

$$\begin{cases} T_r - T_n = \Delta T_{r-n} = B \\ \Delta T_{ol-ot} = a \cdot \Delta T_{r-n} \end{cases} \quad (30)$$

The constant “a” is to be read from the diagram (Fig. 6) or calculated.

After solving the set of equations the relation was obtained which can be used for calculating permissible temperature difference $\Delta T_{ol-ot(MAX)}$ between the hot oil and the cold component:

$$\Delta T_{ol-ot(MAX)} = a \cdot B \quad (31)$$

When the temperature difference ΔT_{ol-ot} between the oil and the hydraulic component is smaller at the initial time than the permissible temperature difference $\Delta T_{ol-ot(MAX)}$ (Fig. 6), the start-up of this component will take a faultless course in thermal shock conditions.

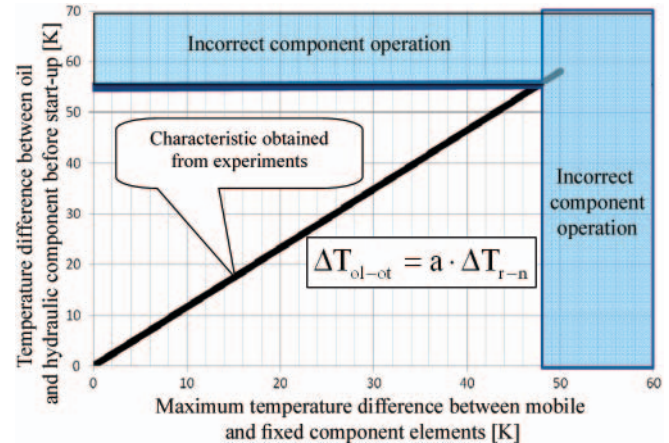


Fig. 6. Experimental assessment of the maximum temperature difference between the oil and the component, at which the component will work faultlessly in thermal shock conditions

Analytical method

Due to its disadvantages, the experimental method cannot be used in all cases. For instance, measuring temperatures of mobile elements is, generally, extremely difficult. Therefore basic parameters of faultless system start-up should be determined using the analytical method or the computer simulation method.

An advantage of the analytical method is its ability to determine the correct operation area using simple equations. Time consumption is smaller than when using complicated computer codes.

In order to determine with the aid of the analytical method the serviceability of the hydraulic component started in thermal shock conditions we have to know the time-histories of average temperatures of mobile and fixed elements of the component.

Figure 7 shows the time-histories of the average temperatures of the fixed elements T_n and their surfaces T_{wn} which are in contact with the flowing oil after the beginning of the start-up. In the initial time interval of heating of the fixed elements, from $\tau = 0$ to τ' , the disordered heat transfer takes place [1, 3, 12, 13].

In the next interval, $\tau > \tau'$, the nature of temperature changes at particular points of fixed elements (T_n, T_{wn}) depends of the shape, dimensions, and thermophysical properties of the element and on heat transfer conditions on the element surface. This is the time of well-ordered heat transfer. After time τ_u the steady state of temperatures in fixed elements is reached.

The time τ' of initial heating of component elements a disordered manner (Fig. 7) is short, as compared to the entire time τ_u of the heating process and is not of high importance for the mathematical description of the phenomenon. To determine the effective clearance with the aid of the analytical method, the author made use of the well-ordered state of heating of component elements.

The temperature time-history $T_n(\tau)$ of the fixed elements can be calculated, for initial conditions (T_{ol}, T_{ot}), making use of the energy balance for those elements:

$$\begin{aligned}\dot{\Phi}_n(\tau) &= \alpha_{wn} \cdot F_{wn} \cdot [T_{ol} - T_n(\tau)] \cdot \psi_n = \\ &= m_n \cdot c_n \cdot \frac{dT_n}{d\tau} + \dot{\Phi}_z(\tau)\end{aligned}\quad (32)$$

where:

- m_n – mass of fixed elements
- $\psi_n = \frac{T_{ol} - T_{wn}}{T_{ol} - T_n} = \frac{\vartheta_{wn}}{\vartheta_n}$ – coefficient of non-uniform temperature distributions in fixed elements, taking into account relations between the temperature differences:
 - ϑ_{wn} – difference between the average oil temperature (higher) and the average temperature (lower) T_{wn} of the surface F_{wn}
 - ϑ_n – difference between the average oil temperature (higher) and the average volumetric temperature (lower) of the fixed elements in the conditions of well-ordered unsteady heat transfer.

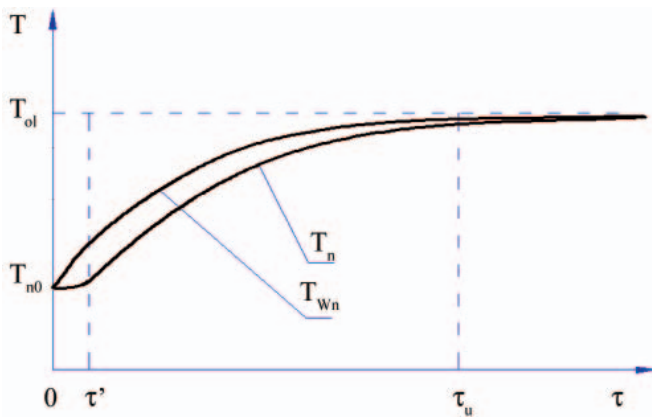


Fig. 7. Time-histories of temperature changes in heated fixed elements. Within time interval from $\tau = 0$ to $\tau = \tau'$ disordered heat transfer takes place, while the interval $\tau = \tau'$ to $\tau = \tau_u$ is characterised by well-ordered unsteady state, and above $\tau = \tau_u$ – by steady state. T_{n0} is the initial temperature of the fixed element

Some quantities in Formula (32), such as masses and heat transfer surfaces of component elements, and specific heats of materials, are known, while the others are to be determined experimentally. The results of experimental tests make the basis for determining the heat transfer coefficient α_{wn} and the coefficient ψ_n of non-uniform temperature distribution in component elements.

The flux $\dot{\Phi}_z$ of the energy passed to the environment, described by Equation (32), has been neglected. The thermal energy passed to the environment during the start-up time is small, as the outer temperature of the component is approximately equal to the ambient temperature $T_z(\tau) \approx T_{ot} \rightarrow \dot{\Phi}_z \approx 0$.

After some transformations of Equation (32) we get for fixed elements:

$$m_n \cdot c_n \frac{dT_n}{d\tau} = \alpha_{wn} \cdot F_{wn} \cdot (T_{ol} - T_n) \cdot \psi_n \quad (33)$$

Equation 33 can be rewritten to the form:

$$\frac{dT_n}{T_{ol} - T_n} = \frac{\alpha_{wn} \cdot F_{wn} \cdot \psi_n}{m_n \cdot c_n} d\tau \quad (34)$$

where:

$$\sigma_n = \frac{\alpha_{wn} \cdot F_{wn} \cdot \psi_n}{m_n \cdot c_n} \quad (35)$$

is the rate of heating of fixed component elements.

After relevant transformations of Equation 34 and introduction of relation 35 we arrive at:

$$\frac{d(T_{ol} - T_n)}{(T_{ol} - T_n)} = -\sigma_n \cdot d\tau \quad (36)$$

After integrating we get:

$$T_{ol} - T_n = (T_{ol} - T_{ot})e^{-\sigma_n \cdot \tau} \quad (37)$$

Having known the initial conditions: oil temperature T_{ol} , ambient temperature T_{ot} and the rate of heating of fixed elements σ_n we can calculate the temperature time-history $T_n(\tau)$:

$$T_n(\tau) = T_{ol} - (T_{ol} - T_{ot})e^{-\sigma_n \cdot \tau} \quad (38)$$

In the analytical method the rate of heating of fixed elements can be determined from Equation 35.

Temperature time-histories $T_r(\tau)$ of mobile component elements can be calculated based on the initial conditions (T_{ol} , T_{ot}) and the rate of heating of mobile elements σ_r :

$$T_r(\tau) = T_{ol} - (T_{ol} - T_{ot})e^{-\sigma_r \cdot \tau} \quad (39)$$

The rate of heating of a mobile element of the hydraulic component can be calculated from the relation:

$$\sigma_r = \frac{\alpha_{wr} \cdot F_{wr} \cdot \psi_r}{m_r \cdot c_r} \quad (40)$$

where:

- α_{wr} – heat transfer coefficient between oil and mobile element
- F_{wr} – area of heat transfer of mobile element
- m_r – mass of mobile element
- c_r – specific heat of mobile element
- ψ_r – coefficient of non-uniform temperature distribution in mobile element.

The rate of heating eg. of fixed elements of the hydraulic component can be established experimentally having known current values of the temperature differences ϑ_{n1} and ϑ_{n2} for times τ_1 and τ_2 [13]:

$$\sigma_n = \frac{\ln \vartheta_{n1} - \ln \vartheta_{n2}}{\tau_2 - \tau_1} \quad (41)$$

The rate of heating of an element can be more precisely determined by measurements of more temperature differences and corresponding time moments, and by making a semi-logarithm diagram. In Fig. 8, of coordinates $\ln \vartheta$ and time τ , time-history of temperature difference is presented using the straight line equation $y = ax + b$, where a is the slope of this line and represents the rate of heating σ ($\sigma = -a$).

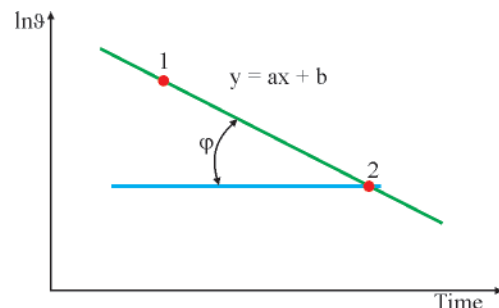


Fig. 8. Determining the rate of heating

Calculating coefficients of non-uniform temperature distribution in hydraulic component elements

The coefficients of non-uniform temperature distribution ψ_r , ψ_n in component elements (Equations 35, 40) can be determined using the relations given by Kondratev [1, 3, 7, 8].

The coefficient ψ depends on the Biot number (Bi):

$$\psi = 1 - 0.73 \cdot \xi^2 \quad (42)$$

where:

$$\xi = \frac{p}{p_\infty} - \text{critical number} \quad (43)$$

The critical number p can be calculated from the formula ($Bi < 1$):

$$p^2 = \frac{L_0}{l} \cdot Bi \quad (44)$$

where:

L_0 – characteristic dimension defining the body, for instance: wall thickness, radius of a cylinder or a sphere

$l = V/F_w$ – linear dimension of a body as the ratio of its volume V to heat transfer surface F_w .

The value of the number p_∞ for fixed elements of hydraulic components can be roughly estimated based on a selected characteristic element having the shape of a plate or cylinder. For the plate the value of the number p_∞ is equal to $p_{\infty pl} = \pi/2$, while for a cylinder - $p_{\infty wa} = 2.4$ [1, 3, 7, 8].

For an arbitrary fixed element of the hydraulic component, the critical number can be assumed from between those for a plate and a cylinder. The averaged value of the critical number for the fixed element is equal to $\frac{p_{\infty wa} + p_{\infty pl}}{2} = p_\infty \cong 2$.

Calculating heat transfer coefficients between oil and surface of the hydraulic component elements

Calculating the heat transfer coefficients between the oil and the surfaces of component elements requires the following data: heat transfer area, mass of the element, specific heat of the element, coefficient of non-uniform temperature distribution in the element, and the rate of heating of the element.

Using Equations (35), (40), the heat transfer coefficients α_n , α_r between the oil and the surfaces of fixed and mobile elements of hydraulic components were calculated, among others, for: proportional spool valve PVG 32 made by Sauer Danfoss (Fig. 9), satellite motor SOK 100 made by Hydroster (Fig. 10).

Determining serviceability of the proportional spool valve PVG 32 with the aid of the analytical method

Proportional spool valves PVG 32 [5] are used in various hydraulic systems. They can consist of up to twelve sections. Using the analytical method we can determine the serviceability of the spool valve working in thermal shock conditions.

In order to determine the average temperatures of the heated elements in the spool valve PVG32 in thermal shock conditions, relations (38, 39), we should know the rate of heating of those elements. This quantity can be determined from formula (35). The required heat transfer coefficient can be determined from curves shown in Fig. 9.

One experimental test of the spool valve PVG 32 was done for the following initial conditions: spool valve temperature -10°C , oil temperature 37°C , and flow rate $39\text{ dm}^3/\text{min}$. Based on those data the equations were obtained to describe time-histories of:

a) spool temperature, $T_s(\tau)$:

$$T_s(\tau) = 37 - 47e^{-0.106\tau} [^\circ\text{C}] \quad (45)$$

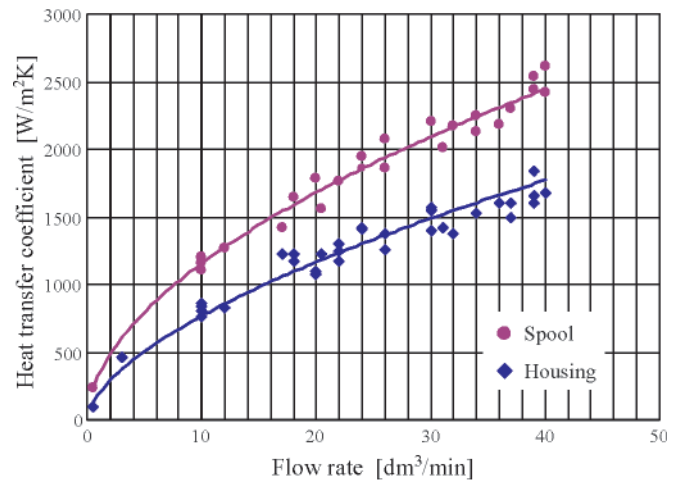


Fig. 9. Heat transfer coefficients between oil and surfaces of spool and housing of proportional spool valve PVG 32 vs. flow rate

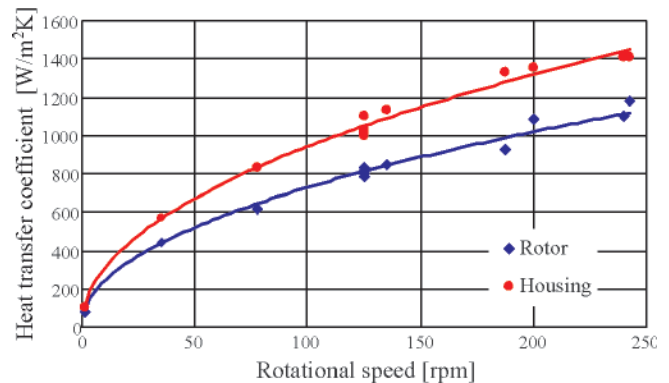


Fig. 10. Heat transfer coefficients between oil and surfaces of rotor and housing of satellite motor SOK 100 vs. rotational speed

b) housing temperature, $T_K(\tau)$:

$$T_K(\tau) = 37 - 47e^{-0.0105\tau} [^\circ\text{C}] \quad (46)$$

The heating rates in Equations (45) and (46) were determined experimentally.

The temperature time-histories calculated using those formulas for the spool and the housing are close to those obtained from experimental tests (Fig. 11).

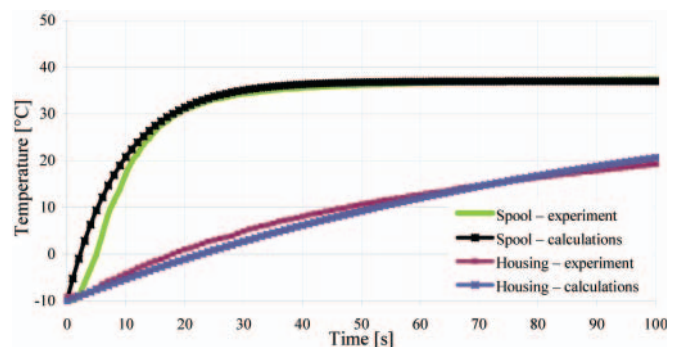


Fig. 11. Temperature time-histories of the spool and housing in spool valve PVG 32 obtained from experimental tests and calculated for initial conditions: spool valve temperature -10°C , oil temperature 37°C , flow rate $39\text{ dm}^3/\text{min}$

The equation of the clearance time-history between the spool and the housing during the spool valve start-up has the following form:

$$l_{suw} = l_m - \beta_s \cdot h_s \cdot [T_s(\tau) - T_0] + \beta_K \cdot h_K \cdot [T_K(\tau) - T_0] \quad (47)$$

After placing relations (38) and (39) into Equation 47 we get:

$$l_{suw} = l_m - \beta_S \cdot h_S \cdot [T_{ol} - (T_{ol} - T_{ot})e^{-\sigma_S \cdot \tau} - T_0] + \beta_K \cdot h_K \cdot [T_{ol} - (T_{ol} - T_{ot})e^{-\sigma_K \cdot \tau} - T_0] \quad (48)$$

where:

- S – spool
- K – housing.

Effective clearance changes between the spool and the housing having the nominal dimension $h \approx h_S \approx h_K$ is given by the relation:

$$l_{suw} = l_m + h \cdot [(\beta_K - \beta_S) \cdot (T_{ol} - T_0) + (T_{ol} - T_{ot})(\beta_S \cdot e^{-\sigma_S \cdot \tau} - \beta_K \cdot e^{-\sigma_K \cdot \tau})] \quad (49)$$

For instance, the equation of the effective clearance time-history between the spool and the housing in the single-section spool valve PVG 32 during the start-up from initial conditions: spool valve temperature -10 °C, oil temperature 37 °C, flow rate 39 dm³/min, heating rates (experimentally determined) for the spool $\sigma_S = 0.106$ [1/s] and housing $\sigma_K = 0.0105$ [1/s], and the clearance 7 μm, can be written as:

$$l_{suw} = 7 + 0.018 \cdot [-8.5 + 47 \cdot (11 \cdot e^{-0.106 \tau} - 10.5 \cdot e^{-0.0105 \tau})] \quad [\mu\text{m}] \quad (50)$$

It results from the characteristics determined with the aid of formula (50) and given in Fig 12, that for from these start-up conditions incorrect spool valve operation will not take place as the minimum clearance for $\Delta T_{ol-ot} = 47$ K is equal to 0.7 μm.

Permissible parameters of the hot oil supplied to the cold spool valve at which the correct valve operation will take place can be calculated. By increasing, in the theoretical analysis, the oil temperature in Equation (49) we get the characteristics of effective clearance changes for increasing temperature differences between the oil and spool valve, (Fig. 12).

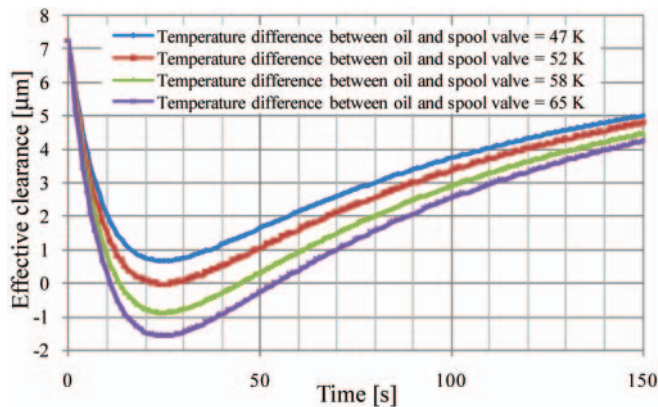


Fig. 12. Time-history of effective clearance between spool and housing in spool valve PVG 32 for initial conditions: spool valve temperatures -10 °C, oil temperature 37, 42, 48, 55 °C, flow rate 39 dm³/min

When the initial temperature difference between the oil and the spool valve is equal to 52 K, the effective clearance will temporarily totally disappear at 25th second (Fig. 12).

When the temperature difference is 65 K (Fig. 12), clearance disappearance and the incorrect operation of the spool valve will be observed between second 12 and 55.

The clearance changes calculated using the analytical method are very close to those obtained from the experiment.

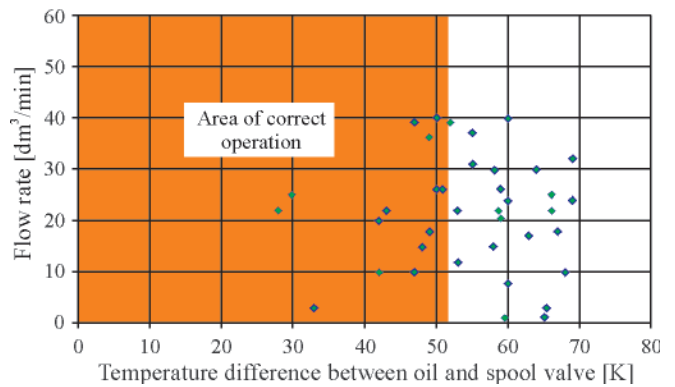


Fig. 13. Areas of parameters of correct and incorrect operation of spool valve PVG 32 with clearance 7 μm

When the temperature difference between the oil and the valve exceeds 52 K, the spool valve PVG32 operates incorrectly in thermal shock conditions (Fig. 13). Here, the calculated results are in full agreement with the experimental tests. In those tests faulty operation of the spool valve was observed when the temperature difference between the oil and the spool valve was larger than 54 K.

Characteristics of the computer simulation method

The computer simulation method for determining the serviceability of hydraulic components in thermal shock conditions makes use of computed temperature distributions in hydraulic component elements. These temperature distributions make it possible to calculate the effective clearance between cooperating component elements using relation (25).

Computing the effective clearances during the component start-up requires the following input data: initial temperature of the component, oil temperature and heat transfer coefficient (stepwise flow rate).

When deciding to solve this task, the author had to select a relevant numerical method.

There are a number of basic numerical codes which make use of the finite element method FEM [3, 6, 9, 10, 11], including: NASTRAN, ABAQUS, ANSYS, COSMOS/M and others.

The numerical calculations of temperature distributions were performed for a number of hydraulic components, including: satellite motors SOK 100 and SOK 1600 made by Hydroster, orbital motor GMR 160 made by Rexroth [3], axial piston pump PWK 27 made by Hydrotor, axial piston pump PV 16 made by Parker, gear pump PZ-2-K-6,3 made by Hydrotor, orbital motor TF 170 made by Parker, radial piston motor MR1000 made by Parker, gear motor PZ-2-K-10 made by Hydrotor, hydraulic cylinder CJ2F-50/28/250 made by Stalko, spool valve RE2510/101 made by Hydrotor, proportional spool valve PVG 32 made by Sauer Danfoss, and hydraulic servovalve 4WS2EM10 - 45/20 made by Rexroth.

Along with temperature distributions, the numerical calculations also produced the time-histories of average temperatures in component elements.

Comparing the numerical results with those obtained from experimental tests has made it possible to conclude that the time-histories of average temperatures of the examined elements are very close to each other.

SUMMARY AND CONCLUSIONS

The summary and conclusions concerning methods used for determining permissible start-up parameters for hydraulic components in low ambient temperatures is given below:

- A basic design factor, deciding about permissible start-up parameters of a hydraulic component in thermal shock conditions, is the effective clearance which defines dimensions of the clearances between the surfaces of the cooperating elements. The effective clearance can be calculated for an arbitrary component based on temperature time-histories of its mobile and fixed elements. If the effective clearance is positive, the component will work faultlessly.
- There are three methods of determining parameters for faultless start-up of the hydraulic component in low ambient temperatures, which are: the experimental method, the analytical method, and the computer simulation method.
- Using the analytical method we can determine the area of correct operation of an arbitrary not loaded hydraulic component during its start-up in thermal shock conditions, depending on the oil flow rate and the temperature difference $\Delta T_{ol-ot} = (T_{ol} - T_{ot})$ between the oil and the environment, according to the following inequality:

$$l_m - h \cdot [(T_{ol} - T_0) \cdot (\beta_r - \beta_n) + (T_{ol} - T_{ot}) \cdot (\beta_n \cdot e^{-\sigma_n \tau} - \beta_r \cdot e^{-\sigma_r \tau})] > 0 \quad (51)$$

The variables in this inequality are: the oil temperature T_{ol} , the ambient temperature T_{ot} and the rates of heating σ_r , σ_n , of mobile and fixed elements. The rates of element heating σ , mainly depend on the average flow velocity of the fluid supplying the hydraulic component.

- The heat transfer coefficient between the oil and the mobile and fixed component elements depends on the average oil flow velocity. The author determined its values experimentally.
- The analytical method of determining faultless component operation can be used in engineering practice. Using this method the area of correct operation of a hydraulic component can be determined with high accuracy.
- The computer simulation method makes it possible to assess the serviceability of the component during its start-up in thermal shock conditions with higher accuracy than the analytical method. The computer simulation method base on the finite element method (FEM) for determining temperature fields in component elements.

The application of the computer simulation method for determining the process of elements heating and the serviceability of hydraulic components will be presented in Part 4 of the article.

BIBLIOGRAPHY

1. Balawender A.: *Energy analysis and methodology of examination of low-speed hydraulic motors* (in Polish). Zeszyty naukowe PG. Gdańsk 1988
2. Balawender A., Bieńkowski A.: *Examining motors SOK 160 in thermal shock conditions*. Report on stage IV of Agreement 780106 commissioned by ZUO Hydroster in Gdansk (in Polish); Gdansk 1981
3. Jasiński R.: *Operation of low-speed hydraulic motors in thermal shock conditions* (in Polish). PhD thesis, supervisor: A. Balawender. Gdańsk 2002
4. Jasiński R.: *Problems of the starting and operating of hydraulic units and systems in low ambient temperature (Part 1)*, Polish Maritime Research 4/2008
5. Jasiński R.: *Problems of the starting and operating of hydraulic units and systems in low ambient temperature (Part 2), Determining the clearance between cooperating elements during the hydraulic components start-up in extremely low ambient temperatures on the ground of experimental research*, Polish Maritime Research 1/2009
6. Kleiber M.: *Introduction to the finite element method* (in Polish); Państwowe Wydawnictwo Naukowe, Warszawa-Poznań 1989
7. Kondrat'ev G.M.: *Regularnej teplovej rezim*. Moskwa: Gosud. Izdat. Tech. Teoret. Literat. 1954
8. Kondrat'ev G.M.: *Teplovyje izmerenija*. Moskwa: Gosud. Nauczno-Tech. Izdat. Maszinost. 1957
9. Kruszewski J., collective work: *Finite element method in dynamics of structures* (in Polish); Arkady, Warsaw 1984
10. Rusiński E.: *Finite Element Method. System COSMOS/M* (in Polish). Wydawnictwa Komunikacji i Łączności, Warszawa 1994
11. Rusiński E., Czmochocki J., Smoliński T.: *Advanced finite element method in supporting structures* (in Polish)
12. Szargut J.: *Numerical modelling of temperature fields* (in Polish). Wydawnictwo Naukowo-Techniczne, Warszawa 1992
13. Wiśniewski S., Wiśniewski T.: *Heat transfer* (in Polish). Wydawnictwo Naukowo-Techniczne, Warszawa 2000.

CONTACT WITH THE AUTHOR

Ryszard Jasiński, Ph. D.
Faculty of Mechanical Engineering
Gdansk University of Technology
Narutowicza 11/12
80-952 Gdansk, POLAND
e-mail: rjasinsk@pg.gda.pl

Optimization of transformation of measurements of ship hull blocks

Aleksander Kniat, Ph. D.
Gdansk University of Technology

ABSTRACT



The paper presents an analysis of measurements taken on ship hull blocks to assess their feasibility for the final stage of assembly in a dry dock or on a slipway. The analysis requires first to check if blocks were manufactured within tolerances assumed in design and then to compare if two neighbouring blocks can be joined to each other. As each block is measured in a different coordinate system it is necessary to make transformations and bring results to a common CAD model without loss of accuracy. An algorithm for optimizing the transformation process to obtain better results, is proposed. The optimization is aimed at minimizing the sum of distances between transformed points and corresponding points in a CAD model. Description of the optimization method and example of its application is also presented. The problem of transformation of measurements or coordinate systems is more general as it can be found, apart from shipbuilding, e.g. in civil engineering, cartography, robot control, pattern recognition, medical imaging.

Keywords: co-ordinate system transformation; ship hull measurements;
ship hull assembly; computer aided design (CAD)

INTRODUCTION

The dimension control of pre-fabricated hull structural units and blocks is very important in the process of building ship's hull. It is crucial for the shipyard to be sure that units and blocks being brought to a dry dock or slipway have dimensions within assumed tolerances and that they do not require corrections as the time necessary to join them should be as short as possible. Corrections of units and blocks, conducted outside workshop where they have been manufactured, are very time consuming. Moreover it slows down the final hull assembly which is usually a bottleneck in every shipyard production process.

Two comparisons should be done to check dimensions of the units and blocks. It is first necessary to check if the dimensions are within design tolerances. If yes, then two neighbouring blocks should be checked against each other to know where differences occur and of what size they are. This information may influence the way in which the neighbouring units and blocks are joined.

Prefabricated elements are usually measured by means of modern laser-optic instruments. Results of the measurements are presented as a set of coordinates of points in three dimensional space. To verify the dimensions it is necessary to compare location of measured points with a CAD model. Thus the measured points must be brought to the CAD model coordinate system. This requires an isometric transformation of the measurement results to be performed. Usually such transformation is done intuitively by an experienced specialist

who checks the dimensions. To avoid human errors and make the process faster an algorithm intended to be implemented as a computer program and hence to solve the problem, is proposed.

MEASUREMENTS – ACCURACY, DIFFICULTIES

Measurements must be done with proper accuracy. Accuracy is one of the main characteristics of measuring instrument. Only measurements taken with the use of a proper accuracy instrument may be further analyzed. Unfortunately most popular instruments used in land surveys or at construction sites are not precise enough for shipbuilding purposes.

Measurements of ship's hull units and blocks are difficult. There are two main reasons of the difficulties. The first reason is location of measured points within unit or block. Measured points are usually not located at the edges, but inside and they are hidden behind stiffeners, longitudinal or transverse elements. The second reason is position of a given unit or block against its neighbourhood. Prefabricated units and blocks are often stored close to each other as shown in Fig. 2, because of limited space in shipyard. In such cases certain measurement points may be accessible only from one side of a unit or block and the rest from the other side. Taking direct measurements is rather impossible in narrow gaps between units and blocks or in hidden locations therefore additional techniques must be applied. It is very important not to lose

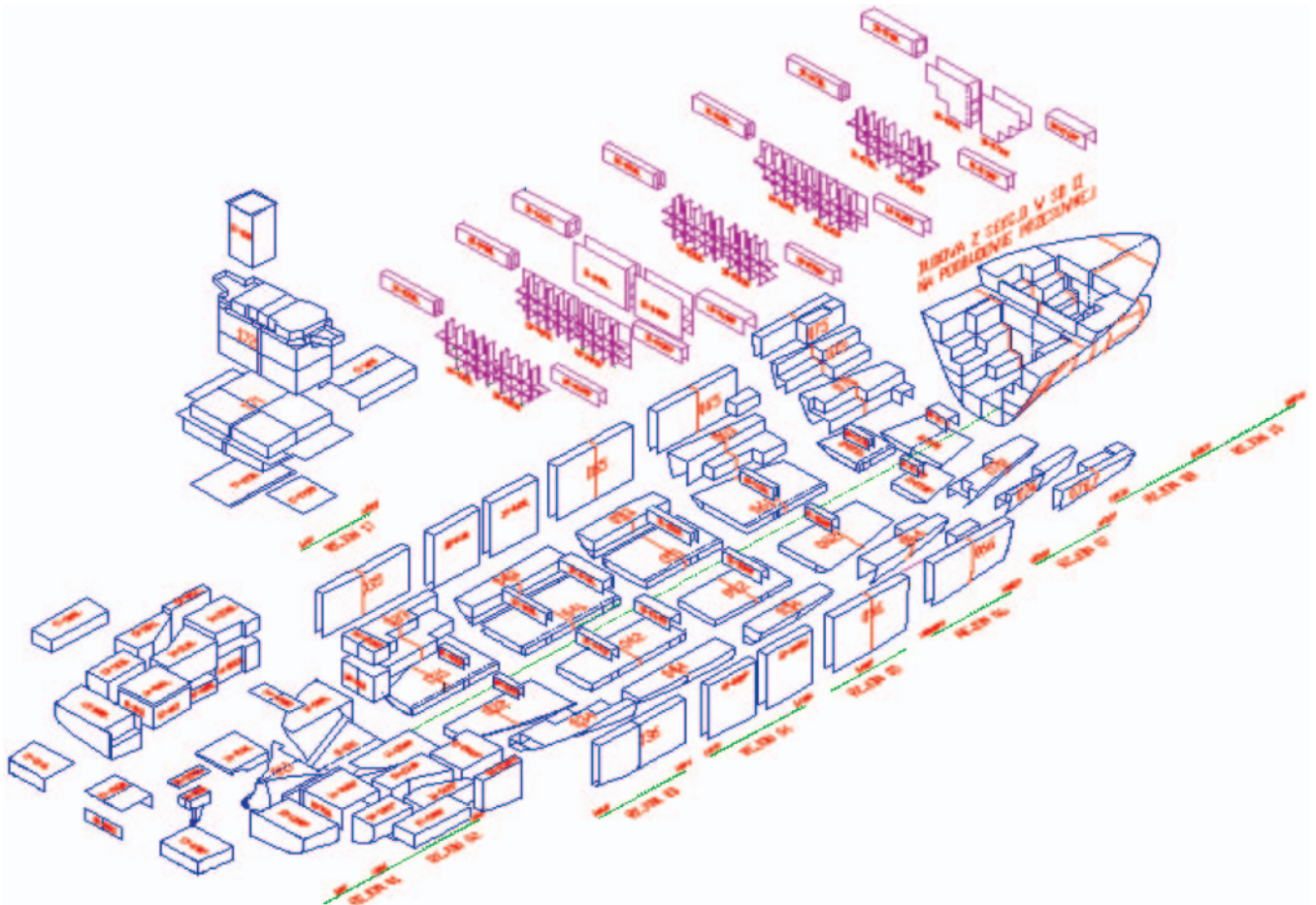


Fig. 1. Units and blocks of ship's hull in an exploded view

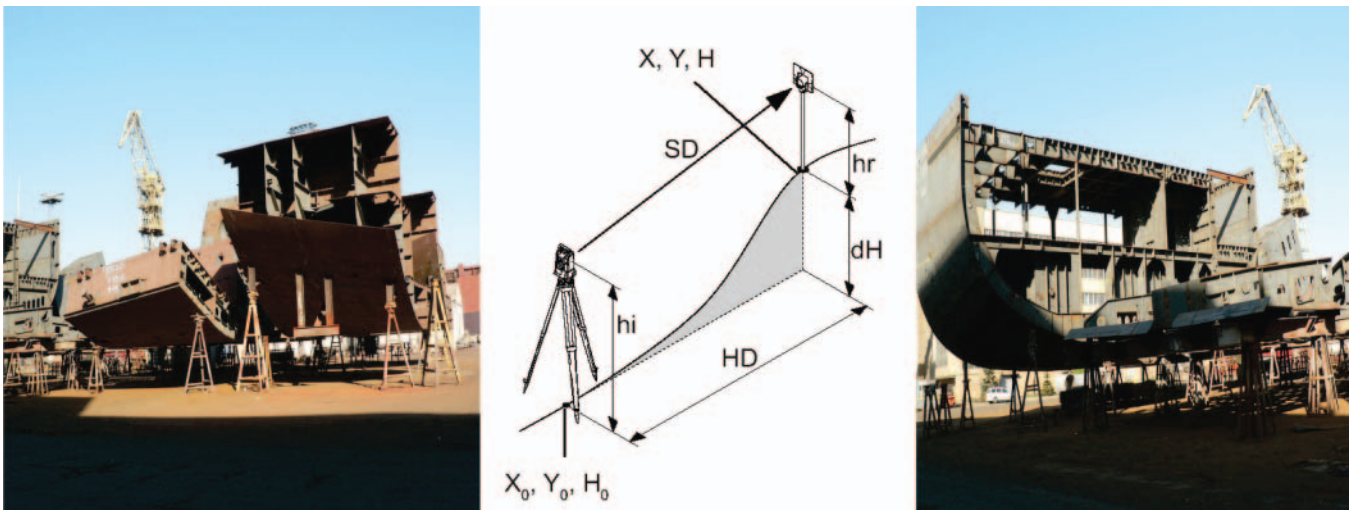


Fig. 2. Prefabricated ship's hull units and blocks in positions in which they are measured

accuracy while applying the techniques because it may lead to incorrect results.

If one unit or block is measured from different positions it is also very important to properly relate both series of measurements to each other. It is achieved either by choosing certain points common for both series of measurements or by establishing a common coordinate system with the use of measuring instrument functions.

There are many different measuring techniques, e.g. with application of visible laser, invisible laser, with reflector, without reflector, automatic search, scanning etc. Each of them has its advantages and disadvantages. However the

problem is not discussed in this paper. Attention is focused on transforming results of measurements to assess if prefabricated units and blocks are suitable for further assembly. It is assumed that measurements are taken with a satisfying accuracy.

TRANSFORMATION OF MEASUREMENTS

Measurements of each unit or block are taken in different coordinate systems. The coordinate system is arranged according to local situation where the measurements are taken. All measured points have corresponding points in the design and in the other unit or block with which it will be

joined. Therefore the transformation is constrained by the following:

- it must keep distances between measured points within a unit or block,
- it must not lose accuracy.

The purpose of the transformation is to obtain the best fit between measured points and points taken from CAD model or the other unit or block. In other words, the transformation of measurement results is aimed at minimization of the sum of distances between corresponding points.

The problem of transformation of measurements is very similar to the shape recognition or pattern recognition problem. In the shape recognition problem, however, we search for transformation of one set of points to best fit to the other set of points in situation we do not know if the two sets of points correspond to each other. Results of the best transformation show how much similar the two sets of points are. In the case of question we know that points in the two sets correspond to each other and we search for an optimum transformation.

Shape recognition problem

Shape recognition is a well known problem. In most general form its definition is as follows:

Definition 1

Given two sets of points $A \{a_1, a_2, a_3, \dots, a_k\}$ and $C \{c_1, c_2, c_3, \dots, c_m\}$ in d -dimensional space, where k is not necessarily equal to m , find the similarity transformation parameters giving the minimum value of the squared distance between corresponding points in these two point sets.

Since the 1980s different solutions of the problem were described in many sources e.g. [1, 2, 3, 5, 7, 8, 9, 10].

There are several kinds of the problem depending on:

- known/unknown correspondence between points in the two sets
- equal/unequal number of points in the two sets (phantom points)
- only distance preserving transformation allowed/scaling transformation allowed.

Flick & Jones [5] give a very general formulation of a d -dimension to d -dimension mapping problem with the possibility of omission, phantom and unknown transformation. Their basic idea is to write down the probability equation for the image based on a given object by all the possible matchings, and then to find the best parameters and the best matching by using the maximum probability principle. However, due to the large number of parameters in the equation and the computational complexity in doing all the possible matchings, a solution is generally intractable unless the number of points is small.

When the correspondences between the point sets are unknown a priori a popular approach to solving the problem is the class of algorithms based on the Iterated Closest Point (ICP) technique introduced by Besl [3] and Zhang [11]. ICP is attractive because of its simplicity and performance. Although the initial estimate does need to be reasonably good, the algorithm converges relatively quickly.

Arun *et al.* [1] address the „absolute orientation problem” of finding the least squares solution of a rotation and translation of rigid body transformation. The algorithm [1] sometimes gives a reflection instead of rotation transformation. Umeyama [10] presents a refinement to [1] that always gives a correct rotation matrix and also handles scaling transformation.

Ramos & Verriest [9] point out that while [10] returns a correct rotation in the degenerate cases where [1] fails, it does so at the expense of larger fitting errors. Ramos & Verriest [9] propose a method based on a mixed least squares - total least squares solution, assuming noises to be present in both point series to be fitted. The methods presented in [1, 9, 10] have the disadvantage of requiring both data sets to have the same number of points, and that the point-to-point correspondence is known a priori. On the contrary, Goodrich *et al.* [6] solve the „approximate geometric pattern matching problem”, based on the approximate minimizing of the direct Hausdorff distance from the pattern set to the background set, conducted by using rigid body transformation. The point sets can be of different size and the point-to-point correspondence is not assumed.

Definition of measurement transformation problem

The problem of measurement transformation is a special case of shape recognition problem. In the case in question we assume that the correspondence between the points in the sets is known exactly and the scaling when transforming one set of points into the other, is not allowed. Formal definition of the problem is as follows:

Definition 2

Given two sets of points $A \{a_1, a_2, a_3, \dots, a_k\}$ and $C \{c_1, c_2, c_3, \dots, c_k\}$, we search for isometric transformation of points in the set A which produces minimum sum of distances with corresponding points in the set C . We assume that each point of the set A has exactly one corresponding point in the set C and each point of the set C has exactly one corresponding point in the set A . Points are labelled and their coordinates in 3-dimensional space are known.

For us, isometric transformation is a composition of translations and rotations. We do not allow symmetry (mirror) which is also isometric transformation. Formula (1) defines isometric transformation matrix \mathbf{I} which depends on six parameters: x, y, z - coordinates of translation and χ, β, α - angles of rotation about X, Y and Z axes.

$$\mathbf{I}(x, y, z, \chi, \beta, \alpha) = \mathbf{T}(x, y, z) \cdot \mathbf{R}(\chi, \beta, \alpha) \quad (1)$$

OPTIMIZATION OF MEASUREMENT TRANSFORMATION

According to *Definition 2* given in the previous paragraph, we must define criterion function for the measurement transformation problem. We assume distance to be the metrics in 3-dimensional space. The square of the distance is also a metrics and it is less complicated for calculation hence the criterion function is presented in the form of the formula (2).

$$f = \sum_{i=1}^k (\|c_i - a_i\|_2)^2 \quad (2)$$

where:

k - number of points in the set C and the set A

Since we transform a_i points with isometric transformation matrix $\mathbf{I}(x, y, z, \chi, \beta, \alpha)$ our criterion function depends on six decision variables as presented in formula (3).

$$f(x, y, z, \chi, \beta, \alpha) = \sum_{i=1}^k (\|c_i - \mathbf{I}(x, y, z, \chi, \beta, \alpha) \cdot a_i\|_2)^2 \quad (3)$$

By using the criterion function (3) it is possible to calculate an approximate value of the sum of distances between

corresponding points in the set **C** and transformed points in the set **A**. The aim is to find such values of the decision variables x, y, z and χ, β, α , which produce the minimum result of the criterion function (3).

Other possible optimization criteria and constraints

Measurement results of sections and blocks are transformed and analyzed to assess if sections and blocks can be joined together. Minimum sum of distances between points on seams on both joined sections or blocks is the most obvious criterion but not the only one to be used. While building the ship's hull it is crucial to keep decks planar and adjusted to axes. A measure of how coplanar or how coaxial the sections and blocks are, might also be used as an optimization criterion. Alternatively, it can be used as a constraint, hence only these transformations which yield coplanar and coaxial results within certain tolerance, are accepted.

Optimization method

There are many methods to minimize function (3). Briefly, they can be divided into two categories: deterministic and probabilistic. Deterministic methods are proven to find a solution when optimized function has certain properties. Not all functions conform to restrictions of deterministic methods.

In our case the criterion function (3) is well defined. To find the minimum for the function (3) we use a deterministic method – the Newton's method described by the formula (4).

$$\mathbf{x}_{n+1} = \mathbf{x}_n - \mathbf{H}^{-1} \cdot \mathbf{g} \quad (4)$$

where:

\mathbf{x} - a vector of decision variables.

This is an iterative method described by Bjorck & Dahlquist in [4], which requires calculation of the gradient \mathbf{g} and Hessian matrices \mathbf{H} of the function (3). To start, we assume some initial values of the vector of decision variables \mathbf{x}_n and calculate next values of the vector of decision variables \mathbf{x}_{n+1} . In each step we receive values of decision variables, which produce smaller result of the function (3). The advantage of the Newton's method is a quick convergence and stability.

Point - to - point correspondence

In case of measurement analysis, exactly one measured point must correspond to exactly one point in a CAD model or located on the other section or block. The one- to- one- point correspondence is a very fundamental assumption. This is so

important, because in contrast to the shape recognition problem, it is not the aim to check whether the point sets resemble each other, which is always true, but to precisely state the minor differences between point sets. In case of shape recognition, it is a perfect match if the two patterns of size of about 10 meters have distances between corresponding points of about 30 mm. In case of measurement transformation it is of a great importance if to minimize this distance from 30 mm to 10 mm, is possible at all.

Labels in point sets allow to control the correspondence between points in the two sets. Assigning labels is time consuming, but prevents from mirror matchings. As the constructions in question are usually symmetric, sometimes about two axes, it is quite easy to lose orientation without a proper labelling. The labelling also prevents from matching sections or blocks which are similar in shape but are not to be joined. Clear labelling system of measured points helps in storing and retrieving measurement results.

Application example results

The above described method was implemented in a program used for visualization and checking of measurements of ship's hull units and blocks. Measurements of two neighbouring sections of a ship's double bottom were taken as an example. Fig. 3 shows a view of both sections.

Tab.1 presents comparison of measured points and points from CAD model of the portside section, where measurement transformation was done by intuition. Tab. 2 presents the same comparison, but the transformation was optimized by the program.

Tab. 3 presents comparison of measured points and points from CAD model of the starboard section, where measurement transformation was done by intuition. Tab. 4 presents the same comparison, but transformation was optimized by the program.

In both cases the optimized transformation is better. In the case of the portside section the sum of distances is only slightly smaller and the maximum distance between points decreased from 19,36 mm to 17,50 mm. In the case of the starboard section the difference is more significant. The sum of distances is two times smaller and the maximum distance decreased from 30,05 mm to 17,21 mm.

DIRECTIONS OF FUTURE RESEARCH

Further research investigations are expected to be conducted in two main directions: the automatic recognition of measured points and the automatic selection of points to be measured. The

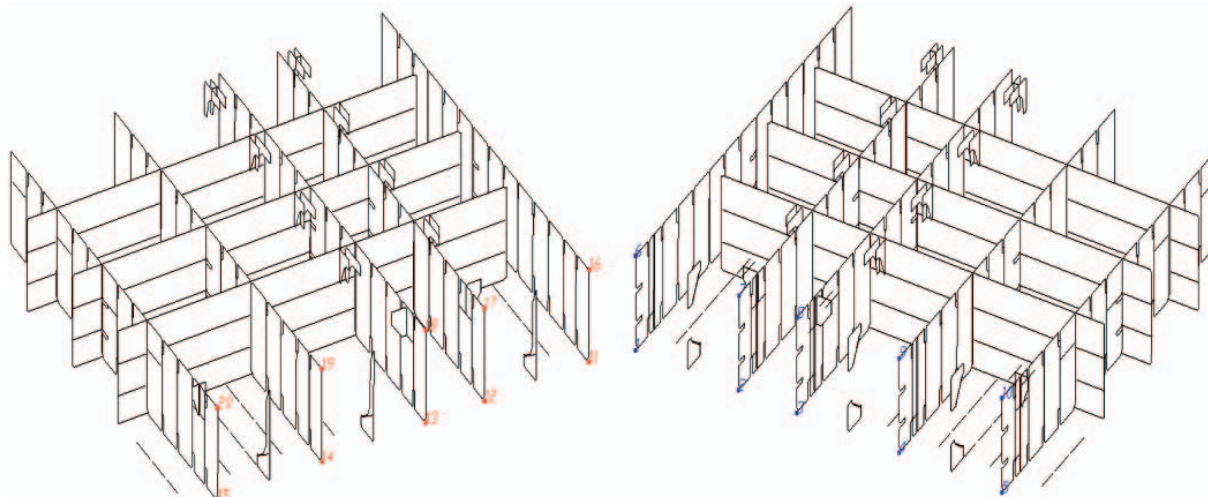


Fig. 3. Neighbouring sections of a ship's hull double bottom with measured points marked with numbers

Tab. 1. Comparison of measured points and points from CAD model of the portside section – intuitive transformation

CAD model points				Transformed measured points				Comparison			
Label	X	Y	Z	Label	X	Y	Z	dX	dY	dZ	dist
101	133400	0	0	01	133413.87	0.00	0.00	-13.87	0.00	0.00	13.87
102	130200	0	0	02	130194.79	1.10	0.18	5.21	-1.10	-0.18	5.32
103	128400	0	0	03	128384.61	0.68	2.49	15.39	-0.68	-2.49	15.60
104	125200	0	0	04	125202.71	0.00	3.83	-2.71	0.00	-3.83	4.69
105	122000	0	0	05	122000.00	0.00	0.00	0.00	0.00	0.00	0.00
106	133400	0	1950	06	133409.37	15.59	1944.57	-9.37	-15.59	5.43	18.98
107	130200	0	1950	07	130192.01	0.54	1950.39	7.99	-0.54	-0.39	8.02
108	128400	0	1950	08	128380.91	0.16	1953.21	19.09	-0.16	-3.21	19.36
109	125200	0	1950	09	125195.10	-0.51	1950.17	4.90	0.51	-0.17	4.93
110	122000	0	1950	10	121995.62	0.00	1951.82	4.38	0.00	-1.82	4.74
Sum of dist											95.51

Tab. 2. Comparison of measured points and points from CAD model of the portside section – optimized transformation

CAD model points				Transformed measured points				Comparison			
Label	X	Y	Z	Label	X	Y	Z	dX	dY	dZ	dist
101	133400	0	0	01	133417.11	-3.66	0.15	-17.11	3.66	-0.15	17.50
102	130200	0	0	02	130198.04	-0.65	-0.14	1.96	0.65	0.14	2.07
103	128400	0	0	03	128387.86	0.00	1.90	12.14	0.00	-1.90	12.29
104	125200	0	0	04	125205.95	1.21	2.77	-5.95	-1.21	-2.77	6.67
105	122000	0	0	05	122003.24	3.11	-1.52	-3.24	-3.11	1.52	4.74
106	133400	0	1950	06	133412.34	9.14	1944.74	-12.34	-9.14	5.26	16.23
107	130200	0	1950	07	130194.97	-4.02	1950.07	5.03	4.02	-0.07	6.44
108	128400	0	1950	08	128383.87	-3.32	1952.62	16.13	3.32	-2.62	16.68
109	125200	0	1950	09	125198.06	-2.10	1949.11	1.94	2.10	0.89	3.00
110	122000	0	1950	10	121998.57	0.30	1950.29	1.43	-0.30	-0.29	1.49
Sum of dist											87.11

Tab. 3. Comparison of measured points and points from CAD model of the starboard section – intuitive transformation

CAD model points				Transformed measured points				Comparison			
Label	X	Y	Z	Label	X	Y	Z	dX	dY	dZ	dist
111	133400	0	0	11	133400.00	0.00	0.00	0.00	0.00	0.00	0.00
112	130200	0	0	12	130185.96	-0.76	-2.74	14.04	0.76	2.74	14.33
113	128400	0	0	13	128375.40	-1.28	-0.42	24.60	1.28	0.42	24.64
114	125200	0	0	14	125186.42	-2.56	-0.45	13.58	2.56	0.45	13.83
115	122000	0	0	15	121986.27	0.00	0.00	13.73	0.00	0.00	13.73
116	133400	0	1950	16	133401.79	0.00	1948.05	-1.79	0.00	1.95	2.65
117	130200	0	1950	17	130178.92	2.05	1945.82	21.08	-2.05	4.18	21.58
118	128400	0	1950	18	128370.33	3.71	1947.05	29.67	-3.71	2.95	30.05
119	125200	0	1950	19	125180.79	0.43	1949.68	19.21	-0.43	0.32	19.21
120	122000	0	1950	20	121980.13	3.76	1950.81	19.87	-3.76	-0.81	20.24
Sum of dist											160.26

Tab. 4. Comparison of measured points and points from CAD model of the starboard section – optimized transformation

CAD model points				Transformed measured points				Comparison			
Label	X	Y	Z	Label	X	Y	Z	dX	dY	dZ	dist
111	133400	0	0	11	133415.46	-1.34	1.56	-15.46	1.34	-1.56	15.60
112	130200	0	0	12	130201.42	-0.35	-1.38	-1.42	0.35	1.38	2.01
113	128400	0	0	13	128390.86	0.32	0.83	9.14	-0.32	-0.83	9.19
114	125200	0	0	14	125201.88	1.84	0.60	-1.88	-1.84	-0.60	2.70
115	122000	0	0	15	122001.72	-0.47	0.86	-1.72	0.47	-0.86	1.98
116	133400	0	1950	16	133417.13	1.56	1949.62	-17.13	-1.56	0.38	17.21
117	130200	0	1950	17	130194.26	-0.24	1947.19	5.74	0.24	2.81	6.39
118	128400	0	1950	18	128385.67	-1.77	1948.31	14.33	1.77	1.69	14.54
119	125200	0	1950	19	125196.13	1.77	1950.73	3.87	-1.77	-0.73	4.32
120	122000	0	1950	20	121995.47	-1.32	1951.67	4.53	1.32	-1.67	5.01
Sum of dist											78.95

points to be measured are now clearly indicated in measurement instructions which are a part of the workshop design. The points are chosen by designers and production engineers who design techniques of the assembly process.

As the ship hull sections and blocks are manufactured it seems possible to use some new marking method to make the points of interest for measurements distinguishable, e.g. paint of a special kind, magnetic or radio location etc. This way, the time-consuming pointing of each measured point by means of a mirror or a pole, could be omitted.

The automatic selection of measured points requires to have knowledge about construction. In order to choose appropriate points this knowledge should be built into the program which makes decisions instead of a human being. It is difficult but might be possible by applying knowledge engineering and artificial intelligence. The other solution could be obtained by using the scanning of entire section or block. The comparing of entire elements may eliminate choice of points to be measured. However the precise scanning of large elements is a problem. Moreover, sections and blocks in a shipyard are usually stored close to each other or close to other constructions like scaffolding, cranes etc. In such conditions separating scanned element from surroundings is a serious task.

CONCLUSIONS

- Optimization of measurement transformation of ship blocks is very important for the assessment if blocks were manufactured within assumed tolerances and if they can be assembled in a dry dock or on a slipway. The presented method was implemented to the computer program for visualisation and assessment of measurements of ship blocks. Transformation of measurements is done while reading results of measurements in 3-dimensional model of a ship hull. Since the iterative optimization method converges quickly, in about 5 iterations usually, the results are immediate.

The method has the following advantages:

- easy for implementing (derivatives of only trigonometric functions and polynomials)
- quick convergence, immediate results – it requires only a few (about 5) iterations to find a minimum,
- it eliminates analysis of how to align measurement results with a CAD model,
- it eliminates human errors when transforming measurements results into a CAD model.
- The only disadvantage of the method is that it requires exact correspondence between measurement points and CAD model points.
- This method is also assumed to be applied to a possible future research. The transformation of measurements is necessary and not dependent on a way the measured points are selected. From the user point of view, the application of the method which automatically transforms measurements to get the best fit with CAD model, saves time and makes results clear to be assessed.

BIBLIOGRAPHY

1. Arun, K.S. et al.: *Least-squares fitting of two point sets*. IEEE Transactions on Pattern Analysis and Machine Intelligence, Vol. PAMI-9, No. 5, 1987
2. Baird, H. S.: *Model-based image matching using location*. MIT Press, Cambridge, MA, 1985
3. Besl, P.J., & McKay, N.: *A method for registration of 3-D shapes*. IEEE Transactions on Pattern Analysis and Machine Intelligence, Vol. 14 (2), 1992

4. Bjorck, A., & Dahlquist, G.: *Numerical methods*. Prentice-Hall, New Jersey, 1974
5. Flick, T. E., & Jones, L. K.: *A combinational approach for classification of patterns with missing information and random orientation*. IEEE Transactions On Pattern Analysis And Machine Intelligence, Vol. PAMI-8, 1986
6. Goodrich, M.T. et al.: *Approximate geometric pattern matching under rigid motion*. IEEE Transactions on Pattern Analysis and Machine Intelligence, Vol. PAMI-21, No. 4, 1999
7. Griffin, P. M., & Alexopoulos, C.: *Point pattern matching using centroid bounding*. IEEE Transactions on Systems, Man, and Cybernetics, Vol. SMC-19, 1989
8. Lavine D., Lambird B. A., & Kanal L. N.: *Recognition of spatial point patterns*. Pattern Recognition, Vol. 16, 1983
9. Ramos, J.A., & Verriest, E.I.: *Total least squares fitting of two point sets in m-D*. Proceedings of the 36th Conference on Decision and Control, 1997
10. Umeyama, S.: *Least-squares estimation of transformation parameters between two point patterns*. IEEE Transactions on Pattern Analysis and Machine Intelligence, Vol. PAMI-13, No. 4, (1991)
11. Zhang, Z.: *On local matching of free-form curves*. Proceedings of the British Machine Vision Conferences, 1992

ADDITIONAL READING

12. Brockett, R.W.: *Singular values and least squares matching*. Proceedings of the 36th IEEE Conference on Decision and Control, Vol. 2, 1997
13. Fitzgibbon, A.W. Robust registration of 2D and 3D point sets. *Image and Vision Computing*, Vol. 21, No. 13-14 Elsevier Science B.V., 2003 <http://www.robots.ox.ac.uk/~awf/lmicp>
14. Gaojin, W., Dengmin, G.Z., Shihong, X., Zhaoqi, W: *Total least squares fitting of point sets in m-D*, Computer Graphics International, 2005
15. Gronwall, C., Anderson, P., Gustafsson, F.: *Least squares fitting of articulated objects*. Proceedings of IEEE Proceedings - Computer Vision and Pattern Recognition (CVPR'05), Computer Society, 2005
16. Gunnarsson, K.T., Prinz, F.B.: *CAD model-based localization of parts in manufacturing*. Computer, Vol. 20, No. 8, 1987
17. Kluth, V.S., Kunkel, G.W., Rauhala, U.A.: *Global least squares matching*. Proceedings of Geoscience and Remote Sensing Symposium (IGARSS '92), Vol. 2, 1992
18. Manninen, M., Kaisto, I.: *3D measurement and analysis of a ship block. Practice report*. A.M.S. Ltd, Oulu/Finland, 1996, http://www.leica-geosystems.com/media/new/product_solution/U1-298-0EN_AMS.pdf
19. Morgera, S.D., Cheong, P.L.C.: *Rigid body constrained noisy point pattern matching*. IEEE Transactions on Image Processing, Vol. 4, No. 5, 1995
20. O'leary, P., Harker, M., Zsombor-Murray, P.: *Direct and least square fitting of coupled geometric objects for metric vision*. IEE Proceedings - Vision, Image and Signal Processing, Vol. 152, No. 6, 2005
21. Tarnowski, W.: *Fundamentals of technical design* (in Polish). WNT, Warsaw, 1997
22. Yang, M.C.K., & Lee, J.S.: *Object identification from multiple images based on point matching under a general transformation*. IEEE Transactions on Pattern Analysis and Machine Intelligence, Vol. 16, No. 7, 1994.

CONTACT WITH THE AUTHOR

Aleksander Kniat, Ph. D.
Faculty of Ocean Engineering
and Ship Technology
Gdansk University of Technology
Narutowicza 11/12
80-952 Gdansk, POLAND
e-mail: olek@pg.gda.pl

Analysis of possible shipbuilding application of friction stir welding (FSW) method to joining elements made of AlZn5Mg1 alloy

Krzysztof Dudzik, M. Sc.
Miroslaw Czechowski, Ph. D.
Gdynia Maritime University

ABSTRACT

In industrial practice the welding of Al- alloys is usually performed under pure argon shielding by means of MIG or TIG methods. In recent years new joining techniques such as friction stir welding (FSW) have appeared. Joints of EN AW-7020 T6 alloy elements welded by using FSW method have been tested. Results of static tensile tests, transverse bending tests as well as tests on stress corrosion susceptibility are presented. Parameters of friction welding (FSW) applied to joints of plates made of AlZn5Mg1 [7020] alloy are given. Stress corrosion tests have been performed by using slow-strain-rate testing method (SSRT) in compliance with PN-EN ISO 7539-7 standard. The tests were conducted in air and 3.5% NaCl water solution. The following parameters have been measured during the tests: time to failure – T [h], maximum failure load – F [N], fracture energy (area under stress-elongation curve) – E [MJ/m²], relative elongation of specimen – A_{10} [%], maximum tensile stress – R [MPa], as well as percentage reduction of area – Z [%]. On the basis of the obtained test results it was concluded that the joints welded by means of FSW method show good resistance to stress corrosion at satisfactory strength properties, which indicates that application of friction welding by using FSW method in shipbuilding industry is purposeful.

Keywords: aluminium alloys, friction stir welding, stress corrosion cracking

INTRODUCTION

Aluminium alloys are materials which find worldwide industrial applications, including shipbuilding. Their application to ship hull structures is increasing as the alloys make it possible to lower significantly mass of structures as compared with that of steel structures. By using Al-alloys lowering the mass by about 50 % can be obtained, which makes it possible to increase ship buoyancy, or at maintained buoyancy to increase its load carrying capacity or speed, as well as to improve its stability. For the reasons Al-alloys are used a.o. for construction of ship hull and superstructures. Among weldable Al-alloys suitable to plastic working the group of Al-Mg alloys (of 5xxx- series) of good weldability and relatively good service conditions are still the most popular. Their relative insusceptibility to layer and stress corrosion is advantageous, and their disadvantage is low strength of welded joints of elements made of them, not exceeding 300 MPa. In the 1990s Al-Zn-Mg alloys (of 7xxx series) attracted high interest. They are characteristic of higher strength properties as compared with those of Al-Mg alloys. Susceptibility to layer and stress corrosion is a disadvantage of Al-Zn-Mg alloys. Multi-year research has revealed that thermal working, chemical composition and welding technology (welding method, kind of added materials and type of joint) are a.o. responsible for stress corrosion susceptibility of the alloys [1÷7]. Practically all welded joints made of alloys of this

group by means of traditional MIG or TIG methods do not show sufficient resistance to stress or layer corrosion, hence only Al-Mg alloys of 5xxx- series are the only materials applicable to hull structures of light-weight ships.

The Friction Stir Welding (FSW) method may appear an alternative to traditional welding methods such as MIG or TIG methods. In the method a tool fitted with rotary mandrel located in the place of welding the pressed-down plates is used to heat and plastify the material. After putting the mandrel-fitted tool into rotation, friction heating and plastifying the plate material in its direct vicinity occurs, and slow sliding the entire system follows along contact line (Fig. 1). As it is a solidstate welding method, i.e. that below melting point of material, strength properties of joints obtained by the method can be better than those obtained from arc welding techniques (MIG, TIG). Main advantage of the method is easiness of producing joints of repeatable high properties [9, 12, 13]. As in FSW method welding is performed in solid state a far smaller amount of heat is delivered to welded materials than that in the case of traditional welding. This greatly limits range of heat-affected zone. Tests on Al-Zn-Mg alloys joined by using MIG and TIG methods, under action of aggressive sea environment, revealed their low resistance to stress and layer corrosion which occurred just in heat-affected zone [8].

Possible application, in shipbuilding industry, of the alloy of 7xxx-series of greater strength than the commonly used

alloys of 5xxx-series, depends on finding a welding method which could ensure its corrosion resistance in sea water. This work has been aimed at determination of possible application, in shipbuilding industry, of a new welding technology for joining elements of 7020 alloy with the use of FSW method. The analysis has been conducted on the basis of results obtained from research on susceptibility to stress corrosion in artificial sea water of strength characteristics of joints made of AlZn5Mg1 (AW-7020) alloy, welded with the use of FSW method, as well as results of bending tests.

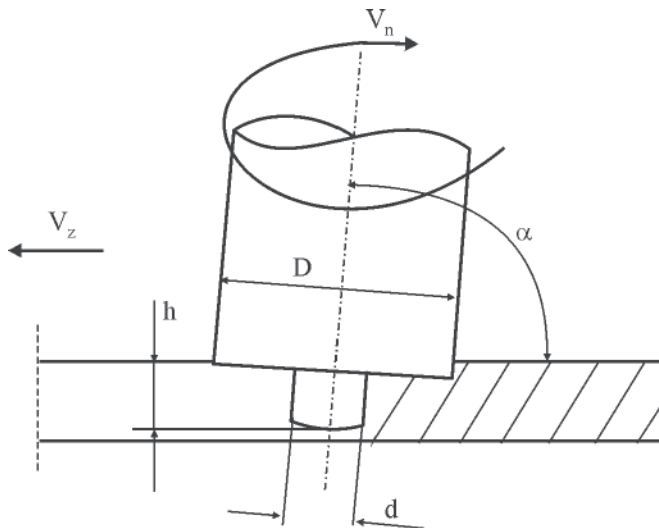


Fig. 1. Schematic diagram of FSW method [9]: D – tool diameter, d – pin diameter, h – pin length, α – angle of tool deflection, V_n – Mandrel's rotary speed, V_z – Welding speed

TESTING METHOD

To the tests the plates of the thickness $g = 10$ mm, made of EN AW-7020 Al- alloy saturated and aged (i.e. in T6 state), were used. Chemical composition of the 7020 Al- alloy is presented in Tab. 1.

Tab. 1. Chemical composition of 7020 Al-alloy

Chemical composition [%]									
Si	Fe	Cu	Mn	Mg	Cr	Zn	Ti	Zr	Al
0.30	0.35	0.10	0.24	1.30	0.14	4.70	0.08	0.07	the rest

Joints were butt ones two-sided welded by using FSW method. The applied parameters of friction stir welding (FSW), i.e. that associated with weld material stirring (see Fig. 1), are given in Tab. 2.

Tab. 2. FSW parameters applied to welding of 7020 Al- alloy plates

D [mm]	d [mm]	h [mm]	α [°]	Mandrel's rotary speed V_n [rpm]	Welding speed V_z [mm/min]
25	10	5.8	88.5	450	180

The stress corrosion tests were conducted with the use of SSRT (Slow Strain Rate Testing) method in compliance with PN-EN ISO 7539-7 standard [12]. The tests were carried out on a special measurement stand which made it possible to stretch specimens at strain rate in the range from 10^{-3} to 10^{-7} s^{-1} in corrosive environment.

The following parameters : the relative elongation of specimen in the instant of its failure A_{10} [%], the maximum

force F_{max} [kN], the maximum stress R_{max} [MPa], the relative fracture energy E [MJ/m³] (area under stress-elongation curve), the reduction of area in the instant of specimen fracture Z [%], duration time till the specimen failure T [h], were recorded with the aid of computer during the tests or just after its termination.

The tests were performed on smooth cylindrical specimens free of notch. They were conducted in artificial sea water (acc. PN-66/C-06502 standard) of +20°C temperature, as well as in a neutral environment – dry air, at the low strain rate $\dot{\epsilon} = 1.6 \times 10^{-6} s^{-1}$, up to complete failure of specimen. Prior to exposition the specimens were polished and degreased.

TEST RESULTS

The results obtained from the static tensile test of AW-7020 alloy and its FSW method -welded joints, conducted on flat specimens (acc. EN 895:1995 standard), are presented in Tab. 3.

Tab. 3. Mechanical properties of the AW-7020 alloy native material and its FSW method - welded joints (average value from two or four specimens)

Material	UTS [MPa]	YS [MPa]	EL [%]
7020/ native material	373	317	14.2
7020/FSW	367	314	13.8
7020/MIG	315	283	8.2

UTS - Ultimate Tensile Strength, YS - Yield Stress, EL - Elongation

Joints of 7020 Al-alloy welded by using FSW method were subjected to the bending test in compliance with PN-EN 910:1999 standard. Flat specimens were used to the test in which bending mandrel of the diameter $D = 60$ mm (sixfold specimen thickness) was applied. During the test no cracks were recorded up to 180° bending angle, which fulfils requirements of classification institutions. A view of specimens after bending tests is given in Fig. 2.



Fig. 2. A view of FSWmethod-welded specimens after bending tests

Results of the SSR tests conducted on smooth specimens in air (marked „pow.”) as well as in artificial sea water (marked „NaCl”), are presented for particular measured parameters (average values from 4÷5 measurements) in Tab. 4.

Fractographic examinations of welded joints made of Al-Zn-Mg alloy were conducted on fractures achieved during the SSRT tests. Analysis of fracture surface of examined specimens was performed with the use of an XL30 Philips scanning electronic microscope (SEM). During the SSR tests the specimens formed of joints welded by using FSW method were tested till the fracture which appeared due to shear in

Tab. 4. Slow strain rate test results

Material	Environment	Elongation A_{10} [%]	Reduction-of-area Z [%]	Fracture energy E [MJ/m ³]	Time-to-failure T [h]
7020	air	8.77	48.3	26.87	12.45
7020	NaCl	8.77	45.8	27.1	12.04
7020/FSW	air	7.32	48.65	19.32	9.86
7020/FSW	NaCl	7.12	48.8	19.17	9.53

their native material. The examinations demonstrated that material decohesion was running through crystals and had plastic character (Fig. 3).

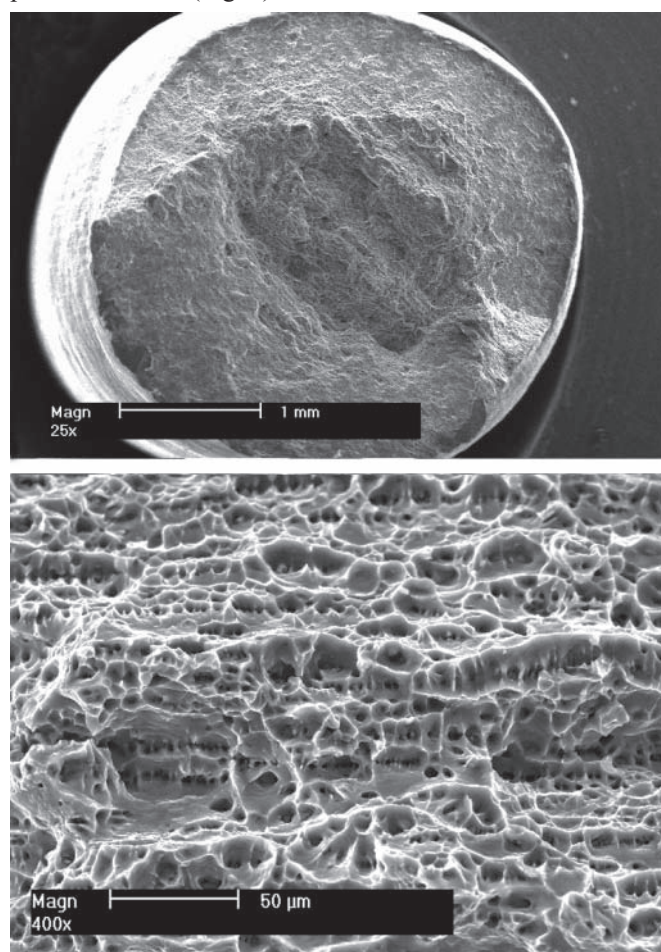


Fig. 3. Fracture of AW-7020 alloy joint welded by FSW, achieved during SSR test

RECAPITULATION

Investigations of mechanical properties demonstrated that strength properties of 7020 alloy welded by using FSW method are better as compared with those of MIG - welded joints of 7020 alloy and AlMg4.5Mn0.7 (5083) alloy presently most used in shipbuilding industry [7]. Such weld is free of typical defects characteristic for arc welding, e.g. gas pores or lack of weld penetration. It was confirmed by bending tests where no fractures were found after bending by 180° angle.

On the basis of the obtained test results it can be stated that the friction-stir-welded AlZn5Mg1 alloy (by using FSW method) is resistant to stress corrosion in sea water. Values of particular measured parameters of friction-stir-welded joints, obtained in air and artificial sea water, do not differ much to each other, respectively (Tab. 4). Relative elongation of FSW

method-welded 7020 alloy specimens stretched in artificial sea water, was lower on average by only 2.7 % as compared with that of such specimens tested in air. Even lower percentage decrease was obtained from the measurements of the relative reduction of area and relative fracture energy (0.77%).

High strength of FSW method - welded joints is confirmed by location of fracture in tested specimens. During the SSR tests cracks appeared beyond weld in their native material. It concerns both the specimens exposed in air and artificial sea water. Specimens subjected to the static tensile test cracked in a similar way. In this case cracks were also located beyond weld in native material.

Summing up, it can be stated that application of the FSW method to welding Al- alloys in shipbuilding industry, seems purposeful. The most important merits of the FSW method are the following :

- the possible welding of butt and overlap joints
- good mechanical properties of welds
- minor welding deformations of elements
- lack of gas pores and cracks in welds
- lack of a shielding gas
- the possible single-run welding of material of up to 15 mm in thickness
- the possible obtaining of repeatable high quality of welds in all positions.

Friction welding by using FSW method has been presently applied in many high-developed industrial countries. It is used in shipbuilding, railway engineering, motor and aircraft industries [1, 14].

CONCLUSIONS

From the performed investigations the following conclusions can be drawn:

- Joints of EN AW-7020 T6 alloy welded by means of the new, FSW method, show higher strength properties as compared with those of joints welded with the use of the traditional method MIG.
- Joints of EN AW-7020 T6 alloy welded by means of the FSW method, show low susceptibility to stress corrosion, determined during the slow-strain-rate test (SSRT).
- AW-7020 alloy can be applied to ship structures welded with the use of FSW method.

BIBLIOGRAPHY

1. Anderson T.: *New developments within the Aluminium Shipbuilding Industry*, Svetsaren, no.1, Vol. 58, 2003.
2. Buglacki H.: *Influence of welding technology on resistance to corrosion of Al-Zn-Mg alloys* (in Polish). International Conference on Environmental Degradation of Engineering Materials, Gdansk University of Technology, Jurata, 1999
3. Cudny K., Puchaczewski N.: *Metal alloys for ship hull structures* (in Polish). Gdansk University of Technology, Gdańsk, 1995

4. Czechowski M.: *Research on effect of electrochemical polarization and thermal treatment on stress cracking of Al-Zn-Mg alloys* (in Polish). Zeszyty Naukowe WSM w Gdyni (Scientific Bulletins of Gdynia Maritime Academy), No. 30, Gdynia, 1996
5. Czechowski M.: *Effect of anodic polarization on stress corrosion cracking of some aluminium alloys*. Advances in Materials Science, no. 1(11), Vol. 7, 2007
6. Czechowski M.: *Optimum methods of welding Al-Mg alloys in the aspect of their resistance to stress corrosion cracking* (in Polish). Materiały i Technologie (Materials and Technologies), Gdansk University of Technology, no. 3 (3), Gdańsk, 2005
7. Czechowski M.: *Properties of butt welds in Al-Mg alloy plates welded by using different methods* (in Polish). Materiały i Technologie (Materials and Technologies), Gdansk University of Technology, no. 1(1), Gdańsk, 2003
8. Czechowski M., Chrzanowski J., Zieliński A.: *Stress corrosion cracking in Al- alloy welded joints* (in Polish). Materials of II Pomorska Konferencja Naukowa - Inżynieria Materiałowa 2001 (2nd Pomeranian Scientific Conference on Materials Engineering), Gdansk University of Technology, Sobieszewo, 2001
9. Czechowski M., Pietras A., Zadroga L.: *Properties of Al- alloys of 5000 series friction- welded by using a new, FSW technique* (in Polish). Inżynieria Materiałowa, no. 6/2003
10. Czechowski M., Zieliński A.: *Effect of cathodic polarization on failure and degradation of mechanical properties of some aluminium alloys*. Scripta Metallurgy Materials, Vol. 30, 1994
11. Czechowski M., Zieliński A., Cudny K.: *Effect of chemical composition and thermal treatment on stress corrosion cracking of aluminium alloys*. Conference on Corrosion-Deformation Interactions, Fontainebleau, 1991
12. Lahti K.: *FSW – possibilities in shipbuilding*, Svetsaren, No.1, Vol. 58, 2003
13. Nicholas E., D., Kalle D., S.: *Process of friction welding with weld material stirring is already 10 years old* (in Polish). Biuletyn Instytutu Spawalnictwa (Bulletin of Welding Institute), no. 3/2001.

CONTACT WITH THE AUTHORS

Krzysztof Dudzik, M.Sc.
 Mirosław Czechowski, Ph.D.
 Faculty of Marine Engineering
 Gdynia Maritime University,
 Morska 81-87
 81-225 Gdynia, POLAND
 e-mail: krysz-r6@wp.pl , czecho@am.gdynia.pl

Water-lubricated bearings of ship propeller shafts - problems, experimental tests and theoretical investigations

Wojciech Litwin, Ph. D.
Gdansk University of Technology

ABSTRACT



In recent years can be met ships whose propeller shaft polymer bearings are lubricated with water. It results from simplicity and associated low cost of such solution which is also environmentally friendly as no risk of pollution is involved. However the solution is not free of disadvantages. The main problem is intensive wear of bush material, occurring in certain cases. It very often results from errors of improper design and machining and mounting operations. Another problem is a limited value of its hydrodynamic load-carrying capacity, resulting from low viscosity of water used as a lubricating medium.

As results from the performed research investigations, bearing of the kind is a highly sensitive unit. Problems of choosing a suitable bearing clearance, designing an optimum bush geometry, selecting a proper bush material are crucial for lifetime of the bearing.

Keywords: bearing; water-lubricated bearings; propeller shaft bearing

INTRODUCTION

Increasing ecological awareness, more and more stringent requirements for environmental protection, fines for emission of noxious substances to sea, and economical calculations have resulted in that shipowners are searching for inexpensive, simple and reliable design solutions for building new ships and modernizing existing ones. These are main reasons for which slide bearings fitted with polymer water-lubricated bush are more and more willingly applied to propeller shaft bearing. Similar reasons are decisive of that water-lubricated bearings are more and more often applied also in water power plants and pumps in which a pumped liquid, usually water, serves as a lubricating medium. They find application also in mining industry, water conditioning stations or land melioration systems.

Worldwide increasing demands concerning durability and reliability make that more and more stringent requirements for bearings are introduced. As results from experience of classification institutions and shipyards, well designed and assembled water-lubricated bearings are able to operate correctly for more than ten years. Unfortunately from the collected data it also results that many failures occur each year on ships, especially in high-loaded propeller shaft bearings. Such failures greatly endanger sea navigation as they may lead to ship disablement. In situation of the kind, when oil serves

as a lubricating medium, its leakage results in pollution of sea water. If ship's crew and owner do not immediately decide on docking and repairing the ship its serious failure will be possible to happen (Fig. 1).

Water-lubricated bearing of ship propeller shaft, like most materials and components for building and outfitting the ships, should be approved by a classification institution. Many kinds of polymer materials for bearings, applicable in shipbuilding, are present on the market today. For instance the list issued by Lloyd's Register of Shipping contains over a hundred kinds of such materials produced in many countries worldwide [1].

Producers of bearing materials, in their catalogues and internet pages, very often present a recommended way of selecting a definite material, bearing clearance as well as possible location of lubricating grooves. Therefore the designing of a slide bearing seems very simple. However as results from experience the methods are not always effective. In certain cases an excessive wear of bushes can happen within a short period. Sometimes fast progressing wear results from its operation in mixed friction conditions. It is very hard to obtain fluid friction in a bearing as water film load-carrying capacity is limited due to low viscosity of water. In spite of that water-lubricated bearings are often used in practice. Their lower price as compared with that of oil-lubricated bearings is not without any importance.



Fig. 1. Completely damaged oil-lubricated slide bearing and sealing of ship propeller shaft



Fig. 2. Cantilever open bearing of yacht's propeller shaft



Fig. 3. Damage of a composite bush, resulting from edge thrust resulting from skew position of shaft axis (up); during repair the damaged edge was grinded to avoid cracks and delamination of the composite (down)

TYPES OF BEARINGS

Range of the materials available today on the market is very wide. The materials approved for shipbuilding applications can be divided into the three groups: homogenous polymers, composites and rubber which is often substituted by nitrile-butadiene rubber.

Each of them is characteristic of different properties and, resulting from them, advantages and disadvantages. Rubber effectively damps vibrations and is not sensitive to contamination, which is the reason for using it in e.g. cantilever open bearing systems (Fig. 2). It is important that contaminations which fell into rubber bearing accelerate its wear process only moderately. This concerns also hard contaminations, e.g. high-silica sand grains.

Homogenous polymers are relatively elastic. Their modulus of rigidity is usually contained within the range from 800 to

2500 MPa. Owing to that such bush is capable of damping shaft vibrations. Polymers, like rubber, relatively well tolerate errors in alignment of shaft axis against bush axis. The thing is in distribution of shaft - to - bush pressure over an extended area as a result of elastic deformation of bush.

Composites, out of all the above mentioned materials, are characteristic of the largest value of rigidity modulus amounting to about 4500 MPa. Therefore they are sensitive to edge thrust in the case of shaft skewing. (Fig. 3), but they also have important merits. They are durable and highly resistant to form distortion which is a disadvantage of some homogenous polymer materials.

The scientific investigations have been so far conducted worldwide justify that ceramics is a good material for bearings operating in water [2]. Slide bearing fitted with ceramic bush can operate in fluid friction conditions at a very small thickness of lubricating film. On the other hand such bearings are especially sensitive to errors in relative position of shaft against bush, particularly to non-parallelism of their axes.

MANUFACTURING AND MOUNTING OF BUSHES

Bushes are usually manufactured by machine cutting a prefabricate - as a rule - a thin-walled pipe. It is only an outwardly simple operation. In practice it turns out that obtaining a demanded form and accuracy is difficult or completely impossible. Elastic bush material undergoes deformations during machine cutting. In consequence, an inaccuracy of form appears. Therefore it is recommended

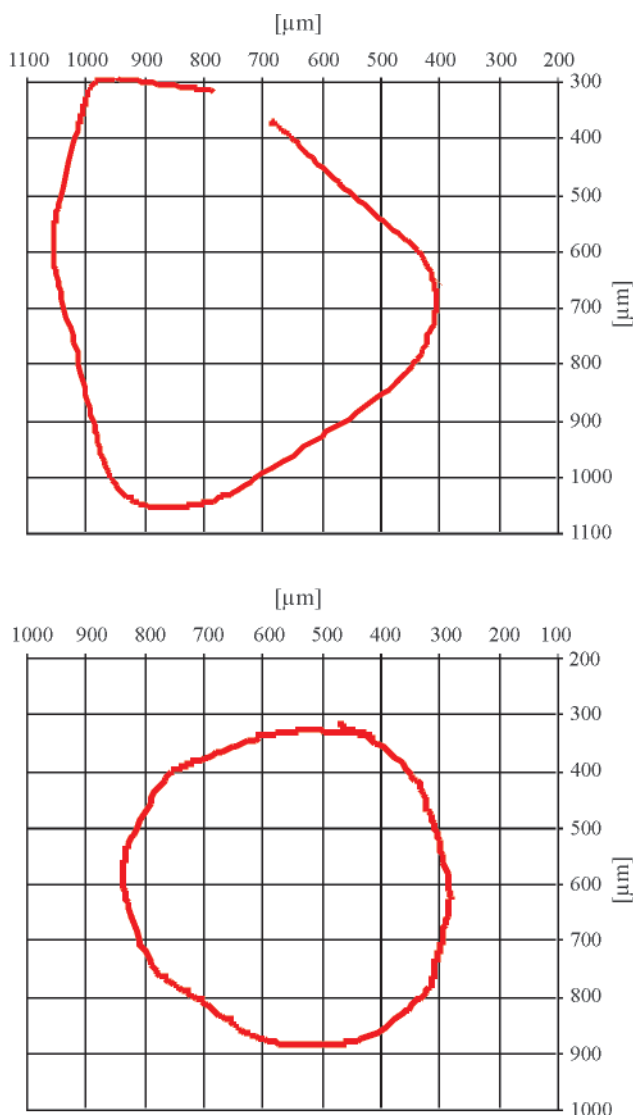


Fig. 4. Circles of gaps measured on both sides of a rubber bearing after its mounting in steel sleeve. Its form errors, especially lack of circularity, can be observed

to machine sliding surface of bearing after fixing its bush in a metallic or stiff composite sleeve. Usually a finished bush is ordered from producer who is usually better equipped with technological means to ensure an appropriate machining accuracy. Then the problem of proper mounting is only left for solving. As a rule the forcing method is not recommended as it may lead to bush deformation. Usually the contraction method is applied. The bush is cooled-down to a low temperature by using liquid nitrogen and next mounted into the sleeve. Unfortunately such method does not guarantee the highest accuracy hence bearing clearance may often differ from a design value. Additionally, if longitudinal lubricating grooves are made in the bush a danger of sliding surface deformation arises as the largest deformations appear usually in areas of the smallest thickness of the bush, i.e. in the vicinity of the lubricating grooves. Errors in manufacturing and mounting very often cumulate, which results in that bearing geometry differs significantly from the initially designed (Fig. 4). As can be observed from the below given diagrams of measured gap circle, significant deformations have appeared after mounting the rubber bearing of 100 mm diameter into the steel sleeve. Cylindricity and circularity errors are found significant. Hence it may be expected that in such bearing an intensive wearing-in process would happen and possible hydrodynamic load-carrying capacity would be very limited.

As results from experience, bearings which practically should be regenerated or replaced are often allowed to be put into operation: for instance a rubber propeller shaft bearing of 385 mm diameter, in which radial gap was in the range from 4 mm to almost 10 mm. In the bearing also shaft journal was subjected to wear, that is typical for rubber bearings.

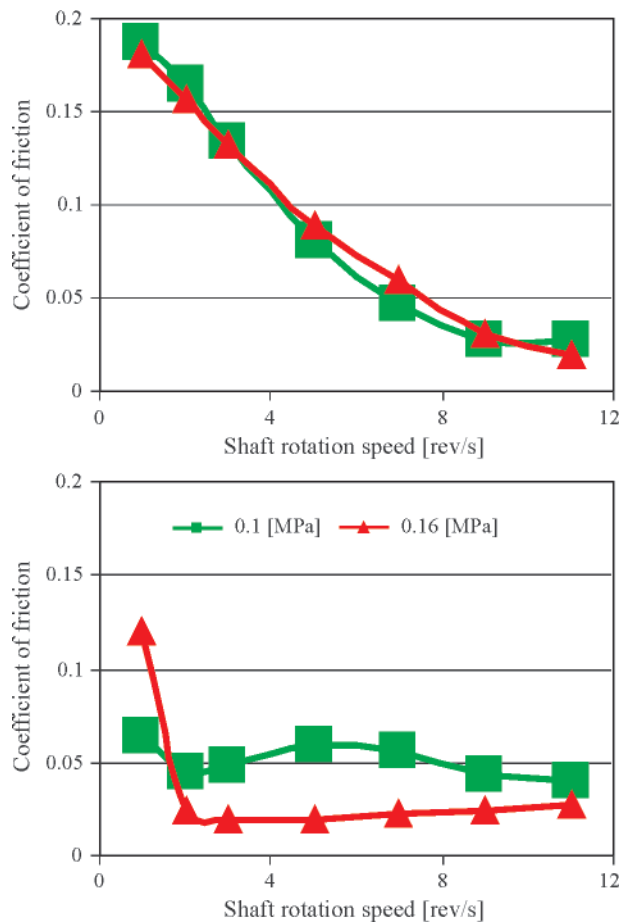


Fig. 5. Diagrams of friction coefficient values in function of shaft rotational speed; up side - the diagram recorded just after mounting the bearing, down side - the diagram obtained after several hours of running-in the bearing

Another technological problem is the achieving of possible high smoothness of co-operating slide surfaces. It is crucial because minimum thickness of lubricating film and hydrodynamic load-carrying capacity of bearing depends on surface roughness height. In the subject-matter literature publications dealing with influence of height and distribution of roughness on operation of hydrodynamic bearing, can be found. However as results from the author's experimental tests, this is bush roughness height which crucially influences hydrodynamical features of bearing [3,4]. The performed tests showed that running-in process of such bearing was very fast and a significant smoothness of slide surfaces was already reached after a few hours of operation. As a result, fluid friction state of operation was achieved faster (Fig. 5).

OPERATIONAL PROBLEMS

Ship water-lubricated bearings can have different forms recommended by their manufacturers. Such differences concern both values of recommended clearance in bearings and magnitude and number of longitudinal lubricating grooves and their suggested location as well. For fear of clamping the bush material exposed to water some producers recommend to increase clearance values. Most of recognized producers of ship slide bearings recommends to make certain number of lubricating grooves led along the bush. They play a significant role. Due to them, cooling water flow rate increasing is possible. It has a great importance as polymer bush practically makes heat transfer from friction zone to housing impossible. Additionally, the grooves, especially in the systems of open cantilever sea-water-cooled bearings, make it possible to more effectively remove wear products and contaminations from the bearings (Fig. 6).



Fig. 6. An unsealed sea-water-lubricated bearing which was exposed to pollution and fouling

Lifetime of ship main shaft bearing depends on many factors. Tribological features of bush material are of a great importance. However to extend lifetime of a bearing significantly it should be so designed as to make it operating in fluid friction regime. As results from the performed tests it is possible to achieve despite water has much lower viscosity than that of lubricating oils [5]. Unfortunately, in consequence, lubricating film thickness is often close to its minimum value. Bearings usually have minimum margin of hydrodynamic load - carrying capacity, and in situations of increased load due to e.g. ship motion in waves, they may operate in mixed friction regime.

Experimental tests showed that even if a high load is imposed on a bearing its operation in fluid friction regime is

possible. It results generally from fast process of bush material smoothing and its operation in fluid friction regime at minimum thickness value of lubricating film. Wrong geometry of slide bearing has definitely detrimental influence on its hydrodynamic features. To excessively increase bearing clearance is not recommended. To locate lubricating grooves in lower part of bush is also not recommended, as they make hydrodynamic pressure developing impossible, and, in consequence, they limit load-carrying capacity of the bearing.

As results from a damage analysis of various bearings of the kind, they suffered failures despite they were correctly designed and manufactured with the use of high-quality materials coming from recognized producers. Reasons of that have been found different. Fast excessive wear resulted sometimes from lack of water flow through bearing due to clogging-up lubricating grooves or faults of crew members who did not put lubricating system circulation pump into operation. In most cases it was changeable heavy operation conditions of ship shaftline, which led to fast progressing wear or even failure of the bearings.

Changeable operational conditions are caused by a few factors. To the most important belong ship's hull elastic structural deformations resulting from ship's motion in waves. During ship motion in heavy waves mass forces applied to shaftline transverse bearings can be risen by dynamic components resulting from ship roll and heave motions. Sometimes loads exerted to bush may be enlarged by dynamic loads due to unbalanced motion of propeller or vibrations generated by its blades passing through non-homogenous pressure field.

Appropriate alignment of shaftline and bushes is the next important factor which directly influences lifetime of bearings; therefore mounting accuracy is of a special importance. In the case when mounting errors happen the skewing of shaft axis versus bush axis may occur. As a result load-carrying capacity of the bearing will be limited. In the extreme case the so-called edging phenomenon and associated fast progressing wear can appear because values of allowable contact pressure are locally exceeded. Bearings fitted with rigid ceramic, metallic or composite bushes are especially sensitive to the phenomenon (Fig.7).



Fig. 7. A white metal bush of oil-lubricated bearing, damaged due to edging

AIM OF THE RESEARCH

The research conducted for several years has been aimed at gathering knowledge on the phenomena which occur in ship main shaft water-lubricated bearings.

Owing to the investigations have been conducted so far it was managed to determine influence of many factors on features

of hydrodynamic bearing fitted with elastic bush lubricated with a low - viscous liquid.

Influence of the following factors on bearing features was investigated:

- diameter clearance
- bush material and sliding surface state
- mounting errors, especially axis skewing
- permanent deformation of lubricating gap, resulting from progressing wear, with taking into account possible mounting errors.

Presently is conducted a research aimed at determination of influence of bush material on bearing lifetime, and estimation of progressing wear rate so as to make it possible to elaborate a computational algorithm to identify bearing lifetime and facilitate setting deadline for necessary friction node regeneration.

EXPERIMENTAL AND THEORETICAL INVESTIGATIONS

The research on ship shaftline bearings has been conducted by Faculty of Ocean Engineering and Ship Technology, Gdańsk University of Technology, for almost ten years. Today three different test stands are applied to the experimental investigations [6]. They provide wide research possibilities, and furthermore, their dimensions make the full-scale testing of bearings possible.

It is possible to record values of resistance to motion, shaft axis trajectory, lubricating film pressure, and such parameters of lubricating medium as temperature, flow rate and pressure,

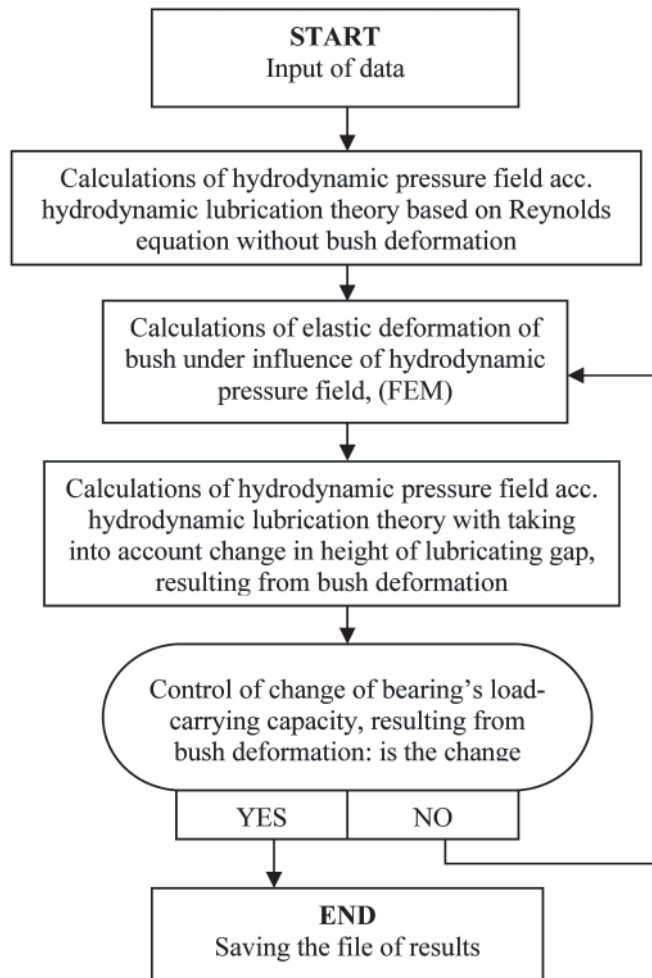


Fig. 8. Schematic diagram of the calculation method

all in function of set changeable working conditions such as shaft rotational speed and load.

Apart from the experimental tests the teoretical research is also conducted. In this paper are presented calculation results obtained by using the author's original software based on hydrodynamic lubrication theory applicable to elastic bush material (EHL). The software is composed of two modules: the program based on hydrodynamic lubrication theory, written in FORTRAN language, and the module based on the finite element method (FEM) in the form of macro to a commercial software. Schematic diagram of the calculation method is presented below (Fig. 8). The calculations are performed in an iterative mode. Generally, a satisfactory result can be obtained after twenty iterations at the most (Fig. 9). Problems with achieving correct results appear in the case of extreme conditions of operation with very thin lubricating films.

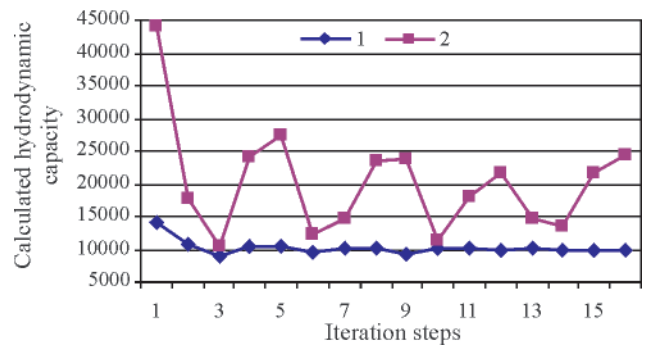


Fig. 9. Diagrams of calculated values of load-carrying capacity of a bearing in function of number of successive iteration steps:
1st series – stable solution was achieved;
2nd series – a convergent result was not achieved

The calculations were performed for the isothermal model. As results from the temperature distribution calculations (Fig. 10) and test-stand measurements the rise of lubricating film temperature is very low and amounts to less than 5°C usually. Therefore in the calculations the minimum change of viscosity of lubricating medium as well as of bush material properties, resulting from local rise of temperature, may be neglected.

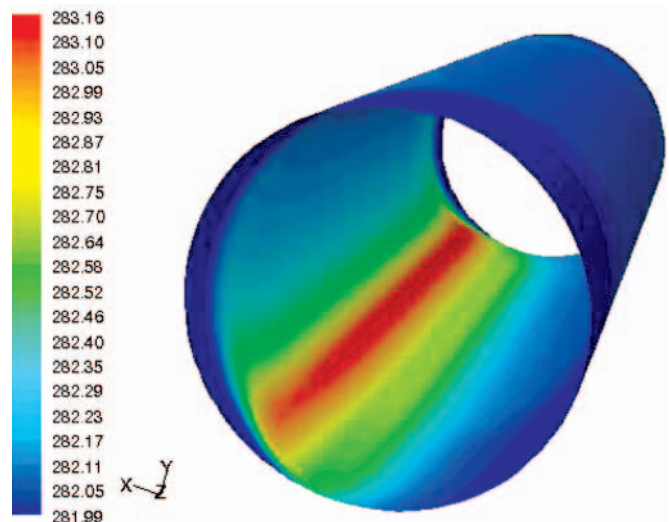


Fig. 10. Temperature distribution in lubricating film of a water-lubricated bearing, calculated by using a commercial software

Results of the calculations were verified experimentally. They confirmed that the applied calculation method is correct. It is rather hard to estimate calculation error as to accurately measure lubrication gap height is deemed questionable. In the author's opinion the calculation error does not exceed 20%.

Results of calculated and measured hydrodynamic pressure distributions in a water-lubricated bearing, are presented below (Fig. 11.)

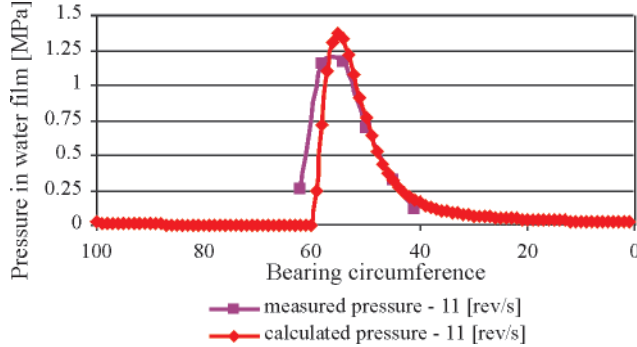


Fig. 11. Comparison of results of pressure field measurements and calculations

INFLUENCE OF CLEARANCE VALUE AND BUSH MATERIAL ON BEARING QUALITIES

Diameter clearance is of crucial impact on slide bearing qualities. The tested bearing achieves usually its largest hydrodynamic load-carrying capacity at the relative clearance value in the range from 0,001 to 0,002 (Fig. 12). However such value would be hardly applicable in practice. It should be remembered that in the typical case a completely finished polymer slide bush is seated by using shrinkage method. Therefore it is usually hard to achieve a precise value of bush inner diameter hence also a precise value of diameter clearance after seating the bearing. An additional problem is water absorption, typical for most polymers. Bush material swells as a result of the process. Because the bush is seated in a steel housing all the swelling of bush material makes bearing inner diameter smaller, which leads to significant risk of clenching the bush onto shaft and bearing blocking. It creates serious danger and therefore bearing manufacturers recommend as a rule to increase bearing gap.

An event of the kind has happened in the past during the tests conducted on one of the test stands. In effect, dismantling the bearing has taken a few days. If such situation happens on a real ship its consequences will be rather unpredictable.

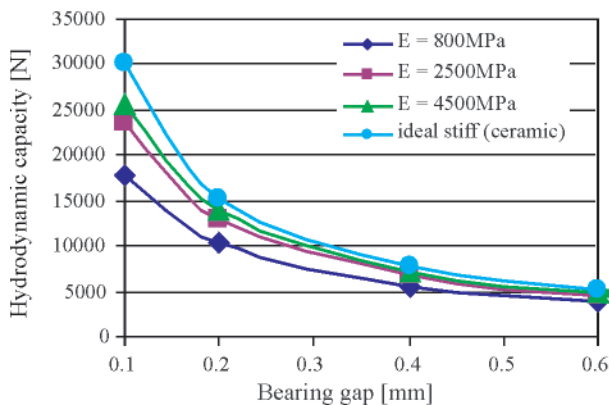


Fig. 12. Influence of bearing diameter clearance (bearing gap) and rigidity modulus of bush material on maximum load - carrying capacity of the bearing; shaft diameter of 100 mm, bush length of 400mm

From the performed calculations it results that rigidity modulus greatly impacts load-carrying capacity of high-loaded slide bearings (Fig. 12). It is associated with elastic deformation of bush material under hydrodynamic pressure

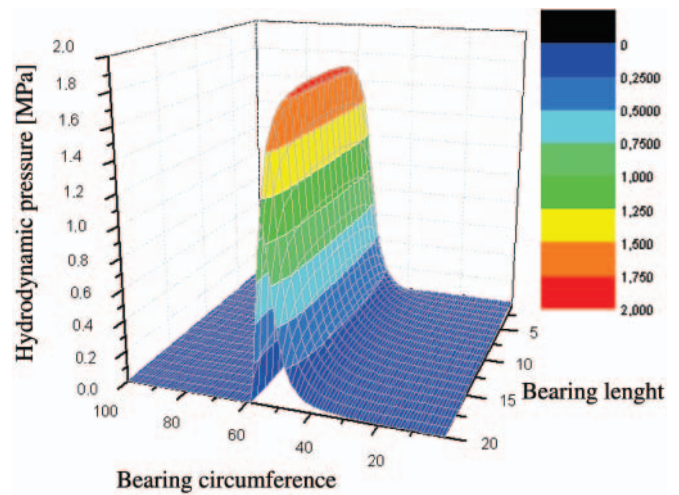


Fig. 13. Diagram of the calculated pressure field in the bearing fitted with perfectly rigid bush

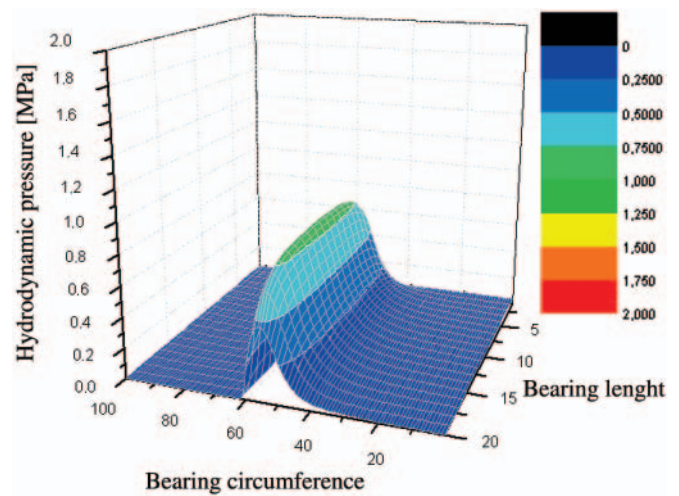


Fig. 14. Diagram of the calculated pressure field in the bearing fitted with elastic bush of 800 MPa material rigidity modulus

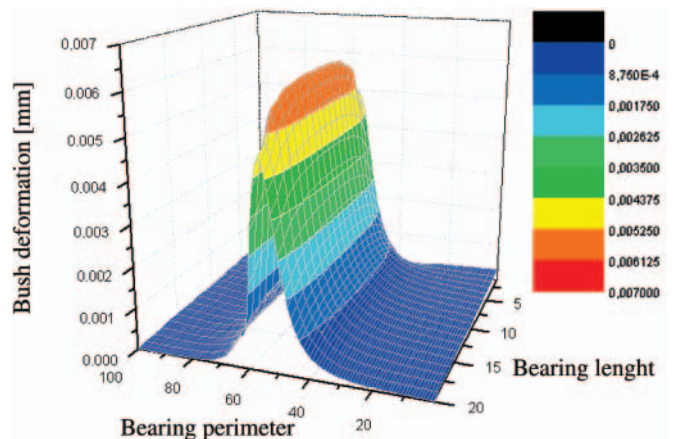


Fig. 15. Diagram of the calculated deformation field in the elastic bush of 800 MPa material rigidity modulus

of lubricating film. In effect the largest deformation takes place in the middle part of the bearing, and only slight ones - near its edges. For this reason in the central part of the bearing the lubricating gap height becomes larger and, in consequence, load-carrying capacity of the bearing - lower. (Figs. 13, 14, 15).

In the diagrams the calculated pressure field of a high-loaded bearing with 5µm lubricating gap height, is presented.

Attention should be paid to the fact that only the central part of the bush has been deformed. Therefore the smallest value of lubricating film thickness has occurred at the bearing's edges. In the case of increasing load specific situation happens in bearing of the kind: its central part operates in fluid lubrication regime but in its near-edge zones mixed friction appears and, in consequence, progressing wear process develops. Occurrence of the phenomenon has been confirmed by the performed experimental tests.

INFLUENCE OF BUSH SURFACE STATE ON BEARING QUALITIES

In the tribology-matter literature many papers dealing with influence of roughness height and distribution on hydrodynamic qualities of bearing, can be found. Slide surface roughness is of a special importance for water-lubricated bearings working under fluid friction regime since values of lubricating film thickness are usually small in them. Shaft journal surface is usually grinded hence its smoothness is high. Then to machine elastic bush is more difficult. Diameter turning operation usually results in a value of roughness height amounting even to a few micrometers.

The experimental tests in question were performed for a few kinds of bush material as well as various clearance values. The bush was turned to achieve roughness direction parallel to sliding direction. A problem was to obtain the roughness having direction perpendicular to rotation direction. Therefore a machining method was elaborated similar to pull-broaching. Through a preliminarily machined opening in the bush were introduced purpose-designed cutting discs of successively larger diameters to perform bush pull-broaching. (Fig. 16).

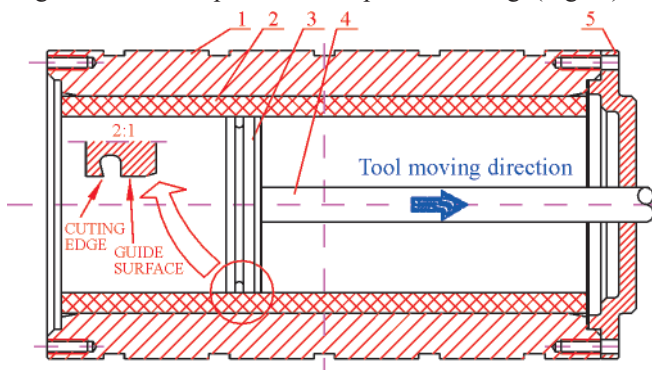


Fig. 16. Internal pull-broaching of polymer bearing bush. 1 – steel sleeve, 2 – polymer bearing bush, 3 – form tool, 4 – pulling rod, 5 – cutting disc

Due to longitudinal motion of the tool roughness arrangement perpendicular to sliding direction was achieved. However in practice it turned out that certain materials, e.g. composites appeared hardly machinable as they deformed elastically. Such polymers, like polyethylene or polyamide, were less troublesome during pull-broaching operation. Despite setting the minimum thickness of cutting layer surface quality after pull-broaching operation was distinctly lower than that after turning.

The performed tests showed that roughness topography, i. e. its arrangement has not any significant impact on bearing qualities [7]. Below, an example comparison of the experimentally recorded shaft axis trajectories, is shown. The observed very small differences in the journal's position demonstrate that the state of surface has negligible effect on hydrodynamic bearing qualities. Worth adding that the tests were performed just after mounting the bearing and before bush material running-in.

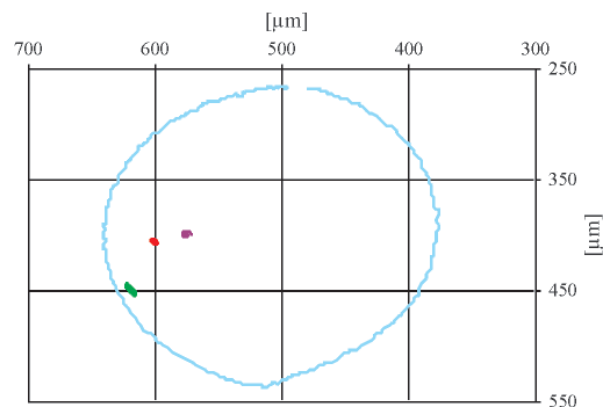
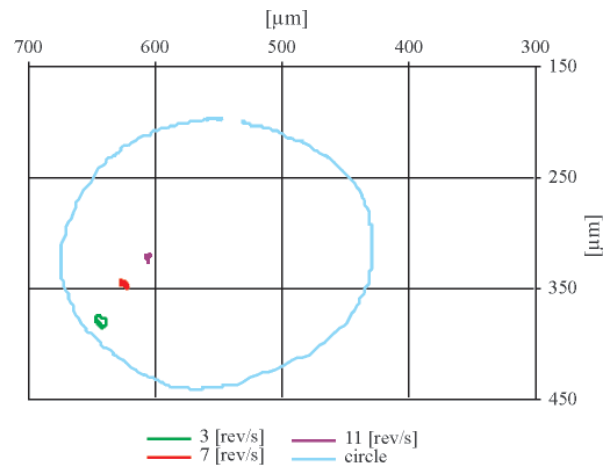


Fig. 17. A bearing fitted with PET polymer bush of 0.0027 relative clearance value; up – the bearing with turned bush; down – the bearing with pull-broached bush

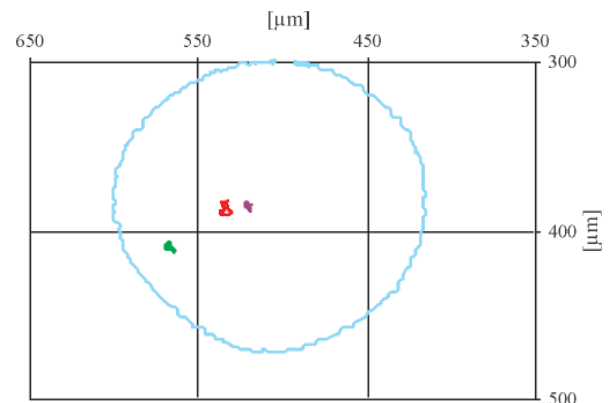
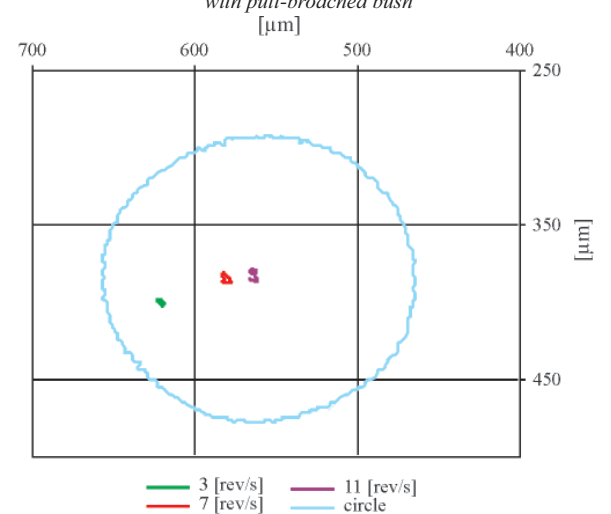


Fig. 18. Bearing fitted with composite bush of 0.0017 relative clearance value; up – the bearing with turned bush; down – the bearing with pull-broached bush

INFLUENCE OF MOUNTING ERRORS, ESPECIALLY SHAFT AXIS SKEWING, ON BEARING LOAD - CARRYING CAPACITY

The skewing of shaft axis against bush axis produces serious danger to bearing. It may appear as a result of the improper machining and mounting of stern tube components. Such phenomenon occurs from time to time also in the case when ship hull deforms elastically during ship loading or sailing in heavy seas. Ships with long shaftlines, e.g. two-propeller double-ended ferries with amidship-located machinery room, are especially exposed to such phenomenon.

The shaft axis skewing leads to decreasing load-carrying capacity of bearing, and in extreme cases, when rigid bush materials are used, the so-called edging occurs as a rule (Fig.7). It results in an intensive local wear of bush material and sometimes also in shaft failure.

Bearings fitted with bushes made of an elastic material well tolerate non-coaxial work as they undergo large deformations and in consequence their load is distributed over an area greater than that in bearings with, for instance, a rigid composite bush.

In the below attached diagrams is presented a change of form of calculated pressure field, which results from the skewing of shaft axis. In the analyzed case the theoretically maximum value of hydrodynamic load-carrying capacity of the bearing decreased by 25% as a result of the shaft axis skewing.

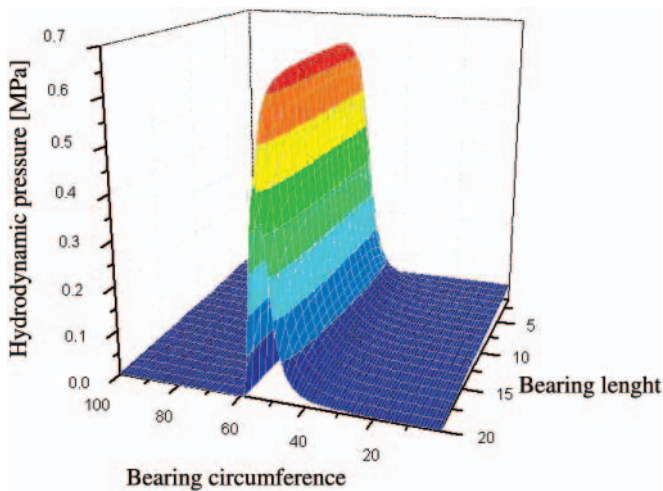


Fig. 19. Calculated pressure field in a bearing fitted with elastic bush of the material rigidity modulus $E=800$ MPa

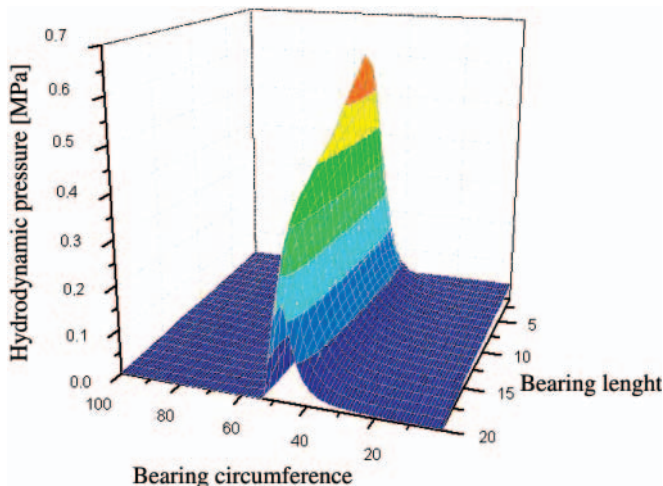


Fig. 20. Calculated pressure field in a bearing fitted with elastic bush of the material rigidity modulus $E=800$ MPa, and shaft axis skewed against bush

INFLUENCE OF BUSH FORM ERRORS AND PROGRESSING WEAR ON BEARING LOAD - CARRYING CAPACITY

Bearing operation performed not always in optimum conditions as well as designing and mounting errors usually lead to fast progressing wear of bush material. Consequently, it is hard to predict which form of bush would be finally obtained. From an analysis of experimental tests with many bushes as well as experience from their long-lasting operation on ships it results that bush loses its initial cylindrical form usually due to progressing wear. It step by step obtains a form of truncated cone and undergoes ovalization. In the below given figure it can be observed that the bush ovalization resulted from its long-lasting work. In the lower part of the bush a significant material wastage occurred and the bush axis was displaced by O_w value.

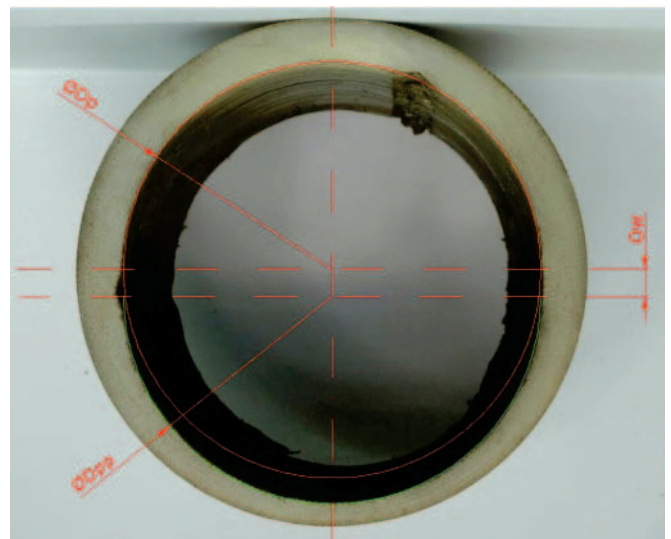


Fig. 21. Sliding bush of a water-lubricated bearing subjected to long-lasting operation which resulted in a significant wastage and associated ovalization of the bush

In practice, during ship's repair very often takes place a conflict between the shipowner who tends to limit extent of repair work and the classification society which surveys the work. For example, repair of 385 mm diameter stern tube bearing was given up despite 5 mm cylindricity errors of the journal and almost 10 mm change of bush diameter found in this case. Diameter clearance value for a bearing as large as that should be smaller than 1 mm, but the really measured was greater than 10 mm.

SUMMARY

The contemporary computational tools make it possible to relatively exactly calculate slide bearing parameters. The available software based on hydrodynamic lubrication theory or other computational methods of fluid mechanics (CFD) taking into account elastic bush deformations calculated by using the finite element method (FEM), makes it possible to conduct experiments and bearing optimization in virtual space. Ship shaft water-lubricated bearings fitted with polymer bush are sensitive units. Because of small thickness values of lubrication film their work in mixed friction regime takes often place. In the case of an erroneous position of shaft axis wear process is often fast developing in such bearings. Nonetheless they are commonly applied to smaller ships owing to their low price, simple design as well as lack of hazard to potential pollution to the environment.

In present, a variety of sliding materials approved for shipbuilding applications can be found on the market. Most of them are products of high quality, rather insensitive to designing and mounting errors and exposure to such aggressive lubricating medium as sea water.

BIBLIOGRAPHY

1. Lloyd's Register: *List of materials approved for application to water-lubricated shaftline bushes on ships* (in Polish)
2. Olszewski A.: *Ceramic transverse bearing of conformal sliding surfaces* (in Polish). Doctoral thesis, Mechanical Faculty, Gdańsk University of Technology, 2002
3. Dymarski C., Litwin W.: *An experiment-based attempt to assessment of influence of surface roughness on operation of hydrodynamic water-lubricated bearing fitted with polymer bush* (in Polish). The Conference „Inżynieria Łożyskowania 2007” (Bearing Engineering 2007), Tribologia, 2007
4. Dymarski C., Litwin W.: *Influence of surface roughness of bearing bush on properties of water lubricated main shaft bearings – experimental tests*. Conference NORDTRIB 2008, Tampere, Finland, 2008
5. Litwin W.: *Calculations of water lubricated main shaft bearings – EHL model*. Conference NORDTRIB 2008, Tampere, Finland, 2008
6. Litwin W.: *The test stands for water lubricated marine main shaft bearings*. NORDTRIB 2006, Helsingor, Denmark, 2006
7. Litwin W., Dymarski Cz.: *Influence of surface roughness of bearing bush on properties of water lubricated main shaft bearings – experimental tests*. Conference NORDTRIB 2008, Tampere, Finland, 2008

CONTACT WITH THE AUTHOR

Wojciech Litwin, Ph. D.
Faculty of Ocean Engineering
and Ship Technology
Gdansk University of Technology
Narutowicza 11/12
80-952 Gdansk, POLAND
e-mail: wlitwin@pg.gda.pl

Calculation of motion trajectory and geometric parameters of the trawl during pelagic fishing

Czesław Dymarski, Prof.
Jacek Nakielski, Ph. D.
Gdansk University of Technology

ABSTRACT

This paper presents a mathematical model of the mass centre motion trajectory of the trawl, its main geometrical parameters, way of solving the model as well as its example results. It could be useful to define optimum parameters of safe, effective and environmentally friendly pelagic fishing.

Keywords: Sea fishing, trawl fishing, physical and mathematical model of trawling

INTRODUCTION

Exploitation of sea life resources undergoes continuous changes which are aimed at fish catch increase on one hand and protection of the resources and ensurance of biological balance to marine ecosystems on the other hand. Various forms of reducing unfavourable consequences of the exploitation are applied a.o. by limiting catch of particular fish kinds as well as by prohibiting application of harmful fishing techniques and preferring environmentally friendly ones. Both worldwide and domestic experience indicate that one of the most important problems is to establish rational technical solutions of exploitation of natural resources especially in the coastal areas and economical zones. In present, greater and greater impact is applied to carrying out selective fishing methods, such as set-nets, drift nets, long lines, drift lines, as well as pelagic and over-seabed trawl fishing. For coastal waters an especially harmful hazard is produced by seabed trawl fishing which results in damaging resident benthonic organisms which play an important role in sea ecosystem. Moreover in Polish coastal zones such kind of fishing produces an additional risk of catching on many obstacles sitting on the sea bed, and in consequence – damage or loss of trawls and caught fishes.

It should be stressed that condition of Polish fishing fleet is very weak today. Majority of Polish ships operating in Baltic Sea waters is in a very bad technical state and use obsolete fishing gear which makes it impossible to carry out highly effective pelagic fishing with controlled position of trawl in sea depth. To compete with fishermen of other EU countries Polish Baltic-Sea fishermen must use modern, economical and ecological ships. To meet the needs relevant research and design projects dealing with modern fishing ships, mainly intended

for individual ship owners, have been carried out by teams of Faculty of Ocean Engineering and Ship Technology, Gdańsk University of Technology, for a dozen or so years.

One of the research tasks realized in the frame of the projects is the below presented mathematical model and software for calculation of mass centre motion trajectory and geometric parameters of trawl during pelagic fishing.

ASSUMPTIONS FOR PHYSICAL MODEL OF THE TRAWL

A fishing cutter together with laid down trawl is presented in a simplified way in Fig. 1.

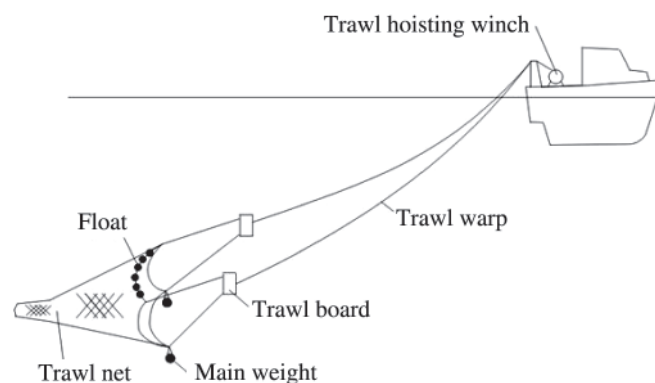


Fig.1. A simplified image of fishing trawl gear

The trawl gear is consisted of trawl warps which are wound around drums of two trawl hoisting winches. The lines go into water through pulley blocks fastened to the aft frame mast.

Deep in the water they are fixed to the trawl boards by which an appropriate divergence (width) of the trawl net is obtained. From the trawl boards four trawl legs go. Two upper ones are mutually connected through the floatline, two lower ones - through the bottom line. The side legs are connected in pairs through two side lines. To the floatline the floats are connected, due to which an appropriate floatability of the gear is obtained, and the bottom line is loaded, additionally onto the lower trawl legs the main weights are hung. Due to the buoyancy force and applied weights the trawl mouth is shaped in vertical plane. The next element of the trawl gear is its net part consisted of a few conical segments ended with a cylindrical tail into which caught fishes fall.

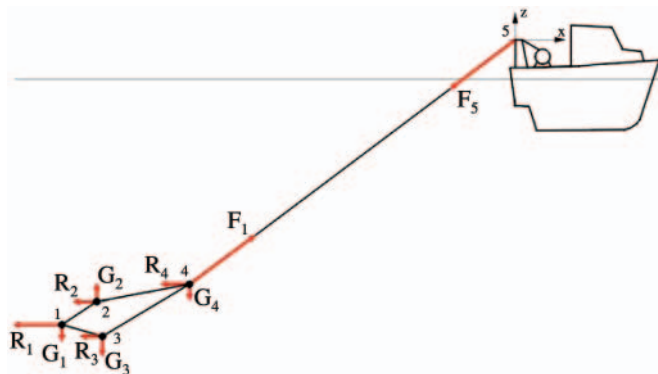


Fig. 2. Simplified model of trawl gear whose particular numbered parts are substituted by their masses concentrated in their gravity centres, namely: 1 – trawl net part; 2 – floats; 3 – weights; 4 – trawl boards; 5 – point of line run-out from the ship; G, R, F – gravity, buoyancy, drag and line stretching forces, respectively.

One of the more important problems which occur during pelagic fishing is to appropriately select operational parameters of ship and trawl winches so as to ensure keeping the trawl in operation in a given water depth. So far not many fishing ships have been equipped with instruments to control trawl position hence choice of the above mentioned parameters is mainly based on crew experience. However not always that will do. Many fishermen resign from carrying out such kind of fishing for fear of catching the trawl on various obstacles placed on the sea bottom and loss of the trawl net together with caught fishes. The situation justifies purposefulness of elaboration of a mathematical model and calculation software based on it, which could make it possible to determine trajectory of trawl motion in water during fishing, depending on main operational parameters. Exact calculation of motion trajectories of particular elements of trawl gear immersed in water is a very difficult task not only with a view of possibility of solving the complex and mutually confounded equations but also due to difficulties in defining and describing randomly changeable sea conditions. For this reason such calculations are to be performed under certain, often very far going, simplifying assumptions depending on a given aim and expected accuracy of results to be obtained, resulting from the aim. Below is presented a relatively simple model which makes it possible to determine motion trajectory of trawl gear gravity centre during fishing in waves and at changeable operational parameters of fishing ship or trawl hoisting winch.

To the model the following simplifying assumptions were introduced to describe the above presented trawl gear:

- the trawl gear is symmetrical with respect to ship plane of symmetry, that means that both trawl warps and the part of the gear, connected with them, are of identical geometric, kinematic and dynamic parameters
- the following parts of the gear, namely: trawl net, floats, weights, trawl boards and warps are assumed to be finite

material points placed vertically in estimated gravity centers of the parts

- the above specified material points have masses and drag areas equivalent to those represented by relevant parts of the gear, and they are connected each to other by means of straight line segments
- motions of the ship, trawl warp and trawl net in waves occur in vertical plane of ship symmetry
- trawl warps are assumed to be uniform, perfectly flexible and inextensible strings with taking into account their deflection due gravity and buoyancy forces and hydrodynamic interaction due to their motion in sea water
- the origin of Cartesian coordinate system is located in the point of contact of the trawl warp with ship stern in the place of going the warp down to water.

Schematic diagram of the trawl gear's physical model which satisfies the above specified simplifying assumptions, is shown in Fig. 2 and 3.

MATHEMATICAL DESCRIPTION OF THE ASSUMED MODEL

To calculate motion trajectory of the trawl gear the equations of component forces applied to its gravity centre can be described as follows:

$$Rw = \sum_{i=1}^{i=4} R_i \quad \text{- total horizontal drag force} \quad (1)$$

$$Gw = \sum_{i=1}^{i=4} G_i \quad \text{- total gravity force in sea water} \quad (2)$$

where:

$$R_i = \frac{\rho \cdot v_{ix}^2}{2} \cdot C_{ix} \cdot A_{ix} \quad (3)$$

- ρ – sea water density
- C_{ix}, C_{iz} – drag coefficients of i -th element of the trawl gear in x - and z - axis direction, respectively
- A_{ix}, A_{iz} – projected areas of i -th element in x - and z - axis direction, respectively
- G_i – weight (buoyancy) of i -th element in sea water
- v_{ix}, v_{iz} – velocity of i -th element in x - and z - axis direction, respectively:

$$v_{ix} = v_{5x} + v_1 \cdot \cos\alpha_{11} \quad (4)$$

$$v_{iz} = v_{5z} + v_1 \cdot \sin\alpha_{11} \quad (5)$$

- v_1 – velocity of running out “+” (or hauling “-”) the line by the trawl winch

$$\alpha_{11} = \arctan(Gw/Rw) \quad (6)$$

(the angle between the line and x - axis at its connection with the trawl net)

- v_{5x} – speed of the ship (and the point 5) in x – axis direction, assumed constant
- v_{5z} – speed of the ship stern (and the point 5) in z – axis direction, under the assumption that motion of the point 5 due to heave and pitch motions of ship in waves is close to sinusoidal, hence it can be described by the equations:

$$z_5(t) = a_{5z} \cdot \sin(\omega \cdot t) \quad (7)$$

$$x_5 \approx v_{5x} \cdot t \quad (8)$$

- a_{5z} – displacement amplitude of the point 5 in z - axis direction

$$\omega = 2 \cdot \pi / T \quad (9)$$

where:

T – ship pitch period
t – time.

Calculation of shape of the trawl warp in vertical plane was performed by using the numerical method in accordance with the model presented in Fig. 3.

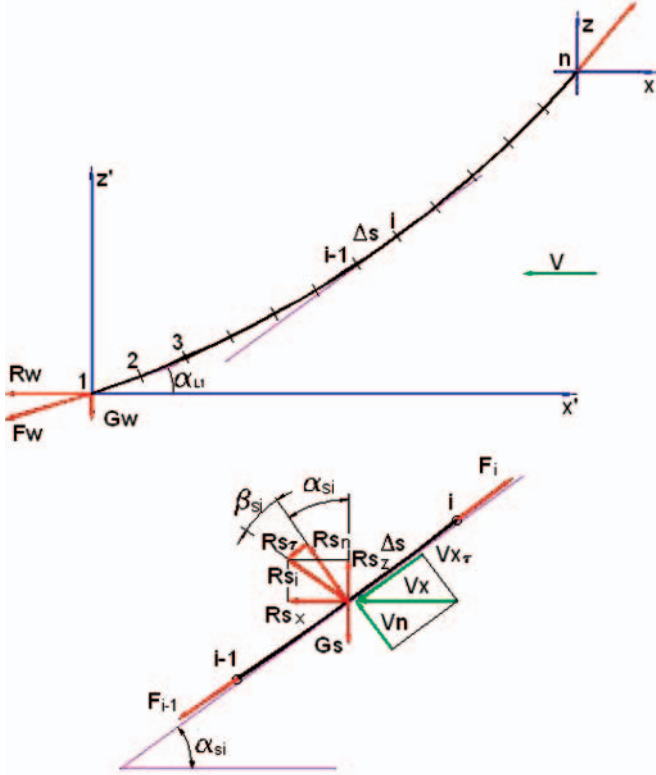


Fig. 3. Simplified model of shape of the trawl warp (line), taken to numerical calculations

The force in the end of the trawl warp at the point of its connection with the trawl body is equal to:

$$F_w = F_{l1} = \sqrt{R_w^2 + G_w^2} \quad (10)$$

and, in an arbitrary point of the line it can be calculated from the relation:

$$F_i = F_{i-1} + \Delta F_i \quad (11)$$

where:

$$F_{i-1} = F_w + \sum_{k=2}^{i-1} \Delta F_{lk} \quad (12)$$

$$\Delta F_i = \sqrt{R_{s_{xi}}^2 + (G_s - R_{s_{zi}})^2} \quad (13)$$

G_s – weight of the calculated segment of the line in sea water

$$R_{s_{xi}} = R_{s_i} \cdot \sin^2(\alpha_{si} + \beta_i) \quad (14)$$

$$R_{s_{zi}} = R_{s_i} \cdot \cos^2(\alpha_{si} + \beta_i) \quad (15)$$

α_{si} – average slope angle of the calculated segment of the line, calculated from the following interpolation:

$$\alpha_{si} = 1.5 \cdot \alpha_{i-1} - 0.5 \cdot \alpha_{i-2} \quad (16)$$

$\alpha_{i-1}, \alpha_{i-2}$ – slope angles of the line in the points $i-1$ and $i-2$, respectively

$$\beta_{11} = \arctan(R_{s_{ci}} / R_{s_{ni}}) \quad (17)$$

$$R_{s_i} = \sqrt{R_{s_{ni}}^2 + R_{s_{ci}}^2} \quad (18)$$

(resultant drag force of the calculated segment of the line)

$$R_{s_{ni}} = 0.5 \cdot C_n \cdot \rho \cdot v_x^2 \cdot d \cdot \Delta S \cdot \sin^2 \alpha_{si} \quad (19)$$

(drag force of the calculated segment of the line in the direction perpendicular to it)

$$R_{s_{ci}} = 0.5 \cdot C_\tau \cdot \rho \cdot v_x^2 \cdot d \cdot \Delta S \cdot \cos^2 \alpha_{si} \quad (20)$$

(drag force of the calculated segment of the line in the direction parallel to it)

where:

C_n – drag coefficient of the line in the direction perpendicular to it

C_τ – drag coefficient of the line in the direction parallel to it

d – diameter of the line

ΔS – length of the elementary (calculated) segment of the line.

Coordinates of an arbitrary point i of the trawl warp relative to the point of its connection with the trawl body were determined from the following relations:

$$x_i^I = x_{i-1}^I + \Delta S \cdot \cos \alpha_{si} \quad (21)$$

$$z_i^I = z_{i-1}^I + \Delta S \cdot \sin \alpha_{si} \quad (22)$$

and the slope angle of the line – from the interpolation formula:

$$\alpha_{li} = \alpha_{li-1} + 2 \cdot (\alpha_{si-1} - \alpha_{li-1}) = 2 \cdot \alpha_{si-1} - \alpha_{li-1} \quad (23)$$

Any motion of the point 5 in z -axis direction will produce definite changes in loads in the line and displacements of the gravity centre of the trawl gear. The equation of forces acting on the trawl gear in z -axis direction takes the following form:

$$m \frac{d^2 z}{dt^2} = mg - F_z - \frac{\rho}{2} \left(\frac{dz}{dt} \right)^2 \cdot \sum_{i=1}^{i=4} (C_{iz} \cdot A_{iz}) \quad (24)$$

where:

$$m = \sum_{i=1}^{i=4} m_i \quad (25)$$

(total mass of the trawl gear elements in sea water)

$$z = -z_n^I \quad (26)$$

(vertical coordinate of the trawl gear gravity centre, relative to the point 5)

$$l = l_0 + v_1 \cdot t \quad (27)$$

(current length of the run-out trawl warp)

$$F_z = R \cdot \operatorname{tg} \alpha_{11} \quad (28)$$

(vertical force component in the line, acting on the trawl gear)

To solve the differential equations Runge-Kutta method was used. At first the following substitution was introduced:

$$y = \frac{dz}{dt} \quad (29)$$

On substitution of Eq. (29) to Eq. (24) and appropriate transformations the following was obtained:

$$\frac{dy}{dt} = g - \frac{\rho}{2 \cdot m} \cdot \sum_{i=1}^{i=4} (C_{ix} \cdot A_{ix} \cdot v_{ix}^2) \cdot \operatorname{tg} \alpha_{i1}(t) +$$

$$- \frac{\rho}{2 \cdot m} \left(\frac{dz}{dt} \right)^2 \cdot \sum_{i=1}^{i=4} (C_{iz} \cdot A_{iz}) \quad (30)$$

The calculation process was realized by applying a constant time step and assuming the results of the preceding step to be initial value for the successive calculation step.

To calculate geometric parameters of the trawl gear in steady operational conditions the above given mathematical description was supplemented by the following additional relations to which the notations complying with Fig. 4 were introduced:

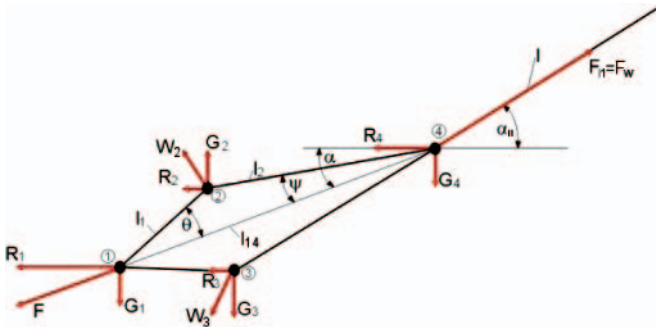


Fig. 4. Simplified model of the trawl gear, with indicated load vectors and main geometric parameters

$$\theta = \arctan \left(\frac{2 \cdot (G_2 \cdot \cos \alpha + R_2 \cdot \sin \alpha)}{\sqrt{R_1^2 + G_1^2}} \right) \quad (31)$$

In the first calculation step:

$$\alpha = \alpha_1$$

$$\psi = \arcsin \left(\frac{l_1}{l_2} \cdot \sin \theta \right) \quad (32)$$

If the above mentioned angles and the line length is known it is possible to determine coordinates of gravity centers of particular parts of the trawl gear, namely:

$$x_4 = -x_n^I \quad (33)$$

$$z_4 = -z_n^I \quad (34)$$

$$x_3 = x_4 - l_2 \cdot \cos(\alpha + \psi) \quad (35)$$

$$z_3 = z_4 - l_2 \cdot \sin(\alpha + \psi) \quad (36)$$

$$x_2 = x_4 - l_2 \cdot \cos(\alpha - \psi) \quad (37)$$

$$z_2 = z_4 - l_2 \cdot \sin(\alpha - \psi) \quad (38)$$

$$x_1 = x_4 - l_1 \cdot \cos \theta - l_2 \cdot \cos \psi \quad (39)$$

$$z_1 = z_4 - l_1 \cdot \sin \theta - l_2 \cdot \sin \psi \quad (40)$$

Then, for the so determined geometry of the gear the moment in the point 4, which tends to rotate the gear with respect to the point, is calculated.

$$M_4 = G_1 \cdot l_{14} \cdot \cos \alpha + G_2 \cdot l_2 \cdot \cos(\alpha - \psi) +$$

$$+ G_3 \cdot l_4 \cdot \cos(\alpha + \psi) - R_1 \cdot l_{14} \cdot \sin \alpha +$$

$$- R_2 \cdot l_2 \cdot \sin(\alpha - \psi) - R_3 \cdot l_4 \cdot \cos(\alpha + \psi) \quad (41)$$

$$l_{14} = l_1 \cdot \cos \theta + l_2 \cdot \cos \psi \quad (42)$$

In the case when a calculated value of the moment is greater than an assumed accuracy, for the next calculation step a little greater or smaller value of the angle α is taken, depending on sign of the moment. When a sufficiently accurate result is achieved the coordinates of the points 1 through 4 and then the moment relative to the point 5 are calculated for the new geometry of the trawl gear.

$$M_5 = G_1 \cdot (l_{1-4} \cdot \cos \alpha + x_4) + G_2 \cdot [l_2 \cdot \cos(\alpha - \psi) + x_4] +$$

$$+ G_3 \cdot [l_4 \cdot \cos(\alpha + \psi) + x_4] + G_4 \cdot x_4 +$$

$$- R_1 \cdot (l_{1-4} \cdot \sin \alpha + z_4) - R_2 \cdot [l_2 \cdot \sin(\alpha - \psi) + z_4] +$$

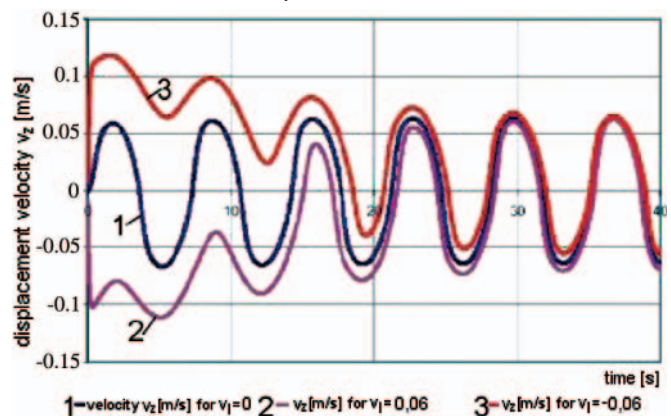
$$- R_3 \cdot [l_4 \cdot \cos(\alpha + \psi) + z_4] - R_4 \cdot z_4 \quad (43)$$

Like before, the angle α_{i1} will be corrected depending on value and sign of the moment until its values in successive iteration steps are sufficiently accurate.

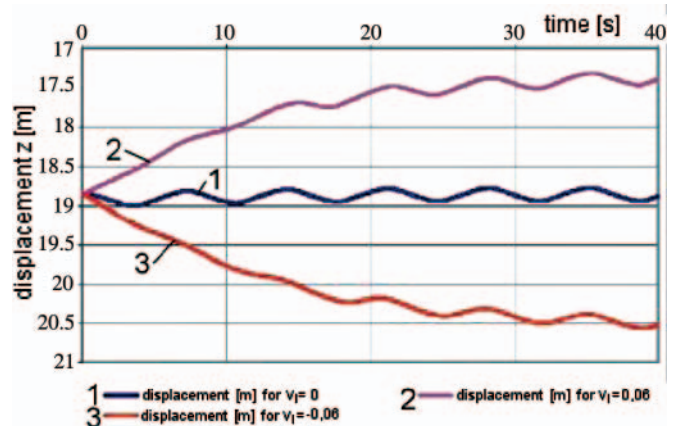
The computer software in question was written in Fortran programming language to make it possible to carry out calculations in various working conditions.

RESULTS OF NUMERICAL SIMULATIONS

Below are presented example results of the calculations of the trawl gravity centre motion trajectory, performed for the following operational conditions: $v_s = 1.5$ m/s; $l = 300$ m; $a_0 = 0.5$ m; $T = 7$ s; $C_n = 1.2$; $C_t = 0.02$; $d = 0.01$ m and three values of rope velocity: $v_1 = 0$; 0.06 ; and -0.06 m/s.



Diag. 1. Diagram of trawl displacement velocity for the parameters: $v_s = 1.5$ m/s; $l = 300$ m; $a_0 = 0.5$ m and $T = 7$ s.



Diag. 2. Diagram of trawl displacement for the parameters: $v_s = 1.5$ m/s; $l = 300$ m; $a_0 = 0.5$ m and $T = 7$ s.

The oscillations of the trawl gear gravity centre of for 300 m length of the laid-down line and the trawling speed of 1.5 m/s, amount to 0.226 m and along with the increasing of trawling speed

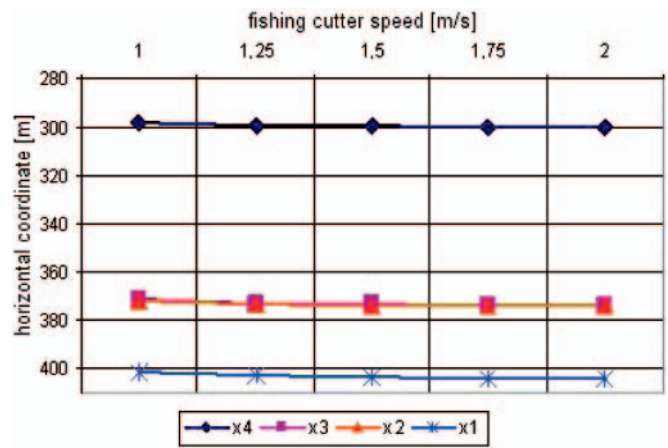
they maintain on similar level. And, the displacement velocity of the gravity centre amounts to $v_z = \pm 0.06$ m/s on average. In the case of decreasing the initial length of the laid-down line the mean value of oscillation amplitude increased up to 0.289 m and the displacement velocity was equal to almost ± 0.09 m/s.

It should be also observed that for 300 m length of the laid-down line, for the first several seconds (one period) after switching the winch on line hauling mode, the „flattening” of the displacement characteristics occurs at simultaneous deviation of its mean value. The emerging of the trawl occurs relatively fast at simultaneous insignificant increasing the amplitude of oscillation, and an increase of its draught with accompanying decrease of the oscillation amplitude takes place during laying down the line. The trawl velocity v_z , after starting the winch and transient disturbances resulting from that, tends to be close to the initial velocity except that, as expected, oscillation amplitude value increases in the case of hauling the line and decreases during laying down the line. The increasing of trawling speed or decreasing of length of the laid-down line does not cause any distinct intensification of the above mentioned phenomena.

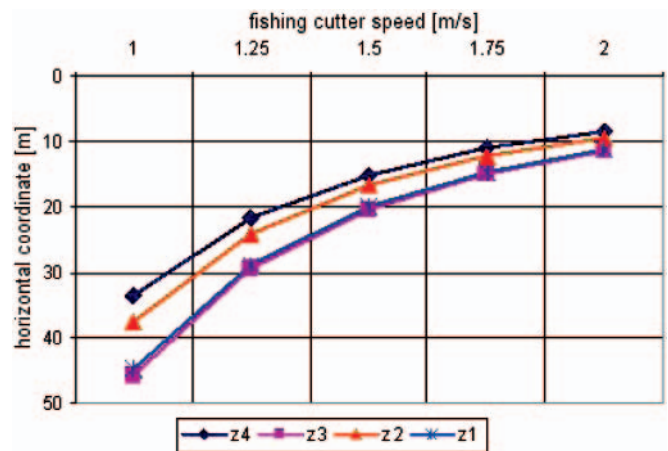
Below in Tab. 1. and the diagrams are presented example results of the numerical calculations performed for two values of the laid-down line length $l = 300$ m and 150 m as well as five values of the ship speed $v_s = 1; 1.25; 1.5; 1.75$ and 2 m/s.

Tab. 1. Results of the simulations

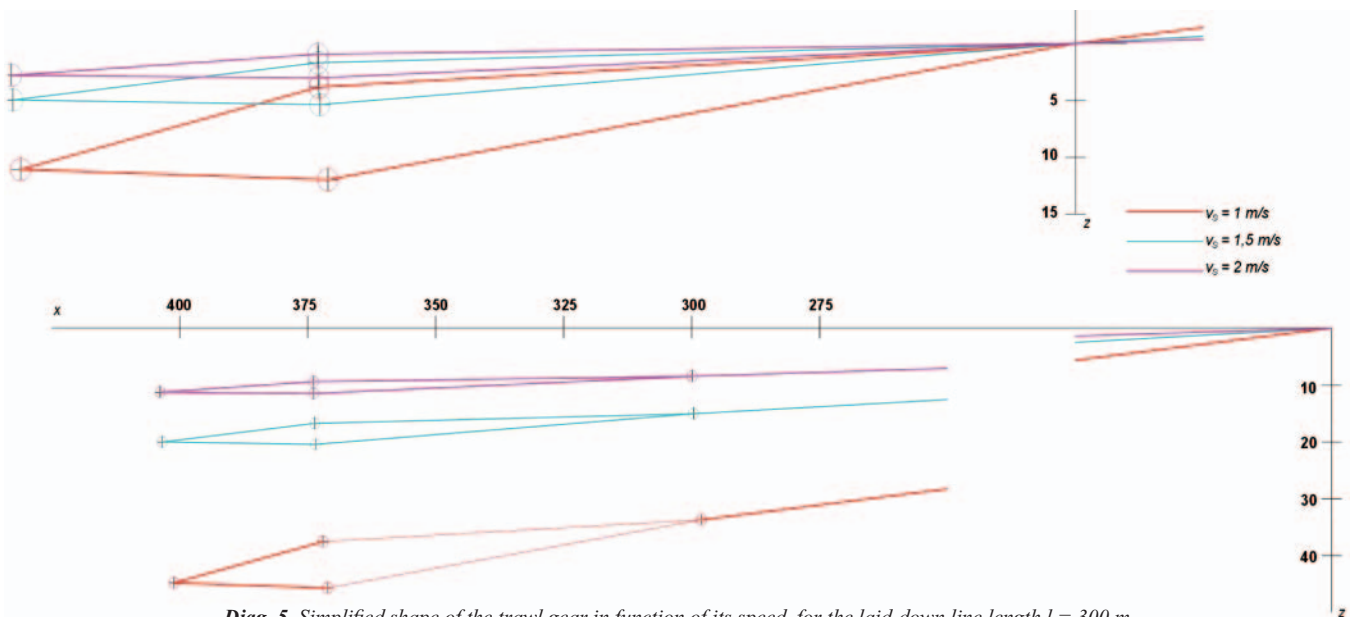
v_x [m/s]	l [m]	α_1 [°]	α [°]	θ [°]	ψ [°]
1	300	6.451	6.138	7.834	3.168
1	150	6.451	5.958	7.834	3.168
1.25	300	4.139	3.941	5.064	2.051
1.25	150	4.139	3.827	5.064	2.051
1.5	300	2.877	2.740	3.530	1.430
1.5	150	2.877	2.661	3.530	1.430
1.75	300	2.114	2.014	3.597	1.053
1.75	150	2.114	1.956	3.597	1.053
2	300	1.619	1.543	1.990	0.807
2	150	1.619	1.498	1.990	0.807



Diag. 3. Calculated values of the horizontal coordinate x of the points 1 ÷ 4 for $l = 300$ m and $v_s = 1 \div 2$ m/s.



Diag. 4. Calculated values of the vertical coordinate z of the points 1 ÷ 4 for $l = 300$ m and $v_s = 1 \div 2$ m/s.



Diag. 5. Simplified shape of the trawl gear in function of its speed, for the laid-down line length $l = 300$ m

FINAL COMMENTS

- The elaborated, relatively simple model of the trawl gear as well as calculation software make it possible to determine the gravity centre motion trajectory of the trawl gear immersed in sea water, depending on the main operational parameters such as: ship speed, speed of hauling or laying-down the line by trawl winches, length of the laid-down line as well as amplitude and period of ship stern displacements.
- The model makes it possible also to determine position of the trawl gear main parts as well as divergence (width) of the trawl mouth for definite values of the main design and operational parameters of the gear. This is as much important that the so obtained data can be used during performance of fishing. By appropriate selecting the operational parameters a current position of the trawl and its mouth width can be adjusted to a localized fish shoal, moreover any danger of catching the trawl on underwater obstacles can be avoided this way.

BIBLIOGRAPHY

1. Bessomneau J.S., Marichel D.: *Study of the dynamics of submerged supple nets (application to trawls)*. Ocean Engineering, 25, 1998
2. Bielański J.: *The analysis of the system towing rope with long underwater object*. Hydroacoustics, 9, Gdańsk 2006
3. Brewek D., Eayrs S., Mounsey R., You-Gan W.: *Assessment of an environmentally friendly, semipelagic fish trawl*. Fisheries Research, 1996
4. Chun-Woo L., Ju-Hee L., Bong Jin Ch., Hyun-Young K.: *Physical modeling for underwater flexible systems dynamic simulation*. Ocean Engineering, 32, 2005
5. Erinfolami L. A.: *Investigations of interaction between ship power system and fishing trawl gear* (in Polish). Doctor thesis, Gdańsk University of Technology, Gdańsk, 2000
6. Huang S.: *Dynamic analysis of three-dimensional marine cables*. Ocean Engineering, 21, 1994
7. Moderhak W.: *A calculation method of total hydrodynamic drag of the pelagic trawl net* (in Polish). Doctor thesis, Gdańsk University of Technology, Gdańsk 1991
8. Piechna J. R.: *Programming in the language Fortran 90 and 95* (in Polish). Publishing House of Warsaw University of Technology (Oficyna Wydawnicza Politechniki Warszawskiej), Warszawa 2000
9. Pogański Z.: *Prospects for Baltic Sea fishery* (in Polish). Nautologia, 2, Gdynia 1998
10. Wu J., Chwang A. T.: *A hydrodynamic model of a two-part underwater towed system*. Ocean Engineering, 27, 2000
11. Wu J., Chwang A. T.: *Experimental investigation on a two-part underwater towed system*. Ocean Engineering, 28, 2001

CONTACT WITH THE AUTHORS

Czesław Dymarski, Prof.
Jacek Nakielski, Ph. D.
Faculty of Ocean Engineering
and Ship Technology,
Gdańsk University of Technology
Narutowicza 11/12
80-952 Gdańsk, POLAND
e-mail: cpdymars@pg.gda.pl

Position accuracy evaluation of the modernized Polish DGPS

Marek Dziewicki, M. Sc.
Maritime Office Gdynia
Cezary Specht, Assoc. Prof.
Polish Naval Academy

ABSTRACT

Polish Maritime DGPS system has been modernized to meet the requirements set out in IMO resolution for a future GNSS, but also to preserve backward signal compatibility of user equipment. Having finalized installation of the new technology L1, L2 reference equipment performance tests were performed. This paper presents results of the long-term signal measuring campaign of the DGPS reference station Rozewie, which was performed in July 2009. Final results allowed to verify repeatable and absolute accuracy of the system after the modernization. Obtained statistics were compared to past measurements performed in 2005 when previous system infrastructure was in operation.

Keywords: radionavigation; DGPS position; DGPS transmission; accuracy evaluation; static position measurement; absolute accuracy; scatter plot; DGPS monitoring; ellipsoid transformation

INTRODUCTION

Maritime DGPS system was developed to provide position and integrity information to maritime users. This service based on reference stations and MF radio beacons can distribute differential GPS corrections to increase position accuracy, distribute integrity warning to satisfy navigation requirements in coastal navigation and hydrographic survey.

The first Polish DGPS station was established by Polish Hydrographic Office in 1994, finally the system was composed of two independent maritime reference stations located in Rozewie and Dziwnów and common control station in Gdynia. Both RS stations equipped with local integrity monitors were remotely controlled by PSTN network. Due to common research projects performed by Polish Naval Academy and Maritime Office Gdynia, the infrastructure of the system was gradually improved. Tests had mainly been focused on coverage, accuracy and availability of beacons' signals. Then hardware and software of the system have been entirely modernized in 2007, by replacing obsolete L1 code receivers with new type L1, L2 as well as a set of new technology antennas.

DGPS-PL NETWORK

National radio-navigation policy assessed the current and potential use of the DGPS in navigation, therefore concluded that there was a requirement to improve functionality while modernized. It was evident, that any new approaches that could meet higher requirements and provide enhanced services, had to

preserve backward compatibility of existing users' equipment. According to IALA recommendation [IALA 2006], the baseline principles for the re-capitalization of the Polish DGPS system were as follows:

- backward compatibility with legacy signals
- solution supported by international standards
- flexibility for future service requirements
- long life-time.

Polish DGPS system has been modernized during the last two years (2007-8) to meet the requirements set out in IMO Resolution A.915(22) to contribute to the provision of navigational and engineering position-fixing, including navigation in harbour entrances, port approaches and other congested waters. The hardware RSIM solution has been adopted for the re-capitalization on grounds of market availability and lowest cost.

A conception of communication in the system (Fig. 1) is based on operation of reference stations (RS) and far field remote integrity monitors (IM) via IT network, continuously controlled by a Control Station.

There are two reference stations: RS Dziwnów – at west coast, and RS Rozewie at north-east, coast, has been equipped with local integrity monitors (RSIM model). Both sites are being under permanent control of Control Station in Gdynia, where a dedicated server continuously gathers operational information from all RS sites and remote integrity monitors. Thus a living data base of system performance is available there in real time.

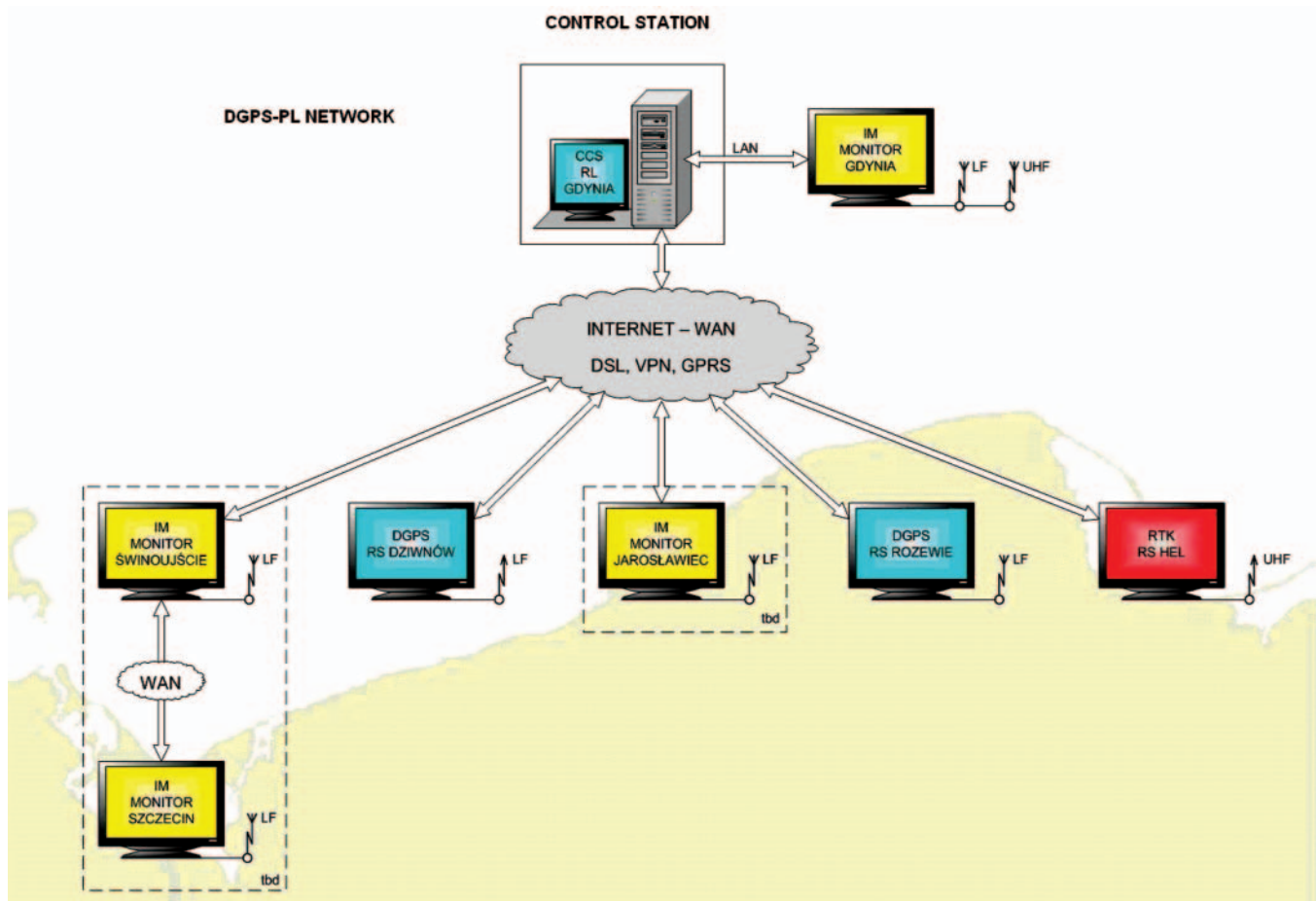


Fig. 1. Block diagram of modernized Polish DGPS and RTK network [1]

SYSTEM COMPONENTS AND PERFORMANCE

Both reference beacon stations Dziwnów and Rozewie are equipped with local PCs remotely operated and controlled via wide area network from Control Station located in Gdynia. Quality of DGPS broadcast is being checked and evaluated by local integrity monitors (IM) and one remote LF DGPS monitor in Gdynia port. The corrected DGPS position accuracy is limited by the quality of the position information of the reference points. For high precision applications, the reference antenna should have a stable center (electrical center of the antenna) and should not be affected by reflected signals (multipath mitigation) and/or radio interference (jamming resistance). To overcome these problems a choke -ring antennas were installed which performance is particularly effective in reducing the effects of multipath. Daily reports and data on availability of the signal are gathered by local PCs then can be transferred to the data base of Control Station in Gdynia.

To ensure signal availability at required level of 99,5% for a single site beacon station, a redundancy of major functions is fundamental, so that station will continue uninterrupted work in case of a single hardware failure. Therefore, main blocks of each RS beacon station are doubled. It contains two independent reference L1, L2 receivers, two MSK modulators and dual MF beacon transmitters. Station integrity is under control of single local integrity monitor (L1 DGPS receiver) plus one broadcast station controller – a high end industrial PC well equipped with multiport cards. Each reference station includes a UPS and a telecommunication equipment: DSL modem, router, network switch. It was recognised that certain reference station and integrity monitor threshold settings are vital to the proper performance of the RS station. A list of parameters and recommended range of settings can be found in IALA recommendation [IALA 2004]. The set of RTCM messages and frequencies being broadcast from Polish DGPS beacon stations is shown in Table 1. The local integrity monitor tests the quality of the own beacon transmission by

Tab.1. Polish DGPS characteristics

Table of DGNSS Stations			Country: POLAND		Date of last amendment: July 2009			
Station name	Identification Nos		Geographical Position Lat/ Lon	Station in operation	Integrity Monitoring	Transmitted message types	Freq (kHz)	Bit Rate (bps)
	Reference Station(s)	Transmitting Station						
Dziwnów	741 742	481	54°01' N 14°44' E	yes	yes	9,3,7,16	283.5	100
Rozewie	743 744	482	54°49' N 18°20' E	yes	yes	9,3,7,16	301.0	100

receiving and applying own corrections. The IM software continuously monitors position accuracy, signal availability, every single tracked satellite, GPS geometry, RTCM data correctness and quality, as well as transmitted signal strength (SS, SNR). When any 'alarm condition' is detected, an alarm message is immediately set for local response and switching to optional station (secondary configuration) can happen. In case of integrity alarm – a warning message will automatically be broadcast to all users/ships in the area within time of 10s.

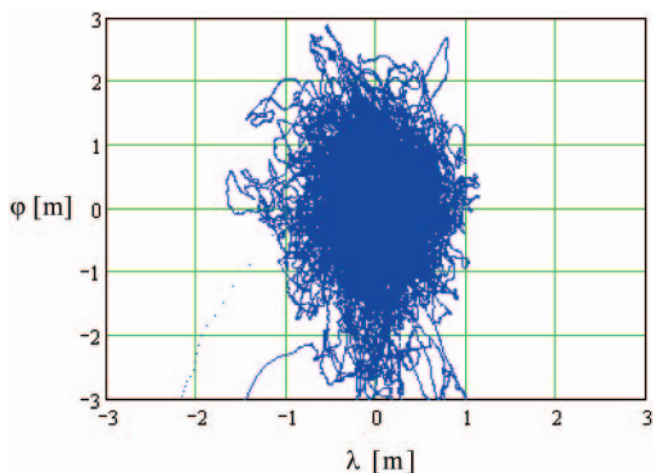
SYSTEM ACCURACY EVALUATION

In order to evaluate new characteristics of the modernized DGPS system, a measurement campaign took place over the time span between 30th of June and 26th August 2009. Pseudorange (PRC) corrections type 9-3 broadcasted from DGPS reference station Rozewie were received and recorded by a single frequency (L1) receiver installed in Gdynia, 40 km from the transmitting MF beacon. These tests were focused on evaluation of horizontal and vertical accuracies of the 3D position. Results were based on long term observations (26 days) registered with 10s sampling rate. Data files were containing position time series in the format of NMEA 0183 standard, GGA referenced to WGS-84 datum (a = 6378137.00 m, b = 6356752314 m). The reference point for the receiver was set in the Port of Gdynia with coordinates: 54 31.75524 N, 18 33.57418 E, H = 68.07 m. The previous one (in 2005) was installed almost at the same position. Obtained results (statistics) has been compared to ones performed in 2005 [4].

Let's define an absolute accuracy as a the statistical difference between position measurements and a surveyed benchmark for any point within the service volume over a specified time interval [SPS 2001]. When there is no information about surveyed coordinates the statistics could be related to estimated (average) position (repeatable accuracy).

Measured ellipsoidal coordinates were transformed to Gauss-Kruger (X,Y) conformal coordinates: based on relations; [2,3,5]

$$Y = R \cdot \left[dL \cos(B) + \frac{dL^3}{6} \cos(B)^3 (1 - t^2 + \eta^2) + \frac{dL^5}{120} \cos(B)^5 (5 - 18t^2 + t^4 + 14\eta^2 - 58\eta^2 t^2) \right] \quad (1)$$



$$X = k \cdot R \left[\frac{S(B)}{R} + \frac{dL^2}{2} \sin(B) \cos(B) + \frac{dL^4}{24} \sin(B) \cdot \cos(B)^3 (5 - t^2 + 9\eta^2 + 4\eta^4) + \frac{dL^6}{720} (\sin(B) \cos(B)^5) \cdot (61 - 58t^2 + t^4 + 270\eta^2 - 330\eta^2 t^2) \right] \quad (2)$$

where:

- B, L – measured ellipsoidal DGPS coordinates (ref. WGS-84)
- R – radius of curvature in the prime vertical
- S(B) – distance from the equator to defined coordinate B
- dL – difference in longitude between L and prime meridian
- k = 0.999923 – scale factor.

Others parameters could be calculated as:

$$t = \operatorname{tg}(B) \quad (3)$$

$$\eta = \frac{e^2 \cos(B)^2}{1 - e^2} \quad (4)$$

where:

- e – eccentricity of ellipsoid
- η – orientation angle of distortion ellipsis.

All calculations were realized in Mathcad, software version 13.1. Drawings below present scatter plots of the position solution for DGPS relative to past and current status. These fixes are presented with reference to average position (average latitude and average longitude).

Figure 3 presents a comparison of the time series of position errors measured during these two campaigns.

Cumulative statistics of accuracies are presented in tables no. 2 and 3.

The same analysis was done for the absolute accuracy – but relative to true (surveyed) coordinates of reference point. (Tab. 3).

Final analysis was done regard to vertical position error - see fig. 4.

Table no. 4 presents final statistics of the measurements realized for both campaigns.

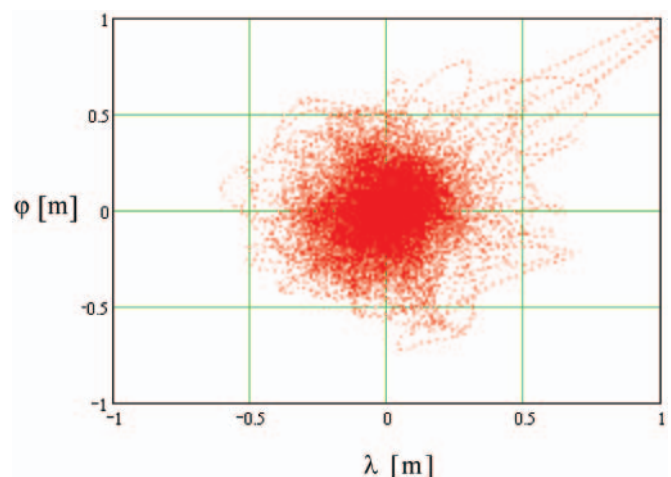


Fig. 2. Scatter plots relative to average position (left - previous, 2005, right - current, 2009)

Tab. 2. Statistic of position repeatable accuracy - results of the Rozewie DGPS station before May 2005 and after modernization (September 2009)

Repeatable Accuracy	Rozewie DGPS before modernization			Rozewie DGPS after modernization		
	rms (p = 0.68) [m]	2rms (p = 0.95) [m]	95 % population [m]*	rms (p = 0.68) [m]	2rms (p = 0.95) [m]	95 % population [m]*
3D position error	1.757	3.515	3.055	0.402	0.804	0.737
2D position error	1.0202	2.040	1.769	0.210	0.420	0.385
1D- Longitude error	0.6204	1.240	1.244	0.127	0.254	0.247
1D- latitude error	0.809	1.619	1.540	0.167	0.334	0.341

Columns rms and 2rms in table 2 assume Gaussian error distribution, while column "95% population" represents measured error value calculated by sorting a population of error values from minimum to maximum.

Tab. 3. Statistic of position absolute accuracy - results of the Rozewie DGPS station before (May 2005) and after modernization (September 2009)

Absolute Accuracy	Rozewie DGPS before modernization			Rozewie DGPS after modernization		
	rms (p = 0.68) [m]	2drms (p = 0.95) [m]	95 % population [m]*	rms (p = 0.68) [m]	2rms (p = 0.95) [m]	95 % population [m]*
3D position error	1.757	3.515	3.039	0.402	0.804	1.204
2D position error	1.020	2.040	1.787	0.210	0.420	0.398
1D- Longitude error	0.620	1.240	1.245	0.167	0.334	0.344
1D- latitude error	0.809	1.619	1.549	0.127	0.254	0.270

Columns rms and 2rms in table 2 assume Gaussian error distribution, while column "95% population" represents measured error value calculated by sorting a population of error values from minimum to maximum.

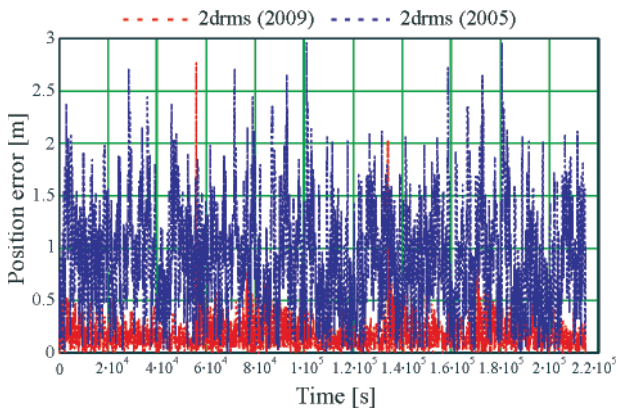


Fig. 3. DGPS position error (2D) as a function of time

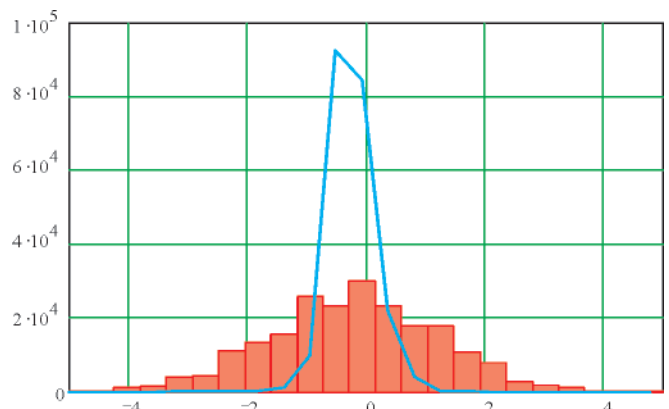


Fig. 4. Histograms of the DGPS vertical position errors measured in 2005 (red) and 2009 (blue) calculated for 2.15.000 position fixes

Tab. 4. Statistics of vertical accuracy results

Type of the accuracy	DGPS before (May 2005)			DGPS after (September 2009)		
	rms (p = 0.68) [m]	2rms (p = 0.95) [m]	95 % of population [m]	rms (p = 0.68) [m]	2rms (p = 0.95) [m]	95 % of population [m]
Repeatable	1.431	2.862	2.834	0.343	0.686	0.674
Absolute	1.433	2.866	2.800	0.341	0.682	1.200

Absolute error of DGPS corrected position estimated by long term static observations allows to calculate error vector between estimated (average) and surveyed position. For 2005 year campaign the differences in 3D cartesian frame were as: $dX = 0.0445$ m, $dY = -0.162$ m and $dZ = 0.034$ m. The same values for present (2009) status are: $dX = 0.013$ m, $dY = -0.046$ m, $dZ = 0.574$ m.

CONCLUSIONS

- Evaluation of the DGPS system was performed to gain a statistical comparison of signal quality before 2005 and current operation. Static test of repeatable and absolute position accuracy was done for the Rozewie reference station.
- It should be noted that 95% current 2D positions calculated was closer to the reference point then 0.42 m.
- Repeatable and absolute accuracies are nearly the same.
- In comparison to former system operation the position error is about 5 times less.
- An absolute error of 2D position was estimated to be 0.047 m.
- Vertical error distribution is shown in fig.4. In comparison to former results (2005), it is also more than 4 times closer to the reference point. However, there is a significant error in absolute vertical error component Z (height): 0.57 m. It is very likely, it happened due to a survey error of the reference point position, which should be checked.

In conclusion, it should be noted that DGPS corrections' quality of the modernized DGPS system was analytically proved to be better then the former one.

BIBLIOGRAPHY

1. Dziewicki M.: *Modernization Of Maritime DGPS in Poland*, TransNav'2009 Conference, Maritime Academy in Gdynia, 2009
2. IALA, Recommendation R-121: *Recommendation on the Performance and Monitoring of DGNSS Services in the Frequency Band 283.5 – 325 kHz*, June 2004
3. IALA, Recommendation R-135: *On The Future of DGNSS, Edition 1*, December 2006
4. Specht C.: *DGPS and EGNOS Systems in Hydrographic Survey – Accuracy Analyses at the Polish Sea Area*, Annual Journal of Hydroacoustics, Committee on Acoustics of the Polish Academy of Sciences, Volume 10, May 2007
5. SPS, Global Positioning System Standard Positioning Service, Performance Standard, Assistant Secretary of Defense, October 2001.

CONTACT WITH AUTHORS

Marek Dziewicki, M. Sc.
Maritime Office Gdynia,
Chrzanowskiego 10
81-338 Gdynia, POLAND
e-mail: marekdz@umgdy.gov.pl

Cezary Specht, Assoc. Prof.
Polish Naval Academy,
Smidowicza 69
81-103 Gdynia, POLAND
e-mail: c.specht@geodezja.pl

On the adaptation of CAN BUS network for use in the ship electronic systems

Andrzej Piętak, Assoc. Prof.
Maciej Mikulski, M. Sc.
University of Warmia and Mazuria in Olsztyn

ABSTRACT

This paper presents an analysis of application of the CAN - based marine electronics standard NMEA 2000, recently developed one, on board sea-going vessels, especially in the context of small, recreational, sailing and motor craft. The idea and development of the system has been briefly presented. The properties of the CAN network has been described and the use of its functions by the NMEA system, discussed. The discussion has been performed for all layers of the communication protocol, according to the Open Systems Interconnection Reference Model worked out by ISO. All the features have been summarized and analyzed in the context of their possible use in various shipboard systems.

Keywords: controlled area network; CAN; CAN BUS; linear network communication; NMEA2000 standard; NMEA 2000 network

INTRODUCTION

In the beginning phase of ship electronics development, each device was an entirely independent unit. Devices such as electronic log, echo sounder or gyrocompass were carrying out their own tasks, being not connected to other instruments. With the development of new technologies it soon became clear that it is crucial for the separate devices to communicate with each other. Introduction of autopilot required to get a signal from gyrocompass and so on. Some producers have introduced their own devices to connect the systems [1,2]. With the development of digital techniques the need of standardization of the communication protocol used by the navigational devices became obvious. The breakthrough came in the year 1980 when the NMEA (National Marine Electronics Association) introduced the NMEA0180 standard. For the following years the standard was being improved. The NMEA0183 standard introduced in 1983 incorporated radical changes in the system which enabled the mutual communication between virtually each device of a vessel's electronics, and also easy exchange of data with PC computer. The NMEA0183 standard, with the passage of years, has undergone significant evolution, and operation of new devices has been added. Towards the end of the 20th century the contemporary standard turned out to be insufficient. The NMEA0183, in principle, provides the linear data transfer only from the transmitter to several receiving devices (the so-called 'listeners'). The progressing strong integration of the on-board systems results in that the modern maritime electronic equipment requires data coming from many sources. Without a network standard which would enable such integration of data, the equipment producers have to provide several inputs or introduce such solutions which

accumulate data from several transmitting devices into one channel. The first solution is connected with a higher cost and additional complication in wiring system. On the other hand the NMEA0186 protocol operating with the speed of 4800 bit/s, is able to provide approximately 10 sentences per second, which is absolutely sufficient when one device transmits, but it fails when the system starts to join the data.

The new standard of the linear network communication - NMEA2000 worked out in 2001 by the National Marine Electronics Association, in which the integrated circuits of the CAN network (Controlled Area Network) is used, was the answer to the growing expectations dealing with joining and exchange of data among the electronic ship devices. The CAN has been originally worked out for the car industry but due to its easy access and low price of the components, is now currently applied in many industrial branches. The standard is becoming more and more popular. The reputable producers of navigational equipment have started to introduce products ready to cooperate with the NMEA2000 network, onto the market. The first applications of the standard have appeared not only in the elaborate on-board systems of big vessels but also in the projects of navigational and propulsion systems of small recreational crafts. Despite the growing interest of the marine equipment producers, the knowledge concerning the new system seems to be not wide-spread especially as far as its use in the yacht industry has been concerned. Also the literature on the standard in question as well as on the possibilities of using the well-known CAN main technology in the electronic systems of small vessels is very scarce. Thus, it seems reasonable to provide a wider commentary on both the systems (i.e. the NMEA2000 and CAN BUS) and to research the legitimacy of using them, especially in the aspect of recreational motor and sailing vessels.

THE NMEA2000 STANDARD

The NMEA 2000 is a cheap linear communication network which operates with the speed of 250 kbit/s using the integrated circuits of the CAN network. The main difference between the NMEA 2000, and the earlier standard, NMEA 0183, apart from the transmission speed (of 4.7 kbit/s for NMEA 0183), is that the first constitutes the whole network of data exchange, and the second one is only the communication protocol. The NMEA 2000 network, unlike preceding standards, enables connecting many electronic devices through one communication channel in which several devices may transmit the data simultaneously. Like the NMEA 0183, the NMEA 2000 introduces standard definitions and formats of a message, but in addition, it provides broader terms of managing the network, device identification, sending the commands and receiving the data. Just as in the case of any network communication, joint between the central units takes place through the solitary lead, which considerably simplifies the installation and lowers its cost in the case of more elaborated systems. In the system, data are transferred in the form of data frames with reserved bits in order to identify and detect errors and confirm the receiving of a message. Each frame consists of 8-byte data space and 29-byte identification field which determines the priority of a message and identifies the broadcasting and receiving element in the network. As only a small part of the frame is allotted to the data, the standard is mainly intended for the transmission of short messages but, owing to the advanced error control, with a high level of reliability. Messages may be transmitted periodically, sent only in given circumstances or at the request of given receivers.

In accordance with the Open Systems Interconnection Reference Model (OSI model) worked out by ISO, [3], the NMEA 2000 standard defines all the layers (the OSI model is based on the seven-layer organization of the communication protocol) essential for proper operation of a network standard, in accordance with the taken-up assumptions. The most important components of the NMEA 2000 network are presented below.

Tab. 1. Elements of the NMEA 2000 standard, with the differentiation into layers in accordance with the ISO/OSI model, based on [3],[4].

Physical Layer	Fully defined in the standard, it normalizes the sort of cables and connectors, the characteristics of signals etc.
Data Layer	Defined by the ISO 11783-3 standard with the additional requirements contained in the NMEA 2000 standard.
Network Layer	Currently non-defined in the NMEA 2000, it will be defined in future versions of the standard.
Network management (includes the transport, session and presentation layers in accordance with the OSI model)	Defined in the ISO 11783-5 standard with the additional requirements contained in the NMEA 2000 standard.
Application Layer	Fully defined in the NMEA 2000 standard

The main characteristics of the NMEA 2000 network, which result from the accepted standards and definition, are contained in Tab. 2.

Tab. 2. Characteristics of the network in accordance with [5]

Characteristics of the network	
Architecture	<ul style="list-style-type: none"> • Wiring of a main by using the twisted-pair cable, intended for the supply, data transfer and functioning of interface. • Linear network with a single backbone cable, separate central units joined to the main through the short cables of the AUI interface.
Functioning	<ul style="list-style-type: none"> • Access to the network: carrier sense / multi-access / access arbitration determined by the CAN network controller. • Network of a multi-master type (lack of a central control unit). • Self-configuring. • Special network tools necessary for the diagnostic purposes, but not essential for the functioning of a network.
Size	<ul style="list-style-type: none"> • Physical central units: 50 connections at max. • Functional central units: 252 IP addresses at max. • Length of a network: up to 200 m (at the 250 kbit /s speed of transfer).

THE CAN BUS – THE BASIS FOR THE PHYSICAL LAYER OF THE NMEA 2000

The physical layer defines mechanical and electrical aspects of connection between the elements of network. The mechanical part of physical layer (kind of cables and the mean joining them) of a network is fully described by the NMEA 2000 standard and is not a subject of this work. Characteristics of the electric physical layer can be covered by the following points:

- Access to media is controlled by the CAN standard defined as in the ISO 11898 standard.
- The CAN uses dominative/recessive bit transmission.
- Time delay and capacity of a network limits the frequency of bit transfer and the length of a backbone cable.
- LVDS method significantly improves the resistance to interferences of transmission.
- The network single-point common signal reference controls ground voltage levels and reduces the RFI.

The CAN network has been worked out in the second half of the 1980s by the Bosch Company. After a number of changes the CAN network specification present in the ISO 1898 standard, has become the international standard to be used in the vehicles. The controllers of the network, owing to its extensive use in the automotive industry, are available at a price lower than most of the ASIC networks used to control the mains of measurement-control systems (such as e.g. Profibus). Thus, the CAN is widely used also in industrial automation systems as a main for the communication with sensors and actuators. Many advantages of the standard have led to its use also in the vessel networks.

The CAN network is a linear, bit-orientated main, to which the CSMA/CA method of the access to the main avoiding the collisions and errors of transmission, is applied. It requires the time of reaction of all drivers to be no longer than the time of transfer of one bit. It imposes significant limitations on the length of a main which has to fulfill the following condition:

$$L \leq C_1 \cdot \frac{1}{K} \quad (1)$$

where:

- L – ength of a main [m]
- C₁ – proportionality constant (of the value varying between 40 and 50, acc. different sources)
- K – transmission speed [Mbit/s].

The length of the main has to be the smaller the bigger the speed of transmission, as all the CSMA/CA devices on the main have to work with the same speed, and as in the transmission line - in case of long lines - the differences of a signal, resulting from delays in the transmitter/receiver or amplifier, may appear. The relation described in Eq. (3.1) is an empirical formula. In the NMEA 2000 standard the CAN network transmission speed has been set to 250 kbit/s which is equivalent to 200 – meter long main cable.

The quick transmission method through copper cables which have low amplitude, power and small interferences (LVDS), is based on the fact that the CAN main has to be closed at both ends with conditioning resistors (so called terminators) of a value depending on cable impedance. The transmitter transmits small electric current which depends on the logical value (usually of 3,5 mA) which is to be transmitted through one cable. After going through the final resistor, the signal comes back in the opposite direction. The receiver measures the difference of voltages in both cables in relation to the joint reference signal in order to determine the logic state. The arrangement of the typical network based on the CAN main is presented in Fig. 1. The small signal amplitude and strong coupling of the electric and magnetic field between the pair of cables results in that the emission of electrical noise (and the loss of energy) is very low.

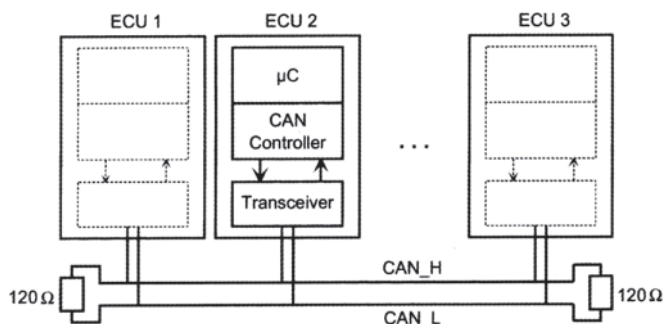
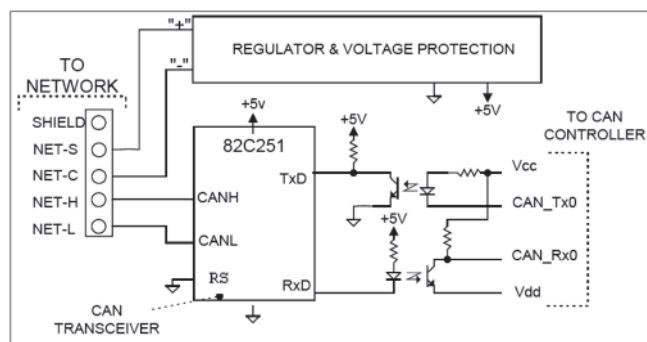


Fig. 1. The arrangement of the typical network based on the CAN main [7]

The LVDS demands powered network interfaces and joint reference signal to all the central units of the network. Two signal lines transmit a differential signal measured in relation to the reference signal. In the CAN networks two logical levels which complement each other, are present, namely: ‘dominant’ or ‘recessive’. During the simultaneous transmission of a ‘dominant’ and ‘recessive’ bit through two different devices the resulting ‘dominant’ level is acquired. Contractually, the ‘dominant’ level is marked “0”, and the ‘recessive’ level “1”. The level “0” has lower priority than the level “1”. The ISO 11898 standard defines the level of individual states as follows:

- Dominant state:
CAN_H = 3,5V, CAN_L = 1.5V,
V_{diff} = CAN_H - CAN_L = 2.0 V
- Recessive state:
CAN_H = 2,5V, CAN_L = 2.5V,
V_{diff} = CAN_H - CAN_L = 0.0 V

The low differential voltage occurring in a system consumes very small amount of energy in comparison to other solutions, which is especially important in case of sailing vessels. The standard also enables the using of typical 12V yacht batteries for the powering of the whole network, in the case when length of a backbone cable and number of central units is sufficiently small. For bigger installations several power sources can be used. Power can be delivered through the main cable or the separate lead (dedicated twisted - pair cable). Such option enables additional power consumption by the device with minimum interface complication. In both the cases the power supply and the reference signal for the interface circuits cannot have direct connection to the power supply circuit or the device grounding in the network. The isolation can be realized in various ways. The most popular one is the using of the optic isolation in the device between the CAN network controller and other circuits. Such isolation which complies with the ISO 11898 standard requirements, is presented in Fig. 2.



Typical Isolated Network Interface

Fig. 2. The example of the optic isolation between the circuits of the interface and devices in the network in accordance with the ISO 11898 standard [6]

THE CAN IN THE DATA LAYER

Like in the case of physical layer, some features of the data connection layer are determined by choice of the CAN as the main of network. The NMEA 2000 fully makes use of the international standard of the ISO 11783-3 data connection layer, which is virtually identical with the SAE J1939-21 standard (i.e. the specification of the CAN for the lorries, delivery trucks and trailers). Additional requirements contained in the NMEA 2000 ensure better copying a system with special types of data and formats transmitted through a navigational device and support special construction of such devices.

In the data connection layer of the NMEA 2000 network, main functions of the CAN interface are: generating the linear stream of bits, controlling the access to the network as well as controlling errors and automatic transmission of messages in which the errors occurred.

The CAN is a broadcast system in which every sender transmits his own messages. Each driver in the network receives messages and, on the basis of a message identifier, decides whether the data will be processed or ignored. In the current specification of the CAN, are incorporated, a. o.,

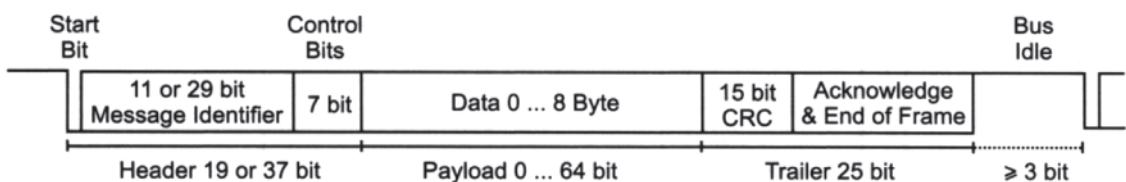


Fig. 3. The CAN communication format (without the separating bits)

29-bits field of identification, the address of a transmitter (specific or global address), type of transmitted data and information about priority. When collision between two devices trying to send data through the main takes place, the CAN compares bit by bit the sent data and this way decides about giving the access, at the same time the arbitration is based on the priority of a message. This method called the Carrier Sense Multiple Access with Collision Avoidance + Arbitration on Message Priority (CSMA/CA + AMP) has such advantage over the standard CSMA/CA protocol that it does not generate time losses.

For error handling and control, each frame contains the so-called cyclic redundancy check (CRC) owing to which the receivers synchronize their execute signal generators with the transmitter. Transmitter, after checking the format and data frame CRC, sends confirmation of receiving the communication by using the ACK bit (Acknowledge) and the end of frame bits. In case of detecting an error by any of the controllers of the network, it sends the application of the error, which results in ignoring the incorrect communication by all the receivers. Owing to this fact the conformity of data in the entire network is guaranteed. The transmitter which has received the error application, immediately and automatically transmits the message in which an error occurred. The CAN detects if a given central unit generates repeating errors and automatically disconnects it from the network to protect the rest of the elements. Results of the research [7] indicate that the error rate of transmission in the CAN system is smaller than 10^{-11} (i.e. percentage of undetectable errors).

The NMEA 2000 standard fully makes use of the described functionality of the CAN network, and in the same time the main tasks it imposes on it in the data connection layer, are the following:

- ensuring the method of transmitting the data which are too big to be contained in a single 8-bit data frame
- defining the set of messages in order to issue a command to the network devices (for example: at the data request or the confirmation request).

The CAN has been originally designed as a transmission network between the sensors/detectors, actuators and the steering system. Such communication does not require the transmission of excessively elaborated messages hence the 8-bit frame was deemed fully sufficient. Due to the specificity of navigational devices, many messages in the NMEA 2000 system exceed the capacity of the standard CAN data controller. In order to deal with this problem, the fast-packet method which enables the transmission of 223 bytes with one identifier, is used for the transmission. This method is about transmitting the frame sequence, the first of which contains the data concerning size of a packet, sequence counter which serves as means for differentiating the messages of the same size in a package and the frame counter. Each additional frame uses one byte of its data space for sequence and frame counters.

The NMEA 2000 expands the capabilities provided by the ISO 11783-3 standard, providing the new type of a message-command, unprecedented in the CAN mains adaptations, which enables setting the specific value or inducing concrete actions

in the receiving device. In addition, the message-command defined in the NMEA 2000, enables setting the time interval of the transmission of concrete data in the transmitting device. For example, a message containing way-points usually consists of the position, name, number and symbol of this point. By using such request the device can force transmitting information concerning certain 'way-point' by providing its name, number or position.

OTHER LAYERS OF THE NMEA 2000 NETWORK

The procedures used in the managing of the NMEA 2000 network result directly from the ISO 11783-5 standard (based on the SAE J1939-81). According to the guidelines the role of this layer can be simply described as: assigning the addresses and identification of devices in the network, as well as initiation of a system after switching-on the power. From among the 256 IP addresses available in the NMEA 2000, only those from 0 to 251 can be assigned to the devices. The set of 255 addresses is the global address used to send messages to all the devices and because of the character of the network (broadcast network) it is the address mostly used while sending messages. Other addresses are reserved to report errors or to be used in next versions of the standard. On the contrary to current CAN applications in accordance with the NMEA 2000, all the devices have to be self-configuring and able to automatically acquire the address while switching-on the system (as devices do not have permanent addresses). The procedure of assigning addresses makes use of the content of the messages data field-command of the address sent by each device during the start. The message contains the name of a device, constituted from the numbers identifying its type and producer and the unique number describing its concrete copy. Assigning the address takes place according to the priority of name. Message-command defined in the data layer of the NMEA 2000 network, can be used to detect information concerning devices connected to the network, to build the map of whole system available to the user. The ability of inserting installation comments by the performer, which can be transmitted at the request, is the additional functionality of the network. The application layer defines composition of all messages which are to be sent in the network. All messages are organized in the parameter groups which are identified by the parameter group number (PGN number), contained in the CAN frame identification field.

ANALYSIS OF THE SCOPE OF APPLICATIONS OF THE CAN TO VESSEL NETWORKS

In the field of vessel systems, their progressing integration takes place. The phenomenon occurs to a different degree on board merchant ships, fishing vessels and yachts. However, irrespective of a purpose, size and complexity level of installed subsystems, to introduce standardization of the process of data exchange between vessel's separate devices, is necessary. The general configuration of a vessel system is illustrated in Fig. 4.

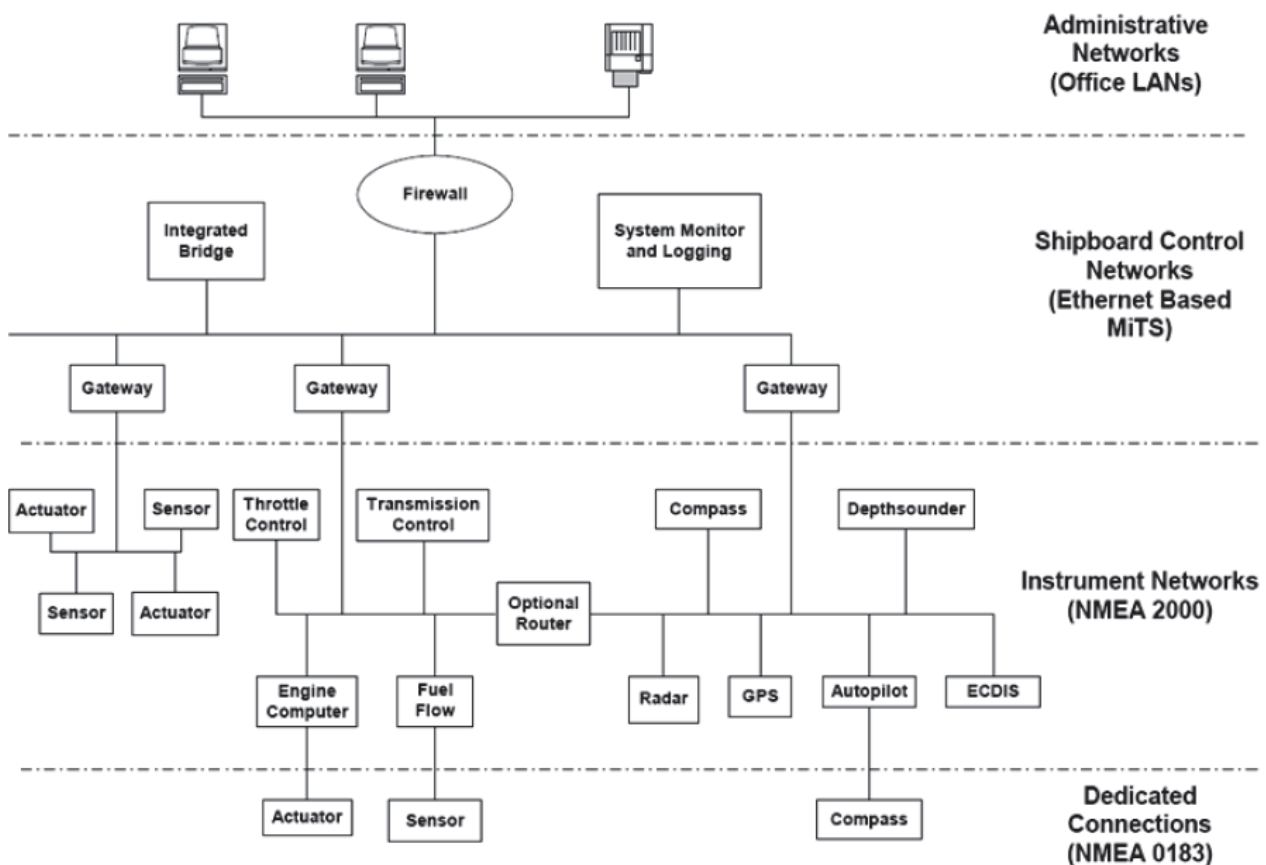


Fig. 4. On-board networks and interfaces [4]

Big merchant vessels, due to their specificity, have the elaborate system of administrative data such as a.o. cargo amount and stowing place. Such databases often have to be accessed not only from the terminals located in different parts of vessel, but also via satellite systems (for example the IMMARSAT C), coupled with the central server in the shipowner's office. However, the administration system is important as far as the effective managing of the vessel is concerned, its efficient work does not significantly influence safety of navigation. Therefore it is not included in the detailed regulations and, out of concern for the users comfort, it was virtually taken over by the PC computers working in the standard LAN network based on the commonly available subsystems.

Decisions which directly influence safety of a vessel and her crew as well as those concerning the ecological safety of greater and greater importance, are taken mostly on the bridge or other control centres being a part of a bridge integrated system. In order to take up such decisions effectively and to guarantee their efficient implementation, captain and officers need the access to data coming from many vessel's systems (of navigation, engine room and fire control etc). The sea transport specificity and special demands concerning reliability eliminate the use of traditional LAN network in such systems despite the requirements concerning the type and speed of data transmission are similar. Big amount of data which has to be sent through the decision support system in the same time disqualifies the CAN network which is dedicated to transmit short messages with high reliability. Requirements concerning the scope of communication between the subsystems of integrated bridge were regulated by the Norwegian Maritime Information Technology Standard (MiTS) [8]. The system based on the TCP/IP protocol (Ethernet network) is currently in the phase of tests and implementation. The surge of interest in Ethernet-based systems in the management layer, is expected [5]. It is also confirmed by the recent application of

the MiTS standard as a basis for the European IEC 61162-4 standard.

However, it appears that systems based on the TCP/IP protocol, propagated by the MiTS, do not fully fit all the vessel communication levels. Separate vessel's subsystems such as engine control or navigational system usually perform strictly defined functions and often regulate processes with the time constant of the order of milliseconds. Therefore they require a real-time data exchange system. The CAN is such system and, on the contrary to Ethernet networks, it is of deterministic kind. Moreover, engine or navigation control, and other control subsystems are usually more autonomic and they transfer relatively small amounts of data (short communications) in relation to other vessel systems. The network dedicated to ensure communication between simple actuators and sensors, i.e. relatively cheap elements, should be of a lower cost per central unit than other vessel networks. All the requirements result in that the choice of an inexpensive CAN network to the subsystem communication, is fully justified.

AN EXAMPLE OF A NMEA 2000 - BASED SYSTEM DESIGNED FOR A MOTOR YACHT

With the introduction of the standard in 2001, attempts to applying it have begun. The test installation has been made on a 25-foot Cherokee class motor boat used by the U.S. Coast Guard. The project assumed the use of electronic throttle and shift controls which transmitted NMEA 2000 - format messages into twin onboard Mercruiser engines equipped with the Teleflex Marine controllers [12]. This way, any mechanical connection between the engine room and the helm station has been eliminated. Beginning from 2008, Yamaha, as the first company, introduced a stock - made motorboat with CAN -based electronic throttle control. In the same time, the largest



Fig. 5. a)¹ Lay-out of the most important elements of the Albatross Control and Management System on a 60 – feet motor yacht.

- 1 - navigation system section, 2 - helm station with data visualization and sections control, 3 - engine room controller,
4 - energy management section, 5 - resources management, 6 - lighting and comfort system controllers,
7 - secondary monitoring station (by means of a multi-function display and wireless network).

b) A fuel filler with an electronic filling percentage indicator – an example of an active NMEA 2000 compatible element used on the yacht

maritime electronics manufacturers began to develop new navigation equipment meeting the requirements of the NMEA 2000 protocol [9], [10].

In the present time, boat yards have a possibility of using full functionality of the new network solution. Examination of yacht systems that are entirely based on CAN protocol, seems most interesting. In Fig. 5 is presented a 60 - feet motor yacht equipped with a complete control and data monitoring system used for many subsystems (sections) of the boat.

In the engine room an ALBA-Engine interface that gathers signals from analog engine sensors, has been installed. The interface is actually a D/A converter and it transmits gathered

data in the NMEA 2000 message format, through the web. Apart from the engine sensors, extra devices that measure propeller shaft vibration and exhaust gas temperature, were added. Every section (lighting, batteries, comfort subsystems) has been equipped with a similar transducer designed for particular types of sensors and actuators. For example the ALBA-Lighting module consists of 8 binary inputs, into which light source circuits are connected, as well as the same number of current relays switched on by the device after receiving a proper command – message from the network. The connection diagram of analog (passive) sensors with the network is shown in Fig. 6.

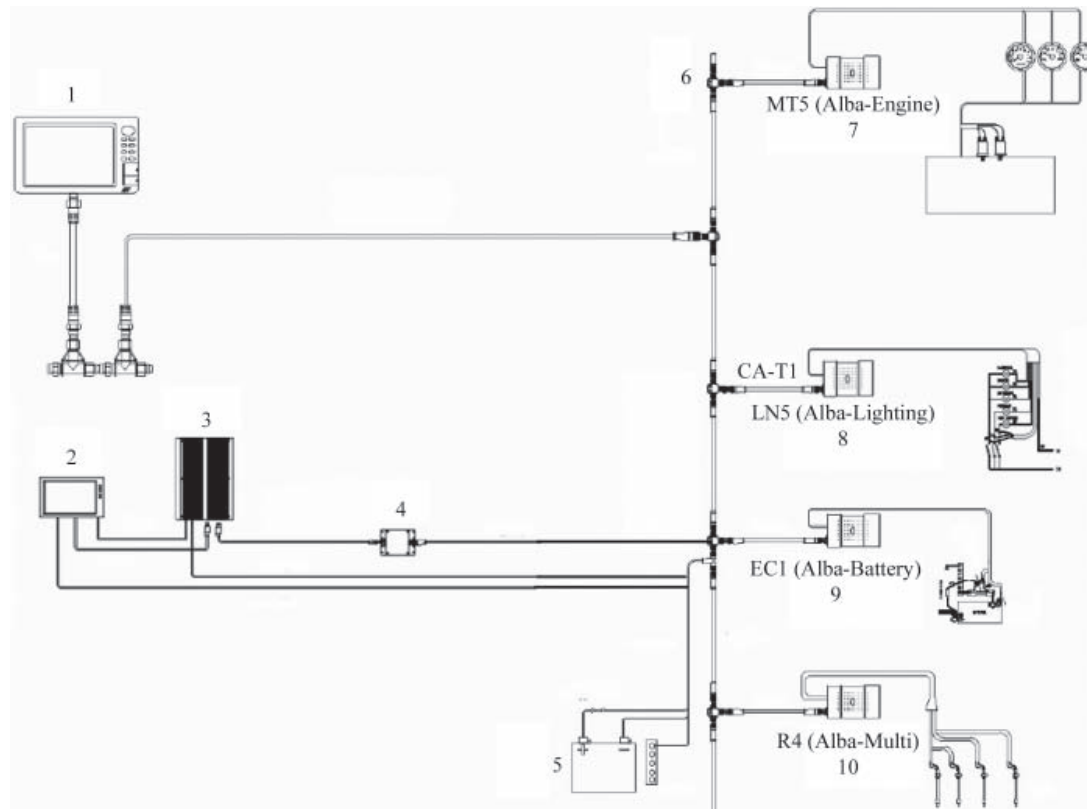


Fig. 6. A part of connection diagram of Albatross Control and Management System: 1 - multi-function display (Raymarine - G-series) at the helm station; 2 - touch screen in the navigation cabin; 3 - ALBA-CPU computer; 4 - ALBA-USB/WIFI - NMEA2000 to USB and Wireless LAN converter (the module enables connecting the onboard computer and a laptop to the ship's network); 5 - network power source; 6 - dedicated "T" junction that connects the device drop cable to the main bus; 7 - ALBA-Engine -engine room controller; 8 - ALBA-lighting - light system controller; 9 - ALBA-battery - energy management; 10 - ALBA-Multi - control and data acquisition from the comfort devices. Notation: in order to simplify the picture not all system elements were shown. The rest of individual sections, converter modules and active network elements are connected similarly by a drop cable and a "T" connection (specified in the NMEA 2000 standard) to the backbone cable

¹ All photos and diagrams of this section are provided by courtesy of Emmi Network [10] – the designer of the system.

Apart from the passive sensors and actuators which communicate with the network by the Albatross system transducers, many active devices (connected directly to the network) have been installed on the ship. The devices are mainly navigational instruments (depth sounder, log, GPS antenna, multi-function displays etc.), dedicated to the NMEA 2000 systems. The characteristics of the standard enables a non-conflicting functioning of devices made by different manufacturers. The application of dedicated NMEA 2000 sensors for fuel, water and wastewater level measurement was a very interesting solution used on board. The whole resource management section has been built by using active elements. Figure 5b presents the fuel filler used in the project. This element is prepared to function as a separate node in the network and it is plugged directly to the main bus with a drop cable.

The heart of the system is an ALBA-CPU water and shock resistant industrial computer. The unit gathers information from all nodes of the NMEA network. The management and visualization software "Albatross On Board Client" has been introduced to the computer. The access to the application is made possible through 3 terminals – a touch screen at the helm station, a similar device in the navigation cabin and through the owner's laptop (by means of wireless network)

The „Albatross On Board Client" software enables the user to freely reconfigure the monitors to customize the way the data gathered in any section, is displayed. Also, interactive fields which can serve to change parameters (like temperature inside), to choose work modes etc, can be put onto the screen. The application terminals configured to visualize engine parameters at the helm station, is shown in Fig. 7.

The down side of the picture shows the visualization of the boat lighting system. The user, by using the interactive screen, can turn the lights on or off in any part of the yacht. Obviously the potential of the system is much greater. It is possible to define alarms when the element status changes or a parameter value exceeds pre-set limit. An automatic reaction can be assigned to any event. For example, a reaction of the system for the voltage drop in one of the battery modules could be either switched to energy saving mode (the system will turn-off non-critical devices) or automatic engine/generator start-up to charge the batteries. All this can be done without the operator's intervention. The owner has the possibility to remotely monitor status of tanks and other parameters as well. Engine warm-up can be initiated in advance of getting onto the yacht etc. Thanks to the use of CAN protocol, the presented system makes it possible to apply the technology of the most exclusive glass-cockpit solutions, with just a fraction of its traditional cost.

SUMMARY

The requirements concerning the on-board communication networks are very demanding. The CAN protocol on which the NMEA 2000 network is based are capable of fulfilling them only as far as the communication between separate sensors and actuators is concerned. The low cost of components and easiness of configuration of the network elements surely contribute to maintaining the standard in this area. The procedure of removing errors in the CAN network is not adaptive hence it takes sometimes more time than in case of other protocols. Unless the very removing of errors is more important than their detecting, the cheap CAN controllers will be a better solution. The CAN has been developed for over 17 years and there is the opinion [9] that elaboration of any other solution capable of replacing it, would take as much time as that.

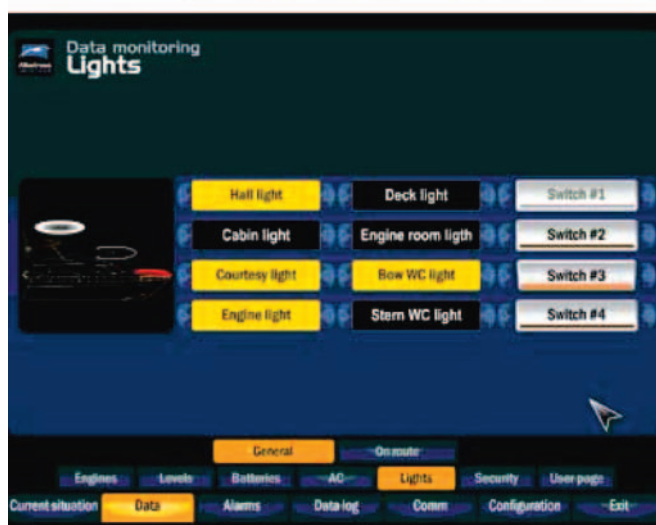


Fig. 7. The helm station in which the monitors were configured to display engine parameters. Down side the control screen of one of the sub-sections (lighting) is visible

- Speed of data transfer depending on the length of the backbone cable, seems to be the main limitation for applying the CAN on board the vessels. It significantly weights in favour of the rival solution - the standardized vessel's LAN (MiTS) networks whose development in the direction of real-time systems is possible along with synchronization of clocks in all the central units. Capacity of the NMEA 2000 network can be further expanded by means of optimizing the electronic equipment as well as data transfer and form, therefore further research should be carried out in this direction.
- It is worth noticing that as far as big vessels are concerned the applying of CAN systems is limited to the actuator-sensor network. Such communication system dominates on small sailing and motor vessels, where it has been implemented till now in the conventional electric control systems with the limited use of the NMEA 0183 protocol. Its low cost and possible simplification of electric installation, as well as easiness of introducing redundancy into critical systems (double main), make the new standard ideal for use on board small crafts. Also, first applications of the NMEA 2000 networks have already appeared on the motor vessels [10], however, the knowledge about the system is

still rather not wide- spread among the designing teams. Taking into consideration the significant share of the products of Polish pleasure craft industry in their market segment, it seems advisable to promote the solution among the producers and designers, as this innovation could strengthen competitiveness of their companies. Also, to conduct further research on possible application of the NMEA 2000 standard on board the recreational vessels is advised.

BIBLIOGRAPHY

1. Simrad AS: *SimNet Installation Manual 2004*
2. Raymarine plc: *SeaTalk Reference Manual 2007*
3. ISO standard 7498-1: *Information technology – Open Systems Interconnection – Basic Reference Model: The Basic Model*, 1994
4. Cassidy F.: *NMEA 2000 Explained - The latest word*. Marine Electronics, 1999
5. Luft L. A., Anderson L., Cassidy F.: *NMEA 2000 - A Digital Interface for the 21st Century*. Institute of Navigation's National Technical, 2002 San Diego, California
6. National Marine Electronics Association: *NMEA 2000, version draft 4.1*, 1999
7. Zimmermann W., Schmidgall R.: *Bussysteme in der Fahrzeugtechnik*. Vieweg & Sohn Verlag, Wiesbaden 2007
8. Rødseth Ø.: *Companion standards for integrated ship control system*. SINTEF Automatic Control N-7034 Trondheim, 1995
9. <http://www.raymarine.com/>
10. <http://www.emminet.com/>
11. Törgren M.: *A perspective to the design of Distributed Real-time Control Applications based on CAN*. 1999
12. Anderson L., Luft L. A.: *NMEA 2000 Applied*. RTCM, May 2002, St Petersburg, FL, (updated in 2006).

CONTACT WITH AUTHORS

Andrzej Piętaś, Assoc. Prof.
Maciej Mikulski, M. Sc.
Faculty of Technical Sciences
Chair of Mechatronics
Słoneczna 46 A
10-710 Olsztyn, POLAND
e-mail: apietak@uwm.edu.pl
e-mail: maciej.mikulski@uwm.edu.pl



The Ship Handling Research and Training Centre at Ilawa is owned by the Foundation for Safety of Navigation and Environment Protection, which is a joint venture between the Gdynia Maritime University, the Gdansk University of Technology and the City of Ilawa.

Two main fields of activity of the Foundation are:

- Training on ship handling. Since 1980 more than 2500 ship masters and pilots from 35 countries were trained at Ilawa Centre. The Foundation for Safety of Navigation and Environment Protection, being non-profit organisation is reinvesting all spare funds in new facilities and each year to the existing facilities new models and new training areas were added. Existing training models each year are also modernised, that's why at present the Centre represents a modern facility perfectly capable to perform training on ship handling of shipmasters, pilots and tug masters.
- Research on ship's manoeuvrability. Many experimental and theoretical research programmes covering different problems of manoeuvrability (including human effect, harbour and waterway design) are successfully realised at the Centre.

The Foundation possesses ISO 9001 quality certificate.

Why training on ship handling?

The safe handling of ships depends on many factors - on ship's manoeuvring characteristics, human factor (operator experience and skill, his behaviour in stressed situation, etc.), actual environmental conditions, and degree of water area restriction.

Results of analysis of CRG (collisions, rammings and groundings) casualties show that in one third of all the human error is involved, and the same amount of CRG casualties is attributed to the poor controllability of ships. Training on ship handling is largely recommended by IMO as one of the most effective method for improving the safety at sea. The goal of the above training is to gain theoretical and practical knowledge on ship handling in a wide number of different situations met in practice at sea.

For further information please contact:

The Foundation for Safety of Navigation and Environment Protection

Head office:
36, Chrzanowskiego Street
80-278 GDAŃSK, POLAND
tel./fax: +48 (0) 58 341 59 19

Ship Handling Centre:
14-200 ILAWA-KAMIONKA, POLAND
tel./fax: +48 (0) 89 648 74 90
e-mail: office@ilawashiphandling.com.pl
e-mail: office@portilawa.com

GDANSK UNIVERSITY OF TECHNOLOGY

is the oldest and largest scientific and technological academic institution in the Pomeranian region. The history of Gdansk University of Technology is marked by two basic dates, namely: October 6, 1904 and May 24, 1945.

The first date is connected with the beginning of the technical education at academic level in Gdansk. The second date is connected with establishing of Gdansk University of Technology, Polish state academic university. Gdansk University of Technology employ 2,500 staff, 1,200 whom are academics. The number of students approximates 20,000, most of them studying full-time. Their career choices vary from Architecture to Business and Management, from Mathematics and Computer Science to Biotechnology and Environmental Engineering, from Applied Chemistry to Geodesics and Transport, from Ocean Engineering to Mechanical Engineering and Ship Technology, from Civil Engineering to Telecommunication, Electrical and Control Engineering. Their life goals, however, are much the same - to meet the challenge of the changing world. The educational opportunities offered by our faculties are much wider than those of other Polish Technical universities, and the scientific research areas include all of 21st Century technology. We are one of the best schools in Poland and one of the best known schools in Europe – one that educates specialists excelling in the programming technology and computer methods used in solving complicated scientific, engineering, organizational and economic problems.

THE FACULTY OF OCEAN ENGINEERING AND SHIP TECHNOLOGY

The Faculty of Ocean Engineering and Ship Technology (FOEST) as the only faculty in Poland since the beginning of 1945 has continuously been educating engineers and doctors in the field of Naval Architecture and Marine Technology.

The educational and training activities of FOEST are supported by cooperation with Polish and foreign universities, membership in different international organizations and associations, as well as participation in scientific conferences and symposia. Hosting young scientists and students from different countries is also a usual practice in FOEST.


The activities of Faculty departments are related to: mechanics and strength of structures, hydromechanics, manufacturing, materials and system quality, power plants, equipment and systems of automatic control, mostly in shipbuilding, marine engineering and energetic systems.

FOEST is a member of such organizations like WEGEMT; The Association of Polish Maritime Industries and the co-operation between Nordic Maritime Universities and Det Norske Veritas. The intensive teaching is complemented and supported by extensive research activities, the core of which is performed in close collaboration between FOEST staff and industry. We take great care to ensure that the applied research meet both the long term and short term needs of Polish maritime industry. FOEST collaborates with almost all Polish shipyards. Close links are maintained with other research organizations and research institutions supporting the Polish maritime industry, such as Ship Design and Research Centre and Polish Register of Shipping, where several members of the Faculty are also members of the Technical Board.

The Faculty of Ocean Engineering and Ship Technology is a unique academic structure, which possesses numerous highly qualified and experienced staff in all above mentioned specific research areas. Moreover, the staff is used to effective co-operation and exchange of ideas between specialists of different detailed areas. This enables a more integrated and comprehensive treatment of research and practical problems encountered in such a complicated field of activity as naval architecture, shipbuilding and marine engineering.


The staff of the Faculty has strong international links worldwide, being members or cooperating with international organizations like International Maritime Organization IMO, International Towing Tank Conference ITTC, International Ship and Offshore Structures Congress ISSC, International Conference on Practical Design of Ship and other floating Structures PRADS just to name a few.

GDANSK UNIVERSITY OF TECHNOLOGY
Faculty of Ocean Engineering and Ship Technology
11/12 Narutowicza Street, 80-952 Gdansk, Poland
Tel (+48) 58 347 1548 ; Fax (+48) 58 341 4712
e-mail: sekoce@pg.gda.pl



Gdansk University of Technology

Faculty of Ocean Engineering and Ship Technology



www.oce.pg.gda.pl